UNIVERSITÀ DEGLI STUDI DI MILANO

DOTTORATO DI RICERCA IN SCIENZE DELLA TERRA

Ciclo XXXV

DIPARTIMENTO DI SCIENZE DELLA TERRA

PhD THESIS

Combining Geochemical and Numerical Modeling for Chlorinated Solvents Groundwater Contamination

Giulia Casiraghi

(ID Nr. R12561)

Supervisor

Prof. Daniele PEDRETTI

Co-supervisor

Prof. Giovanni Pietro BERETTA

Coordinator

Prof.ssa Maria Iole SPALLA

Academic Year

2021-2022

Abstract

Chloroethenes represent a serious risk to aquatic ecosystems and human health on a worldwide scale. Chloroethenes contamination is difficult to solve due to the different optimal redox conditions needed to obtain efficient degradation of each chloroethene. The more chlorinated ones such as tetrachloroethene (PCE) and trichloroethene (TCE) are better degraded via reductive dechlorination (RD) under anaerobic conditions, while the less chlorinated compounds such as dichloroethene (DCE) and vinyl chloride (VC) are better degraded via oxidation (OX) under aerobic conditions. Thus, sequential bioremediation systems (SBSs) able to stimulate anaerobic and aerobic biodegradation are preferred over traditional bioremediation systems targeting single degradation pathways.

Assessing the efficiency of SBSs is a challenging task that requires a multidisciplinary approach, spanning from hydrogeology, organic geochemistry and microbiology. While expert knowledge and laboratory analyses provide initial inputs for the design of SBS, field monitoring data are needed to evaluate if and how bioremediation is carried out.

Reactive transport models (RTMs) are suitable tools to assist decision makers when designing and monitoring bioremediation efficiency. To date, no applications to SBSs have been reported, possibly owing to the relative novelty of SBS and to the additional modeling challenges (e.g., more complex parameterization) that sequential systems pose over traditional bioremediation systems. RTMs have the capability to integrate and harmonize multiple data and, when properly tailored, to make useful predictions about a system's behavior when different remediation set-ups are tested in order to optimize the cleanup operations.

The general objective of this thesis was to develop methodologies for the evaluation of the efficiency of SBSs applied to chloroethenes aquifer contamination. As case study, we investigated one the largest SBS currently implemented in a polluted alluvial aquifer in Italy. The SBS is about 800 m-long and was created to remediate organic pollutants such as chloroethenes and petroleum hydrocarbons (PHCs). The SBS is made up of a hydraulically upgradient anaerobic (AN) biobarrier, where a reducing substrate is injected to stimulate RD of higher chloroethenes (PCE, TCE), and downgradient aerobic (AE) biobarrier, where OX of lower chloroethenes (DCE, VC) is stimulated through nutrients and oxygen injection. In addition, P&T wells are active downgradient of the two biobarriers in order to intercept the remaining contaminants exfiltrating from the SBS.

The first part of the thesis evaluates the initial characterization activities propaedeutic to the installation of the operational (full) scale SBS: Microcosm experiments and in situ tests were carried out to assess the biodegradation potential of the autochthonous microbial communities in the laboratory and in the site under both natural and biostimulated conditions. Both investigations showed a satisfactory efficiency of aerobic and anaerobic degradation only after biostimulation, proving the feasibility as well as the necessity of the full-scale SBS for the cleanup of the site. The analysis of these data constitutes an improvement of the current state of the art in the design and implementation of large-scale SBS.

The second part of the thesis is dedicated to the analysis of time series of chloroethenes concentrations and environmental parameters observed during periodic monitoring of groundwater in the site piezometers of the full-scale SBS. Carbon compound-specific isotopic analysis (C-CSIA) were carried out on chloroethenes PCE, TCE, *cis*-DCE and VC in samples acquired along a flow path crossing both biobarriers. Target chloroethenes concentrations and isotopic compositions were interpreted through a one-dimensional (1D) geochemical model in order to assess the processes controlling the sequential bioremediation and to obtain a first-cut evaluation of the effectiveness of the SBS. The active SBS proved to be efficient in reducing chloroethenes concentrations along the investigated flow path (reduction of concentrations up to 100%). The AN barrier proved to be able to significantly enhance RD of PCE and TCE mainly, increasing natural anaerobic degradation up to 30 times. The AE barrier, instead, proved to have a fundamental role in enhancing OX of *cis*-DCE and VC.

The third part of the thesis focuses on the development of a multidimensional model with enhanced predictive capabilities compared to the 1D model.

Different degrees of spatial heterogeneity of degradation efficiency were taken into consideration by setting up two models with different parametrization of degradation constants (i.e. homogeneous and heterogeneous distribution). Moreover, it was also possible to model the P&T system. and simulate different scenarios by deactivating the P&T to determine the most efficient setup of the system (i.e. with or without P&T). Contaminant loadings exfiltrating from the site were quantified and compared between the different scenarios and Damköhler numbers (Da) were calculated to evaluate the spatial heterogeneity of degradation efficiency. The 2D model showed the importance of choosing a spatially heterogeneous configuration rather than a homogeneous one in order to obtain an accurate reproduction of contaminant loadings. Da permitted to prove the heterogeneity of degradation efficiency and pinpoint critical areas in the site where bioremediation is less efficient. Another important result was the demonstration of the P&T importance in abating contaminant loadings and providing a better containment of the plume of contaminants, specifically the more toxic VC whose loadings resulted to be the highest in the site.

Overall, the multiscale experimental activities were fundamental for the assessment of the site suitability to sequential bioremediation and for the subsequent implementation of the SBS. The multidisciplinary approach adopted permitted to evaluate the efficiency of the remediation system.

Abbreviations

Capital letters

AE	Aerobic
ALRC	Artificial land reclamation canal
AN	Anaerobic
CAHs	Chlorinated aliphatic hydrocarbons
CSIA	Compound-specific isotope analysis
DCE	Dichloroethene
ISB	In situ bioremediation
ISB	In Situ Bioremediation
K	Horizontal hydraulic conductivity
K'_D	Distribution coefficient (mg sorbed/kg solid)/(mg solute/L pore water) (L kg^{-1} or cm^3 g^{-1})
L	Unit of length
M	Unit of mass
OHR	Organohalide respiration
OX	Oxidation
PCE	Tetrachloroethene
PHCs	Petroleum hydrocarbons
RD	Reductive dechlorination
RZ	Reactive zone
SBS	Sequential Bioremediation System
T	Unit of time
TCE	Trichloroethene
VC	Vinyl chloride

Lower case letters

D_m	Molecular diffusivity coefficient (m^2 d^{-1})
$\overline{D_m}$	Average molecular diffusivity coefficients (m^2 d^{-1})
f_{oc}	Fraction of organic carbon (-)
k_{oc}	Partition coefficient between organic carbon and water (Lkg^{-1} or cm^3 g^{-1})
k_{OX}	Degradation rate constant for OX (y^{-1})
k_{RD}	Degradation rate constant for RD (y^{-1})
q	Seepage rates (m d^{-1})
r_c	Aquifer recharge (m d^{-1})
v_r	Retarded velocity (m d^{-1})
v_{nr}	Non-reactive velocity or tracer velocity (m d^{-1})

Greek symbols

α_{L}	Longitudinal dispersivity (m)
α_{Th}	Transversal horizontal dispersivity (m)
β	Retardation factor (-)
$\bar{\beta}$	Average retardation factor (-)
ε	Enrichment factor (-)
ρ_b	Bulk density
ϕ	Porosity (-)

Table of Contents

1 Preface

1.1 Introduction

1.1.1 Overview of chloroethene contamination in aquifers

Groundwater represents an essential resource for natural ecosystems as well as human life and activities. Aquifers provide about one third of the globally available freshwater. Many economic sectors depend on the availability of clean groundwaters, since they supply as much as 65% of drinking water as well as 25% of water for agricultural irrigation in Europe (European Environment Agency, 2022). Thus, protection of this vital resource should be a priority. In the EU, the Water Framework Directive (EC 2000) currently represents the main water protection law, and it compels European countries to take action in order to restore a good chemical and quantitative status of aquifers. Specific environmental objectives regarding chemical pollution are specified in the Groundwater Directive (EU 2014). Notwithstanding, in 2016 a percentage as high as 25% of the total European groundwater body area failed to classify as in good status: 12% resulted in of poor quantitative status, while as much as 29% was of poor chemical status, according to the second River basin management plan reporting cycle of 2016 (Kristensen et al., 2018).

Chloroethenes are a widespread and problematic class of contaminants that can endanger the aquifers quality (Futagami et al., 2008; Matteucci et al., 2015a). Due to their toxicity and recalcitrant nature (Henschler, 1994), chloroethenes lead to dangerous and persistent contamination situations (e.g. Pedretti et al., 2012, 2013). Their ability to accumulate in organic tissues poses a serious problem for human and ecosystems health (Häggblom and Bossert, 2004; Koenig et al., 2015). VC, in particular, is the most problematic due to its known cancerogenic nature (Fralish and Downs, 2022)

Chloroethenes are hydrocarbons composed of two carbon atoms and between one and four chlorine atoms in place of hydrogen, which are part of a wider class of organic contaminants called chlorinated solvents. From the most to the less chlorinated species we define tetrachloroethene (or perchloroethylene) (PCE) with four chlorine atoms, trichloroethene (TCE) with three chlorine atoms, dichloroethene (DCE) with two chlorine atoms and vinyl chloride (VC) with only one chlorine atom.

In particular, PCE and TCE fell within the 15 contaminants that caused the failure to achieve groundwaters good status in more than 5 EU Member States, compromising each 1% of the total groundwater body area of the EU (Kristensen et al., 2018). Moreover, these chlorinated solvents pose a serious problem in many other non-EU countries too (Baek and Lee, 2011; Kawabe and Komai, 2019; Leeson et al., 2004; Yang et al., 2018), making it a worldwide problem**.**

Groundwater pollution by chloroethenes has been a serious issue since the last century. From the 1940s to the 1970s chloroethenes were extensively used for dry-cleaning and degreasing purposes, as well as for the production of other chemicals. The adoption of inadequate disposal practices in the past led to their current widespread presence in aquifers throughout the world (Kristensen et al., 2018; Lecloux, 2003). Old industrial landfills represent a common source of chloroethenes due

to the high contaminant mass accumulated without proper safety measures (Christensen et al., 2000; Cozzarelli et al., 2000; Kromann et al., 1998; Nielsen et al., 1995; Ravina et al., 2020; Rügge et al., 1999; Sizirici and Tansel, 2010; Wood and Porter, 1987). Prior to the 1970s, the lack of regulation for disposal of municipal and industrial solid waste in landfills led to inadequate storage of huge volumes of hazardous materials (Pedretti et al., 2012; Reinhart, 1993). Without proper impermeabilization, meteoric water can easily seep through the waste and collect organic and inorganic substances. The resulting polluted leachate can lead to the formation of solute plumes, potentially extended over several km from the source (Calloni et al., 2002; Pedretti et al., 2013; Petitta et al., 2013; Suflita et al., 1992).

More stringent regulations were introduced in the 1980s and 1990s to reduce the risk related to landfills. The use of liners or leachate collection systems was imposed as an approach to minimize water infiltration into landfills and prevent groundwater contamination. While these solutions may slow down the formation of polluted leachate, the long-term effectiveness of engineered waste containment systems is limited and may eventually fail. While authorities need to find solutions that permanently eradicate the problem at the source, aquifer cleanup operations become urgent to stop the contaminants to move downgradient and try to restore aquifer quality to the pre-contamination levels.

1.1.2 Traditional aquifer cleanup with pump-and-treat systems

Pump and Treat (P&T) systems, or pump-and-stock, has been adopted since the early 1980s for the remediation of chlorinated solvents in contaminated sites (EPA, 1996). P&T systems consist of a network of pumping wells, which extract polluted water from a targeted aquifer. While providing hydraulic containment of contaminant plumes, groundwater is treated off-site by means of physical and biochemical methods (e.g., through active carbon filtering), and eventually reinjected to the ground or more commonly delivered to surface water bodies for further dilution.

The effectiveness of P&T as principal remediation option for aquifers polluted by chloroethenes has long been questioned (Freeze and Cherry, 1989; Haley et al., 1991; Keely, 1989; Mackay and Cherry, 1989). Using P&T, contaminant removal rates tend to be low; in most cases, concentrations cannot be reduced to the maximum contaminant levels imposed by the jurisdiction in cost-effective times (Mackay and Cherry, 1989; Olsen and Kavanaugh, 1993; Travis and Doty, 1990). The key reason is that chloroethenes can occur as non-aqueous phase liquids (NAPLs). Their low solubility in water means that these contaminants can persist as a separate phase from groundwaters in soils. The presence of contaminated low permeable layers is particularly critical, as these layers act as slow-release and virtually endless source of contaminant (Mackay et al., 2000; Mutch et al., 1993; NRC, 1994).

If P&T is the sole aquifer remediation approach, its poor effectiveness determines high operational and management costs as well as a high environmental footprint. In fact, their functioning over prolonged time frames and the management of solid residuals produced by the offsite treatment entail energy waste needed for the functioning of the wells and CO_2 emission (Casasso et al., 2019). These issues prompted researchers and administrators to evaluate more cost-effective and sustainable solutions to perform aquifer cleanup.

1.1.3 In Situ Bioremediation

As of the 1980s, evidence of chloroethenes biodegradation started to be gathered. Whilst before these contaminants were not considered degradable at the hand of microorganisms, many studies suggested the contrary.

PCE and TCE transformation to dichloroethene (DCE) and vinyl chloride (VC) under anaerobic conditions (Barrio-Lage et al., 1990, 1987; Bouwer et al., 1994; Norris, 2018; Vogel and McCarty, 1985) as well as VC biodegradation under both aerobic (Hartmans et al., 1985; Phelps et al., 1991) and anaerobic (Bradley et al., 1998; Bradley and Chapelle, 1996) conditions was demonstrated. Microbes that biodegrade chloroethenes as their main mean of support were also identified (Bradley et al., 1998; Holliger et al., 1993; Maymó-Gatell et al., 1997; Sharma and McCarty, 1996).

Further studies were carried out in the successive decades to gain a better understanding of chloroethenes biodegradation pathways and the microorganisms involved (Dolinová et al., 2017a; Xiao et al., 2020) in order to be able to exploit microbial activity in remediation activities directly in the field. Such practice is known as “in situ bioremediation” (ISB) (Thomas and Ward, 1989). In the 1990s the combination of P&T with ISB started to be considered to improve the effectiveness of remedial activities (Marquis Jr, 1995). As of 2015 conventional methods (i.e. P&T) were still predominant to carry out aquifer restoration in most European countries, although ISB was starting to gain a foothold (Majone et al., 2015). The main reason that hindered the spread of bioremediation in aquifer restoration was the need to extensively characterize the site from a microbiological and biochemical as well as hydrogeological and geochemical point of view (Majone et al., 2015).

In the USA between 1982 and 2005 P&T was still the preferred remediation approach, too (EPA, 2007). Since 1997, however, a slow but steady increase in ISB applications started, coupled to a decrease in P&T applications which resulted in the years 2005-2011 in ISB being the most applied in situ remediation approach (EPA, 2013).

Essentially, ISB exploits microbially mediated reactions that affect the stability of organic pollutants (such as chloroethenes) in soils. Both metabolic and co-metabolic processes can concur to transform organic contaminants into harmless compounds (such as ethene in the case of chloroethenes), biomass, CH_4 or CO_2 (Chandra, 2016; Thomas and Ward, 1989). Different approaches to ISB can be taken (Pandey and Singh, 2020; Shivalkar et al., 2021).

In Monitored Natural Attenuation (MNA), the natural capability of the autochthonous microbial communities to degrade the target contaminants is only subject to monitoring activities without direct human intervention. This approach is undertaken when there is evidence of an efficient natural biodegradation which does not require human intervention.
Enhanced ISB, instead, involves different kinds of active intervention. Bioaugmentation enhances degradation by introducing in the aquifer microorganisms able to biodegrade the target contaminants. Biostimulation aims to enhance the activity of microorganisms already present in the aquifer by injection of rate-limiting nutrients. Biosparging involves air injection at low rates of flow in groundwater in order to increase oxygen levels and enhance aerobic biodegradation (Moussa and Khalil, 2022; Speight, 2020; Vidali, 2001). It can also be coupled to inorganic nutrients addition to promote microbial growth (Bell et al., 2022; Moussa and Khalil, 2022).
Compared to P&T, in situ Bioremediation (ISB) offers various benefits. First of all, it allows the treatment of polluted waters directly in the aquifer (Antelmi et al., 2021; Devlin et al., 2004; Leeson et al., 2004; Tiehm and Schmidt, 2011), which eliminates the issue of extracting huge volumes of groundwaters and their reinjection after treatment. The treatment equipment and infrastructures needed are also reduced. The disposal of treatment residuals and wastes is no longer an issue. Overall bioremediation leads to a reduced environmental impact.

During bioremediation, organic contaminants can be transformed to harmless compounds by specific microorganisms which carry out biotransformations with the final aim to increase their population size. To reach this end they need energy for the transformation of nutrients into forms usable by cells. Such energy is produced during biotransformations when electrons are transferred from a so-called electron donor to an electron acceptor.
The biotransformations exploited in bioremediation to solve chloroethene contamination are mainly three: anaerobic reductive dechlorination (RD), aerobic metabolic and cometabolic oxidation (OX).
The first and more used is reductive dechlorination (RD) (Antelmi et al., 2021; Tiehm and Schmidt, 2011). RD is the most popular choice since it potentially permits to obtain the complete dechlorination of PCE to ethene. During this process chloroethenes are utilized as electron acceptors and hydrogen or acetate as electron donor (Aulenta et al., 2006a; He et al., 2002; Kouznetsova et al., 2010).
During RD PCE is transformed to ethene by progressive substitution of one chlorine atom with one hydrogen atom, which transforms PCE to TCE, TCE to DCE (mainly its *cis*-1,2-DCE isomer), DCE to VC and finally VC to ethene, the last (non-toxic) compound of the transformation chain (Frascari et al., 2015).
Microbial genera able to carry out RD are called anaerobic dechlorinators. Most of them are able to carry out the first two steps of RD (i.e. transforming PCE to TCE and TCE to DCE). *Dehalobacter* (Holliger et al., 1993; C. Holliger et al., 1998), *Geobacter* (Sung et al., 2006)*, Desulfitobacterium*

(Maillard et al., 2005), *Dehalospirilum* (Neumann et al., 1994), *Desulfuromonas* (Krumholz et al., 1996; Sung et al., 2003) *and Sulfurospirrillum* (Luijten et al., 2003) are among them.

Even though in limited number, microbial species able to carry out the complete dehalogenation of PCE to ethene also exist. *Dehalococcoides mccartyi (*Maymó-Gatell et al., 2001; Stroo et al., 2013) and *Dehalogenimonas species* (Yang et al., 2017) are some of such species. However, the efficiency of the successive transformation steps drastically decreases with the number of chlorine atoms of the contaminant molecule, due to the lower energetic yields associated with lower chlorinated compounds (Dolinová et al., 2017a; Futagami et al., 2008; Tiehm and Schmidt, 2011).

Moreover, dechlorinators have to compete for the use of electron donors with other bacteria such as sulfate reducing bacteria and methanogens, which gain energy by using sulfate and methane as electron acceptors, respectively (Fennell et al., 1997; Matteucci et al., 2015a; Yang and McCarty, 2002). The activity of such bacteria is optimal under ranges of redox potential that partially or totally overlaps those of dechlorinators. In fact, RD of chloroethenes is optimal with a redox potential lower than -200 mV (Dolfing, 2016), sulfate reducing bacteria best operate at a redox potential between -50 to -250 mV and methanogens activity .is optimized between -175 and -400 mV (Norris, 2018).

To circumvent the problem of lack of electron donors to carry out RD, in the practice of biostimulation they are provided to the microorganisms by injection of organic substrates (e.g. butyrate, propionate , lactate, ethanol, methanol) (Aulenta et al., 2006a) that produce hydrogen and acetate by fermentation.

However, the difficulty associated to reach the optimal conditions for the last two less-favorable steps of chloroethenes transformation can still easily lead to DCE and especially VC accumulation in the site (Aulenta et al., 2006a; Chambon et al., 2013; Němeček et al., 2020). The accumulation of this mono-chlorinated compound is particularly cumbersome due to its cancerogenic nature, which makes it a compound with an even greater toxicity than the other chloroethenes (Fralish and Downs, 2022).

On the contrary, lower chlorinated ethenes like DCE and VC are preferentially degraded by aerobic bacteria via metabolic or cometabolic OX (Davis and Carpenter, 1990; Dey and Roy, 2009; Dolinová et al., 2017a; Mattes et al., 2008; Schmidt and Tiehm, 2008).

During metabolic OX, chloroethenes are used by these bacteria as electron donors. Chloroethenes act as the growth substrate for aerobic bacteria, providing them with carbon and energy.

In cometabolic OX, instead, chloroethenes degradation only happens fortuitously at the hands of enzymes, which are produced by aerobic bacteria for the scope of degrading (and thus gaining energy) their actual target growth substrate (e.g. ammonium, methane, ethene as well as aromatic pollutants).

A comprehensive list of bacteria able to carry out metabolic and/or cometabolic OX can be found in (Dolinová et al., 2017a).

In bioremediation oxidative degradation is favored by creating aerobic conditions with oxygen injection in the subsurface (i.e. biosparging) as well as delivering nutrients that can act as growth substrates for bacteria, when in the aquifer suitable substrates are lacking.

1.1.4 Sequential In-Situ Bioremediation

A limitation of ISB when applied to chloroethenes contamination is that a single system is not able to target the stimulation of anaerobic and aerobic biodegradation simultaneously, i.e., either RD or OX can be stimulated in a single ISB system (Tiehm and Schmidt, 2011). In a site where PCE and TCE are present, the application of anaerobic ISB can thus lead to incomplete chloroethenes degradation and the accumulation of VC.

Sequential anaerobic/aerobic in-situ bioremediation systems (SBS) have been introduced to bypass the limitations of single biodegradation systems (Frascari et al., 2015; Lai et al., 2017; Němeček et al., 2020; Tiehm and Schmidt, 2011). In SBS, chloroethenes in groundwaters undergo a two-stage bioremediation. First, anaerobic conditions are induced at a hydraulically upgradient biobarrier in order to stimulate RD of higher chlorinated ethenes. Downgradient of the anaerobic zone, aerobic conditions are instead favored by injection of oxygen in order to stimulate OX of the residual less chlorinated chloroethenes. If optimal conditions are created and proper biostimulation is attained, a complete dechlorination of chloroethenes can be reached with SBSs. Moreover, since chloroethenes can be found together with petroleum hydrocarbons in landfills, a sequential approach is also useful to target these additional contaminants, since they are generally degraded under aerobic conditions (Fritsche and Hofrichter, 2005). Only less frequently they are degraded under anaerobic conditions (Vogt et al., 2011).

Although SBS is well-studied in the laboratory and shows promise, examples of real-life applications are limited in the literature to date (Devlin and Parker, 1996; Tiehm and Schmidt, 2011). This could be readily ascribed to the higher complexity and costs associated to the implementation of a double ISB system compared to a relatively simpler single ISB system.

1.2 Current gaps in literature

The effectiveness of bioremediation in aquifer restoration has been widely demonstrated (Kao, 2003; Xiao et al., 2020). Notwithstanding, a major issue with bioremediation is the technical complexity associated with the assessment of its actual efficiency. This means proving that contaminant concentration drops observed in space and time at the investigated site are consequence of microbially mediated degradation processes (i.e. contaminant mass destruction) rather than dilution after release from the source.

The major gaps in the current state-of-the-art to properly assess SBSs are the following.

Lack of published data related to SBSs implementation and monitoring. The first technical challenge that arises in SBS is the sheer amount of different data to be collected. Both laboratory analysis and field investigations are in fact required in order to gain a proper initial assessment of the situation and a subsequent continuous monitoring of the system to evaluate its efficiency is essential. First of all, a thorough hydrogeological characterization of the aquifer is necessary, in order to identify heterogeneities in aquifer properties. Geochemical characterization of groundwaters by continuous monitoring of contaminants concentrations and environmental parameters (e.g. TEAs concentrations, pH, temperature, electrical conductivity) is also required. In addition, microbiological characterization is essential before and during bioremediation activities for the initial assessment of the autochthonous microbial communities, the identification of useful bacterial species, their quantity and the effect of bioremediation on their activity. Understanding the interdependence of different microbial species is also a key point for the evaluation of the situation (Xiao et al., 2020).

Having detailed reports of such investigations and analysis of the data acquired would provide a useful guide for future implementation of other SBSs.

Lack of studies applying compound-specific isotope analysis (CSIA) to SBSs. Compound-specific isotope analysis (CSIA) represents another powerful tool for the assessment of biodegradation efficiency and degradation pathways of contaminants in the field (Antelmi et al., 2021; Blum et al., 2009; D'Affonseca et al., 2011; Pooley et al., 2009; Van Breukelen et al., 2005; Zimmermann et al., 2020). CSIA involves monitoring the isotopic composition of the target contaminants in space and time in order to pinpoint an isotopic enrichment that can be evidence of ongoing degradation. The use of CSIA as support to concentration data in SBSs could help obtain a better assessment of both anaerobic and aerobic biodegradation to ensure the efficiency of both pathways.

Lack of modeling applied to SBSs. Once all the aforementioned data have been collected a new challenge arises in their interpretation, especially when dealing with sites characterized by a complex hydrogeology and hydrogeochemistry. Nowadays, the use of numerical models in the design and management of aquifer clean-up sites has become a state-of-the-art approach. Groundwater models

can support the design of bioremediation systems as well as P&T systems (Pedretti, 2020). Geochemical models permit to simulate hydrogeochemical processes (Haest et al., 2010; Kao, 2003; Kao et al., 2003; Kouznetsova et al., 2010; Lee et al., 2004). In the last decades, the combined simulation of hydrogeochemical and transport processes in reactive transport models (RTM) has become an essential tool in assessment of bioremediation systems efficiency (Alvarez-Zaldívar et al., 2016; Antelmi et al., 2021; Clement et al., 2000; D'Affonseca et al., 2011; Pooley et al., 2009, 2009). Yet, cases of RTM applied to SBSs evaluation cannot been found in literature to date.

RTMs have the capability to combine physical and biochemical processes through coupled partial differential equations that reproduce most of the currently known processes occurring in polluted sites undergoing bioremediation (Steefel et al., 2015). They are able to simulate microbially-mediated geochemical reactions occurring during advective and dispersive solute transport in groundwater (Barajas-Rodriguez et al., 2019; Prommer et al., 2009; Schäfer and Kinzelbach, 1992; Scheibe et al., 2009). RTMs have also the potential to reproduce biodegradation via different pathways within the same system, making it feasible their application to bioremediation systems as complex as SBSs.

1.3 Motivation and thesis structure

The general objective of this thesis was to develop methodologies to determine bioremediation efficiency in SBSs, for which no modeling attempts have been reported in the literature so far. As a case study, we investigated an alluvial aquifer in Italy where the country largest SBS was installed to remediate to a chloroethene pollution (the site is described in the following section). The assessment was carried out by setting up a multidisciplinary approach entailing multiscale experimental activities and models of different complexity. The combined methods helped evaluate the importance of an accurate reproduction of the behavior of the pollutants in order to obtain an accurate assessment of the SBS efficiency and reliable predictions of the system's response to a modification in remediation design.

1.3.1 Study site

The polluted aquifer object of this study is located in Northern Italy and is displayed in Figure 1.1. The site is bounded to the south by a lagoon, and to the north by the agricultural land reclamation canal (ALRC) (Figure 1a), an artificial drainage system built specifically to allow agricultural activities on the land surface. The ALRC is connected to a pumping system that keeps the water level inside the canal at constant value of about -2 m above sea level (a.s.l.). Figure 1b provides a conceptual geological cross section of the study area (cross section A-A' in Figure 1a), which also shows the salient hydrogeological features of the site. Except for the top parts of the landfill, the whole area (including the contaminated aquifer) is located between 0 and -1 m a.s.l. (i.e., below the sea level). From a geological point of view, the subsurface is characterized by an alternation of sandy and silty clay horizons. The local lithological characteristics of the subsurface horizons can be summarized as follows.

- From the ground level down to about 1–3 m depth: silty clays and clayey silts.
- From 1–3 m down to about 9–12 m depth: silty fine sand and sandy silt with rare medium sand lenses (forming the "shallow aquifer")
- From 9–12 m down to about 20–22 m depth: dense alternation of clays, silts, and silty clays, intercalated with more or less silty sands ("intermediate aquifers").
- From 20–22 m down to about 34–36 m depth: dense alternation of silty clays and lenticular decimeter levels consisting of clayey silts and silts with fine sand components.
- From 34–36 m down to 50–51 m depth: alternation of sand and silt soils with sandy soils ("deep aquifers").

The hydraulic conductivity (K) of the sandy horizons constituting the main aquifers is close to $K = 10^{-4}$ m s^{-1}, based on the slug and pumping tests. The silt and clay horizons are aquitards/aquicludes with low to very low K ($< 10^{-7}$m s^{-1}). The low permeability layer capping the aquifer is locally absent, making the aquifer unconfined or semi-confined based on the spatial continuity of such layer. The

geological configuration is similar to that of other adjacent sites described by Beretta and Terrenghi, 2017; Carraro et al., 2015; Dalla Libera et al., 2020.

The shallow aquifer is more vulnerable to contamination originated from the ground surface than the intermediate and deep aquifers, which tend to be more confined and therefore better protected from contamination sources.

The piezometric level of the shallow aquifer is close to the ground surface. Groundwater flows from the lagoon to the mainland, crossing the landfill, as schematically depicted by the blue arrows in Figure 1a. The lagoon and rainfall events recharge the aquifer, which is drained by the ALRC. Groundwater head levels are affected by daily tide variations. The average hydraulic gradient (i) is close to i=0.1%, with minor variations throughout the year. All piezometers show a similar trend in groundwater head levels, with winter minima and summer maxima.

Groundwater in the shallow aquifer crossing the landfill is likely in direct contact with the landfill waste. Groundwater is therefore enriched in the solute-form byproducts linked to the landfill's leachate losses. Solutes are transported towards the ALRC, forming an extended plume of pollutants in the shallow aquifer, which is the target of the bioremediation system. The groundwater quality between the landfill and the canal is monitored through an extended network of boreholes screened in the shallow aquifer as well as through the P&T system.

The landfill responsible for the shallow aquifer contamination is an historical waste disposal site which was closed in the 1970s. The plume was first detected in 2001, when high concentrations of chlorinated aliphatic hydrocarbons (CAHs) and petroleum hydrocarbons (PHCs) were observed outside the landfill. These observations prompted several interventions, which included the installation of a pump-and-treat (P&T) system outside the landfill. The P&T consists of seven wells close to the landfill and seven wells along the ALRC (Figure 1a). The latter wells are still active nowadays. Pumped water is treated *ex situ* through a sequential combination of filtering and precipitation, air stripping and catalytic oxidation and activated carbon adsorption. Although the P&T system was useful for the hydraulic confinement of the site, it was not efficient for its cleanup. This is not uncommon, as P&T systems entail long remediation times as well as elevated operational and management costs (Casasso et al., 2019; EPA, 2001; Pedretti, 2020). New investigations started in 2005-2006 to prepare an overall plan for site clean-up by selecting the best intervention technology. This is when the idea of an ISB was conceived as a viable cost-effective alternative to the P&T, eventually leading to the experimental activities described in Chapter 2 and eventually to the implementation of the full-scale ISB system described in Chapter 3.

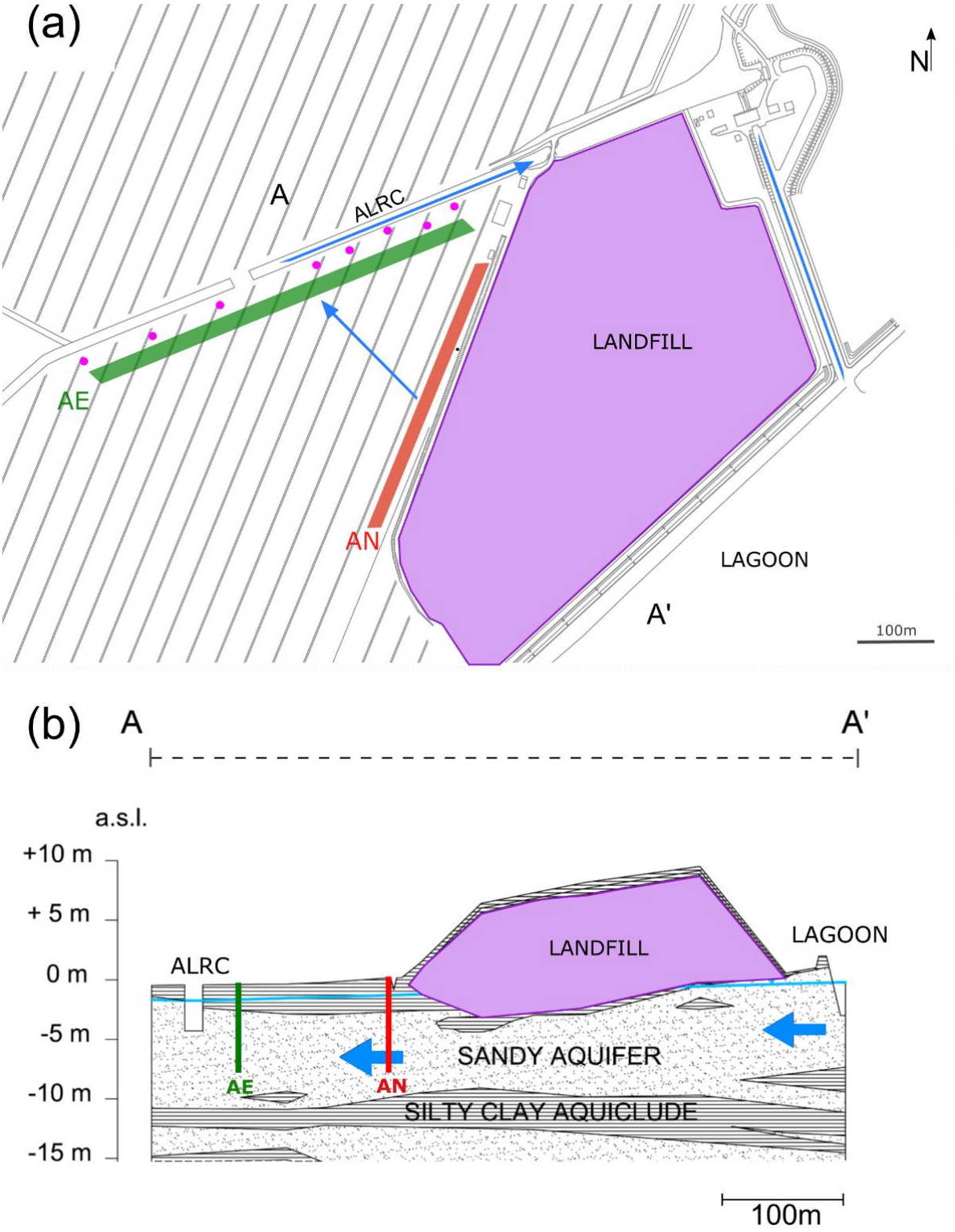

Figure 1.1. (a) Map of the study area, showing the landfill (lilac area) and the position of the ISB systems (AN—anaerobic barrier, AE—aerobic barrier) and the five boreholes utilized in the analysis. The wells of the P&T system are represented as purple dots. (b) Schematic geological cross-section of the study area (corresponding to the A–A' trace indicated in (a)), highlighting the top aquifer (first 10–12 m from the ground surface). The vertical axis represents the topographic elevation above sea level (a.s.l.). The blue arrows indicate the groundwater flow direction, which was oriented from the lagoon in the southeast to the agricultural land reclamation canal (ALRC) in the northwest.

1.3.2 Specific objective and thesis structure

The thesis was organized into three main chapters.

Chapter 2 introduces the site's history and the results from the multiscale characterization activities propaedeutic to the construction of the SBS are reported. These activities include microcosm experiments as well as pilot tests in the field.
The specific objective of this chapter is to provide a detailed description of the multi-scale experimental activities carried out for the design and successive implementation of a large-scale SBS in order to improve the current state of the art of SBS to facilitate its future implementations.
Chapter 2 is based on Casiraghi et al. (2022a), *Water Air Soil Pollut* 233 (425) (https://dx.doi.org/10.1007/s11270-022-05886-1).

In chapter 3 the full scale ISB system is introduced. The analysis of geochemical data collected in multiyear monitoring, as well as compound-specific isotopic data (CSIA) are reported. A conceptual model of the biodegradation processes taking place in the site is developed based on geochemical and microbiological evidence and is applied for the setup of a 1D geochemical model, which allowed the interpretation of CSIA data and a first assessment of the SBS efficiency.
The specific objective of this chapter was to improve the state of the art of SBSs assessment by providing an application of CSIA combined with geochemical modeling to the efficiency evaluation of a SBS. Chapter 3 is based on Casiraghi et al. (2022b), *Pollutants, 2 (4)* (https://doi.org/10.3390/pollutants2040031).

Chapter 4 presents the 2D RTM and its application for the evaluation of degradation efficiency on the whole site area as well as for the estimation of the total loading of chloroethenes exiting the remediation system and reaching the ALRC canal.
The specific objective of this chapter is to propose a general methodology that can be reproduced in other sites affected by chloroethenes contamination where a SBS (and possibly P&T) is implemented.
This last chapter is a draft of a manuscript to be submitted to Journal of Contaminant Hydrology.

The thesis general conclusion encompassing the whole study is reported in the last section "Conclusion", where possible future developments are also addressed. Each chapter is supported by Supplementary Material, that can be accessed at the online repository.

2 Piloting activities for the design of a large-scale biobarrier involving in situ sequential anaerobic-aerobic bioremediation of organochlorides and hydrocarbons

2.1 Introduction

The polluted aquifer object of this study is affected by a wide range of contaminants, among which petroleum hydrocarbons (PHCs) and chlorinated solvents. While PHCs are generally best degraded via aerobic biodegradation (Fritsche and Hofrichter, 2004) and only rarely via anaerobic pathways (Vogt et al., 2011), chlorinated aliphatic hydrocarbons (CAHs) can behave very differenlty. Dechlorination of highly chlorinated CAHs like tetrachloroethylene (PCE) or trichloroethylene (TCE) usually takes place more efficiently via organohalide respiration (OHR) under anaerobic conditions (Aulenta et al., 2006b). However, their less-chlorinated products (e.g. vinyl chloride (VC)) are generally recalcitrant under anaerobic conditions and more easily biodegraded via aerobic pathways. This was the reason that led to consider the setup of a sequential bioremediation system (SBS) targeting anaerobic and aerobic biodegradation sequentially in order to achieve complete mineralization of chlorinated pollutants (Frascari et al., 2015).

Although sequential ISB has already been proven to be efficient in the laboratory, examples of field applications are scarcely documented to date (Devlin and Parker, 1996; Tiehm and Schmidt, 2011). This could be ascribed to the higher demand in terms of both site characterization as well as costs of a SBS compared to single ISB system.

In this chapter, the multiscale experimental activities propaedeutic to the construction of the full SBS were reported and the data collected were analyzed. The objective is to improve the current state of the art in the design and implementation of large-scale SBS with the aid of multi-scale experimental activities. The methods presented in this chapter can serve as an example for future applications of ISB systems, both single and sequential.

The contents of this chapter has been published in Casiraghi et al. (2022a) and the work is complemented by Supplementary Material (SM2), deposited in the online repository.

2.2 Background information

2.2.1 Contaminant plume

Table 2.1 provides a summary of the aqueous concentration of selected compounds sampled in May 2013 (i.e. before the sequential bioremediation system was installed). The concentrations of aromatic hydrocarbons, such as BTEX or monochlorobenzene (MCB), and chlorinated aliphatic hydrocarbons (CAHs), such as PCE, TCE, dichloroethenes (1,1-DCE, *cis*-1,2-DCE, trans-1,2-DCE), VC

and chlorinated ethanes, as well as metals like As, Fe and Mn, largely exceed the Maximum Contaminant Level (MCL) set by the Italian law (Table 2.1).

Table 2.1. Minimum and maximum concentrations of major compounds and contaminants, observed in May 2013 and respective Maximum Contaminant Level (MCL) (In Italian, "Concentrazioni Soglia di Contaminazione", CSC) according to the Italian law (D.Lgs. 152/2006).

Compound	Acronym	Units	MCL / CSC	Min	Max
Sulfates		mg L^{-1}	250	640.00	1970.00
Nitrates		mg L^{-1}	-	0.05	1.85
Phosphates		mg L^{-1}	-	0.05	0.05
Ammonia		mg L^{-1}	-	4.63	19.26
Organic compounds					
Hydrocarbons (n-hexane)		µg L^{-1}	350	162.00	6680.00
Benzene		µg L^{-1}	1	6.20	280.00
Ethylbenzene		µg L^{-1}	50	8.30	43.00
Styrene		µg L^{-1}	25	0.05	0.98
Toluene		µg L^{-1}	15	10.20	73.00
pXylene		µg L^{-1}	10	3.10	19.00
Monochlorobenzene	MCB	µg L^{-1}	40	43.00	1140.00
1,2-Dichlorobenzene	1,2-DCB	µg L^{-1}	270	0.73	26.00
1,4-Dichlorobenzene	1,4-DCB	µg L^{-1}	0.5	0.78	27.00
1,2,4 -Trichlorobenzene	1,2,4-TCB	µg L^{-1}	190	0.05	0.34
1,2,4,5- Tetrachlorobenzene	1,2,4,5-TTCB	µg L^{-1}	1.8	0.01	0.14
Pentachlorobenzene		µg L^{-1}	5	0.02	0.05
Hexachlorobenzene		µg L^{-1}	0.01	0.05	0.05
Chlorometane	CM	µg L^{-1}	1.5	0.05	0.05
Trichlorometane	TCM	µg L^{-1}	0.15	1.85	120.00
Vinyl chloride	VC	µg L^{-1}	0.5	1340.00	77000.00
1,2-Dicloroethane	1,2-DCA	µg L^{-1}	3	176.00	19700.00
1,1-Dichloroethene	1,1-DCE	µg L^{-1}	0.05	48.00	30000.00
1,2-Dichloropropane	1,2-DCP	µg L^{-1}	0.15	0.30	7.30
1,1,2-Trichloroetano	1,1,2-DCA	µg L^{-1}	0.2	0.88	32000.00
Trichloroethene	TCE	µg L^{-1}	1.5	43.00	10400.00
1,2,3-Trichloropropane	1,2,3-TCP	µg L^{-1}	0.001	0.05	104.00
1,1,2,2-Tetrachloroetane	1,1,2,2-TeCA	µg L^{-1}	0.05	0.05	41.00
Tetrachloroethene	PCE	µg L^{-1}	1.1	1.19	1730.00
∑ carcinogenic CAHs		µg L^{-1}	n.d.	3172.35	163184.00
1,1-dichloroethane	1,1-DCA	µg L^{-1}	810	330.00	28000.00
1,2-dichloroethene	1,2-DCE	µg L^{-1}	60	237.00	19300.00
cis-1,2-Dichloroethene	*cis*-1,2-DCE	µg L^{-1}	-	145.00	13900.00
trans-1,2-Dichloroethene	t-1,2-DCE	µg L^{-1}	-	9.00	1500.00
Metals					
Arsenic		µg L^{-1}	10	640.00	1970.00
Iron		µg L^{-1}	200	0.05	1.85
Manganese		µg L^{-1}	50	0.05	0.05

2.2.2 Assessment of degradative microbial communities

A preliminary molecular analysis based on quantitative real time polymerase chain reaction (q-PCR) was conducted on a groundwater sample (2 L) obtained by mixing equal volumes of water from two piezometers. Such piezometers, now dismissed, were located in the proximity of the aerobic and anerobic pilot area. The purpose of the analysis was to prove the biodegradation potential of the site by providing a first-cut estimation of the indigenous bacterial population able to conduct OHR. Detailed information about the specifics related to the experimental analysis is provided as Supplementary Material (SM2).

The results showed that the total amount of bacteria was in the order of $3.5x10^5$ ($\pm 1.75x10^5$) 16S rRNA gene copies m L^{-1}. OHR bacteria *Dehalobacter restrictus* and *Dehalococcoides ethenogenes* were $3.13x10^0$ ($\pm 3.33x10^{-1}$) and $1.68x10^2$ ($\pm$ $8.07x10^1$) gene copies mL^{-1}, respectively. Genes for lower-chlorinated ethenes reductases *bvcA* and *vcrA* were identified, being $2.65x10^2$ ($\pm$ 5.38 10^1) and $7.18x10^2$ ($\pm$ $1.95x10^2$) gene copies m L^{-1}, respectively.

This data indicate that specific bacteria involved in the process of OHR are present at the site. Both *Dehalobacter restrictus* and *Dehalococcoides ethenogenes* are known to conduct OHR of CAHs. *Dehalobacter restrictus* is known to dechlorinate higher CAHs, such as PCE and TCE (Christof Holliger et al., 1998). *Dehalococcoides ethenogenes* can also transform lower CAHs, such as DCE and VC, to ethene (Christof Holliger et al., 1998). Although concentrations were clearly too low to sustain an efficient natural attenuation (Lendvay et al., 2003), the presence of specific bacteria involved in the process of OHR suggested the potential of the natural microbial community to sustain bioremediation of CAHs at the site, if properly stimulated.

2.3 Experimental activities

In this study we focused on two experimental activities that were carried out in the site. Firstly, microcosm experiments were performed to evaluate the biodegradation capabilities of the indigenous bacterial community under natural and biostimulated aerobic and anaerobic conditions. Secondly, the efficiency of coupled anaerobic and aerobic biodegradation in the field was evaluated by setting-up two 40-m-long pilot biobarriers (Figure 2.1a and c).

2.3.1 Microcosms

Microcosms were prepared to evaluate anaerobic and aerobic degradation in the presence of native microbial communities, able to perform OHR of CAHs and oxidation of PHCs. The addition of reducing substrates, oxygen and nutrients (phosphorus and nitrogen) was performed to assess the potential benefit of biostimulation on the above-mentioned microbial activities.

After stabilization of physical parameters, groundwater samples were withdrawn from three boreholes located in different parts of the plume, put into sterile glass bottles and kept refrigerated upon

arrival to the laboratory. Aquifer sediment samples were collected (at a depth of -4.5 m a.s.l.) after drilling procedure, by choosing the internal portion of the sediment core to avoid contamination.
Anaerobic microcosms were prepared under anaerobic glove box ($N_2/H_2/CO_2$, 85:10:5). Glass serum bottles (120 mL) were filled with 70 mL groundwater:sediment phase (50:50 [v/v]) and sealed with Teflon® coated septa. Where appropriate, reducing substrates (molasses, cheese whey and soy oil) were added to a final TOC of 180 mgC L^{-1}.
Aerobic microcosms were prepared with 70 mL of groundwater in glass serum bottles (120 mL) sealed with Teflon® coated septa. To prevent volatilization of organic compounds, water was transferred from sampling bottle to serum bottles by gas-tight peristaltic pump. Along with unamended microcosm, oxygen and oxygen and nutrients (phosphorus and nitrogen) amended microcosms were prepared.
Microcosms were incubated at RT for 9/14 months. Abiotic microcosms were also prepared for each condition. All the study was conducted on triplicate samples. Benzene, MCB, toluene and CAHs were analyzed by gas chromatography mass spectrometry (GC-MS) method at VITO laboratories (Boerateng, Belgium). Analyses were conducted on headspace gas, sampled by static headspace sampling method (APAT, 2003). A 5975B Gas Chromatograph-Mass Spectrometer (Agilent Technologies, Santa Clara, CA, USA) equipped with D3792 PoraBOND Q column (25m x 0.32 mm, 5.00 µm) (Agilent Technologies, Santa Clara, CA, USA) was used. Helium at 250°C was the carrier gas. Samples were injected manually with a split ratio of 3:1 and a split flow of 7.5 mL. Oven temperature conditions were 40°C for 2 minutes and then 10°C min^{-1} to 260° for 7 minutes. Arsenic was analyzed by the ICP-MS method on filtered (45 µm Millipore filters) water samples (Corsini et al., 2014). The determination of volatile fatty acids was carried out with GC-FID, after their extraction from groundwater samples with diethyl ether, as described in Vanbroekhoven et al., 2007.

2.3.2 Pilot biobarriers

Two pilot biobarriers were installed and monitored to evaluate *in situ* aerobic and anaerobic bioremediation processes. The anaerobic biobarrier was created in the proximity of the landfill, while the aerobic biobarrier was created hydraulically downgradient of the anaerobic site and in the proximity of the ALRC (Figure 2.1a). The layout of each biobarrier is shown in Figure 2.1c. The two biobarriers were installed along the same hypothesized groundwater flow path, such that the upgradient anaerobic barrier triggered anaerobic bioremediation, while the downgradient site targeted aerobic degradation. A key hypothesis was that the downstream aerobic barrier intercepts and degrades the plume of lower CAHs, forming as a consequence of the incomplete dechlorination of the higher CAHs occurring in the upstream anaerobic barrier. In the case of chloroethenes, the dechlorination of PCE and TCE occurs mainly via OHR under anaerobic conditions, producing DCE and VC, whose

degradation is favored under aerobic conditions. The sites of the two pilot biobarriers were therefore chosen such that:

- anaerobic conditions were enhanced close to the contamination source (the landfill) by injecting a reducing substrate, to promote the degradation of more chlorinated compounds;
- aerobic conditions were enhanced downgradient of the source and in the proximity of the ALRC, to promote the degradation of less-chlorinated compounds (mainly VC) produced by the activity of the anaerobic biobarrier.

The anaerobic biobarrier included four observation boreholes (labeled as “ANPM” in Figure 2.1c), two pumping wells for groundwater extraction (“EXTAN”) and three wells for reinjection of the extracted water (“INJAN”) amended with a reducing substrate to stimulate microbial activity in the aquifer. A total volume of 5.5 m^3 of substrate-dosed water was injected into the ground during the 475 testing days by continuous injection through wells INJAN1, INJAN2 and INJAN3, corresponding to a total injected COD of 3575 kg. To evaluate the effectiveness of the biostimulation process, two piezometers (ANPM1, ANPM2) were located upgradient of the injection-extraction wells and two piezometers (ANPM3, ANPM4) were located downgradient. The inter-axis between wells was about 10 m.

The aerobic barrier included four observation boreholes (labeled as “AEPM” in Figure 2.1c), four air sparging wells (“ASAE”) for oxygen injection, two extraction wells (“EXTAE”) for groundwater withdrawal and three injection wells (“INJAE”) for reinjection of water amended with nutrients (nitrogen and phosphorus-containing compounds). Specifically, each AS well injected at a rate of 1600 L h^{-1}, resulting in a total cumulative injected air volume of about 73000 m^3 and a total injected mass of oxygen of about 18800 kg. The total volume of recirculated water was about 1100 m^3, with an average flow rate of about 10 L h^{-1}. The total mass of injected nitrogen and phosphorus was about 93 kg and about 38 kg, respectively.

All boreholes were drilled using destructive core methods, except for ANPM1 and AEPM1, where continuous cores were obtained. The drillings reached the low-permeability layer at the bottom of the shallow aquifer at about 10 m depth. The well and piezometer cases were made of HDPE, respectively of 3” and 4” diameters.

The tests were conducted between June 2013 and September 2014. A first monitoring survey of the pilot sites was performed in May 2013 in order to assess the contamination prior to the start of biostimulation activities (Table 2.1). Subsequently, monitoring campaigns were carried out with an average frequency of 45 days to evaluate the effectiveness of the biodegradation processes. In each monitoring survey, concentrations of key contaminants, dissolved oxygen, oxidation-reduction potential (ORP), temperature, electrical conductivity and pH were measured. The well-known statistical Mann-Kendall test was used to verify the presence of trends in the concentration time series collected in the different experiments.

Ultimately, benzene-, chlorobenzene-, toluene-, VC-, and DCA-degrading bacteria active in the aerobic pilot test were determined through the “most probable number” (MPN) method. Samples collected from piezometers located inside and outside the aerobic biobarrier were analyzed and compared. Details about the underpinning methods are provided as Supplementary Information (SM2).

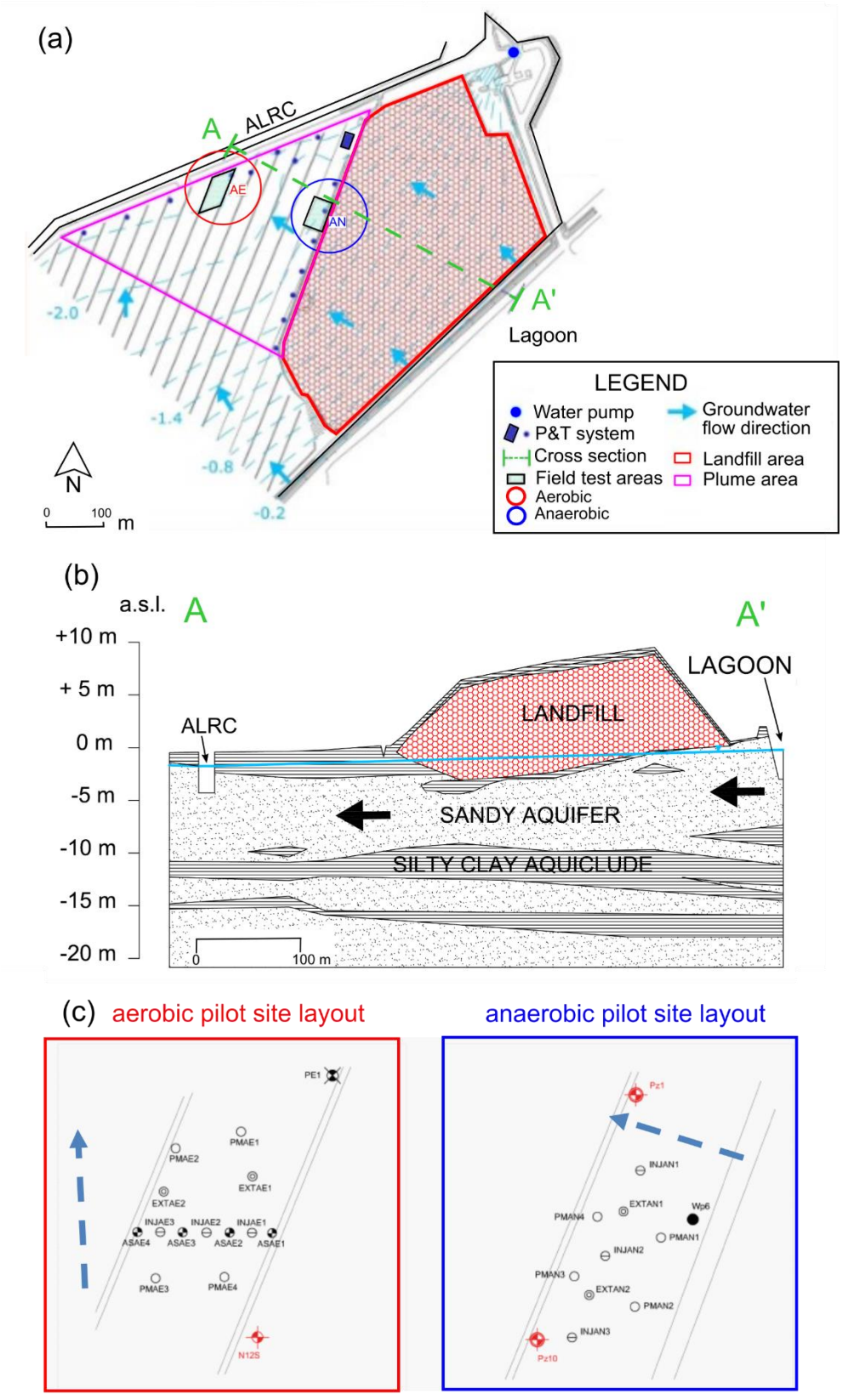

Figure 2.1. (a) Map of the landfill. (b) Schematic geological cross section (A-A') of the study area. The black arrows indicate the mean groundwater flow direction, which is oriented from south-east to north-west. (c) Lay-out of the pilot biobarriers for the aerobic (left) and anaerobic (right) biodegradation test. The blue arrow indicates the expected flow direction. PM: observation piezometers; INJ: injection wells; EXT: extraction wells; AS: air sparging wells. ALRC= agricultural land reclamation canal. Vertical axis represents the topographic elevation above the sea level (a.s.l.).

2.4 Results

2.4.1 Laboratory analysis

2.4.1.1 Anaerobic microcosm experiments

The anaerobic microcosms showed an overall efficient biodegradation of CAHs (Figure 2.2) under both natural and biostimulated conditions, although the addition of nutrients significantly enhanced biodegradation. In all microcosms, pH remained at circumneutral values after 4 and 9 months. The ORP (expressed as Eh) in the unamended microcosms was around -200 mV. Cheese whey amended microcosms reached the lower ORP (-350 mV), followed by the molasses and soy oil amended microcosms (-300 mV). In abiotic microcosms, ORP was around -35 mV. In unamended microcosms (which reflect the natural attenuation capability of the aquifer), high yields of TCE, *cis*-1,2-DCE, 1,1-DCE and 1,1,2-TCA biodegradation were reached after 9 months, although concentrations were still much higher than the MCL for each of these contaminants (several tens of µg L^{-1}). For 1,2-DCE the law limit is imposed for the sum of *cis*- and *trans*-1,2-DCE at 60 µg L^{-1}. Therefore, even if the concentration of *cis*-1,2-DCE after 9 months was equal to 20 µg L^{-1}, the concentrations of trans-1,2-DCE at 9 months (above 300 µg L-1) still exceeded the MCL.

Biostimulating the microcosms with the addition of nutrients increased the biodegradation rates up to five times compared to the natural degradation rates Figure 2.2 shows that biostimulation helped reaching an almost complete removal of most of the studied compounds (concentrations <5 µg L^{-1}) after 2 months. Instead, such results could only be reached after 10 or more months with natural attenuation.

Specifically, *trans*-1,2-DCE, 1,1-DCA and 1,2-DCA proved to be more recalcitrant. Scarce biodegradation was observed in unamended microcosms (meaning that natural attenuation in the site was not efficient), while the addition of substrates was able to enhance the degradation of *trans*-1,2-DCE and 1,2-DCA. While significant drops in concentrations were observed for these two compounds, they still remained in the order of several hundred µg L^{-1}. 1,1-DCA was not degraded at all, not even under biostimulated conditions. 1,1,2,2-TeCA concentrations could not be determined during the experiments due to analytical interferences. The addition of substrates produced a dramatic variation in VC response. In the amended microcosms, concentrations dropped from about 3000 µg L-1 to values under 5 µg L^{-1} within 4 months. In the unamended microcosms, an accumulation of VC took place, with concentrations eventually reaching >6000 µg L^{-1}.

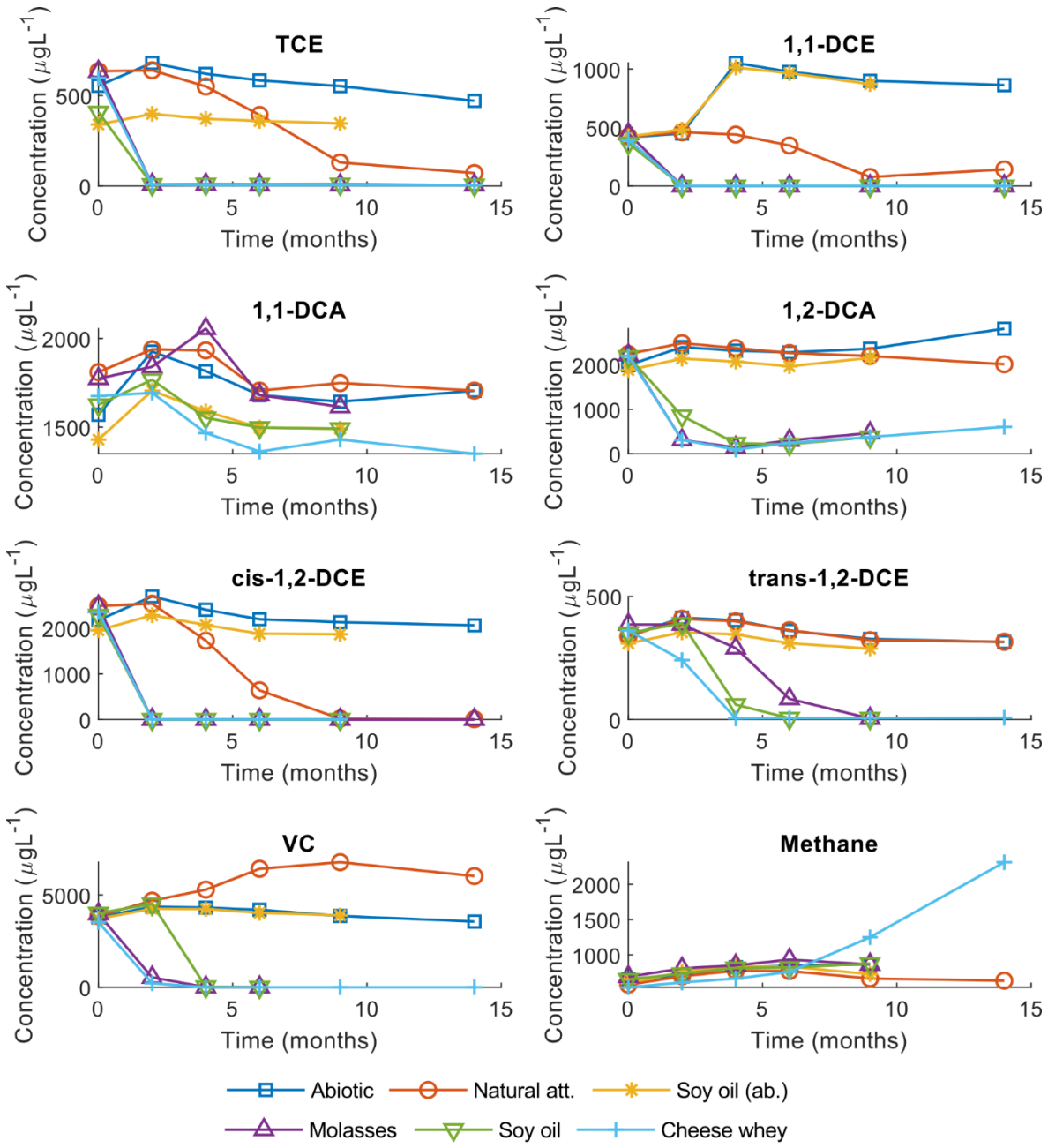

Figure 2.2. Main results from the anaerobic microcosms. “Natural attenuation” refers to unamended microcosms; “Abiotic and Soy oil (ab.)” are the control microcosms for unamended and amended microcosms, respectively; “molasses”, “soy oil” and “cheese way” refers to the amended microcosms. Incomplete time series are due to missing data not communicated by the laboratory performing the analyses.

The addition of substrates increased methane production. In microcosms amended with molasses and soy oil methane concentrations increased from about 650 µg L^{-1} to about 800 µg L^{-1}. In the microcosms with cheese whey addition, concentrations above 2000 µg L^{-1} were reached. No increase in arsenic was observed. An increase in volatile fatty acids, particularly acetic acid (CH_3CO_2H), was observed after four months in the microcosms with the addition of soy oil and cheese whey (from less than 0.5 mg L^{-1} to tens of mg L^{-1}). These acids are a product of organic substrates fermentation as well as byproducts of contaminants biodegradation. Moreover, they can be further fermented to produce hydrogen which is used in the OHR processes.

2.4.1.2 Aerobic microcosm experiments

The results of aerobic microcosm experiments are shown in Figure 3. VC was efficiently degraded with and without the addition of nutrients under aerobic conditions. However, the addition of nutrients sped up the reaction, leading to an almost complete removal of VC after only 28 weeks in the amended microcosms, compared to 41 weeks required in unamended microcosms. Similar benefits of nutrients were observed for the biodegradation of *cis*-1,2-DCE, although no complete removal of this compound was observed at the end of the experiments (concentrations of almost 1 mg L^{-1} were still observed after 41 weeks). The concentrations of other CAHs such as 1,1-DCA, 1,1-DCE, *trans*-1,2-DCE, TCE and PCE did not decrease significantly under aerobic conditions, not even in amended microcosms (data not reported). An accumulation of 1,2-DCA was observed, leading to an increase of concentrations with time. This effect resulted stronger with addiction of oxygen and nutrients. Aerobic conditions were able to reduce the concentration of benzene by 33% (i.e., from about 300 µg L^{-1} to about 200 µg L^{-1}) at week 28, with a rebound at week 41. The behavior of benzene was not affected by the addition of oxygen nor by the addition of oxygen and nutrients. Similar results were observed for MCB, whose concentrations were reduced by about 25% (i.e., from about 400 µg L^{-1} to about 300 µg L^{-1}) at week 28.

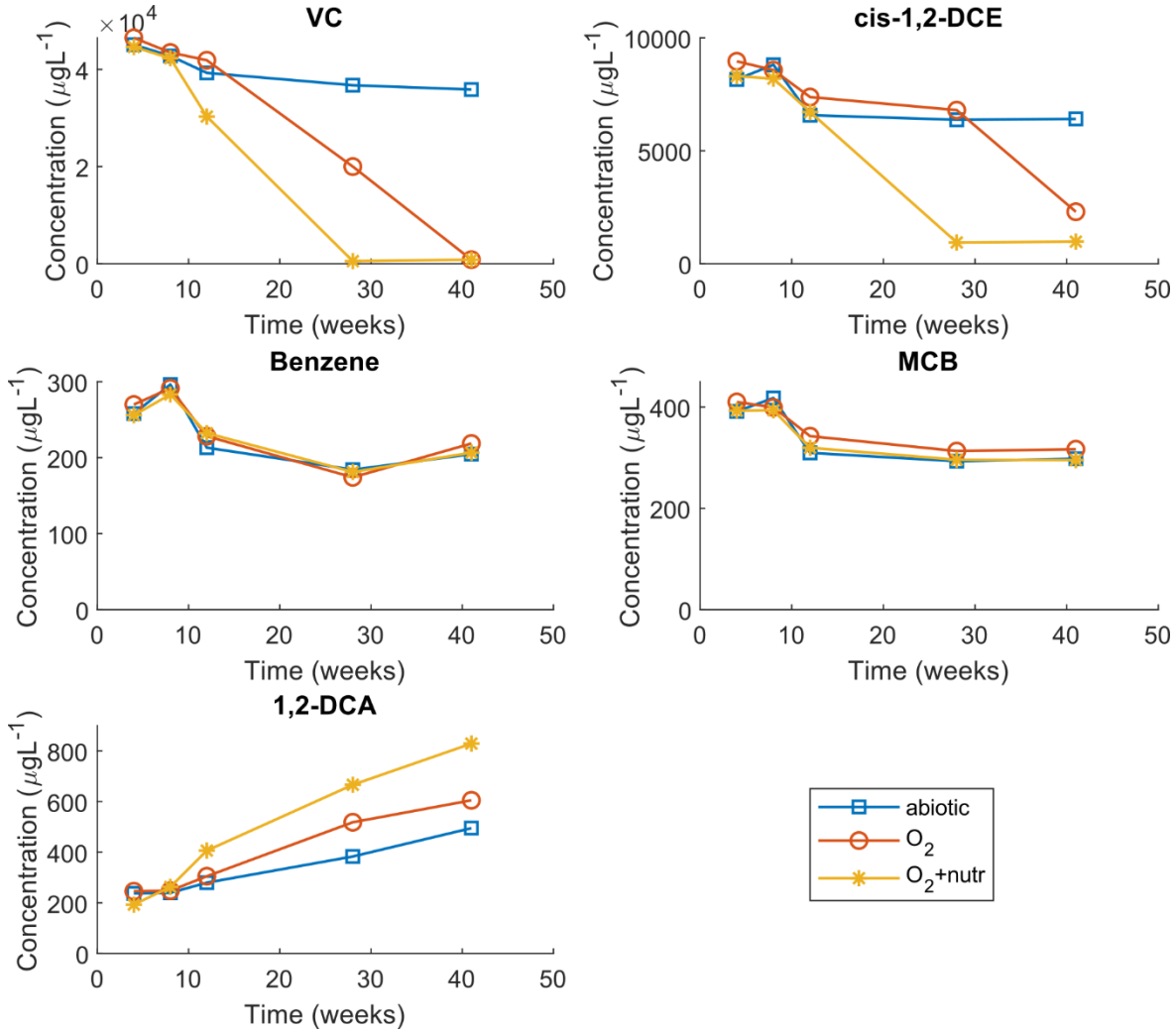

Figure 2.3. Main results of the aerobic microcosms. The control microcosms for unamended and amended microcosms are referred to as "abiotic"; "O_2" indicates the microcosm with only oxygen added; "O_2+nutr" refers to the microcosms amended with the addition of oxygen and nutrients.

2.4.2 Pilot biobarriers

2.4.2.1 Anaerobic biodegradation

The concentrations of PCE, its degradation products, TCA and 1,2-DCA at the anaerobic biobarrier are shown in Figure 2.4. During the experimental time, PCE concentrations at ANPM4 (one of the piezometers downgradient of the injection wells) decreased by nearly 100%, reaching values below the MCL. According to the Mann-Kendall test, ANPM3 (the second downgradient piezometer) showed a negative trend in concentrations too, which confirmed the degradation of this compound induced by the anaerobic pilot barrier, although with different degrees of efficiency. On the other hand, Mann-Kendall tests indicated that no statistically significant trend was observed for piezometers ANPM1 and ANPM2 located upstream of the injection wells, as expected, since they represent the concentrations entering the biobarrier. Similar trends were observed for TCE, 1,1-DCE and VC. For this last compound, a decrease in concentrations up to three orders of magnitude was observed

in the downstream piezometer ANPM4. Nonetheless, VC concentrations remained much above the MCL. For TCA and 1,1-DCA, the Mann-Kendall test showed no statistical significance for the two upgradient piezometers, while the opposite was found for the two piezometers downgradient of the wells, which showed a progressive decrease in concentrations with time. For TCA, concentrations dropped by about 96.8% between the beginning and the end of the experiments. For 1-1-DCA the drop was close to 97.8%. For benzene and MCB, no statistically valid trends were detected in the upgradient piezometers and in the downgradient piezometer ANPM3. At ANPM4, negative trends for both compounds were instead observed.

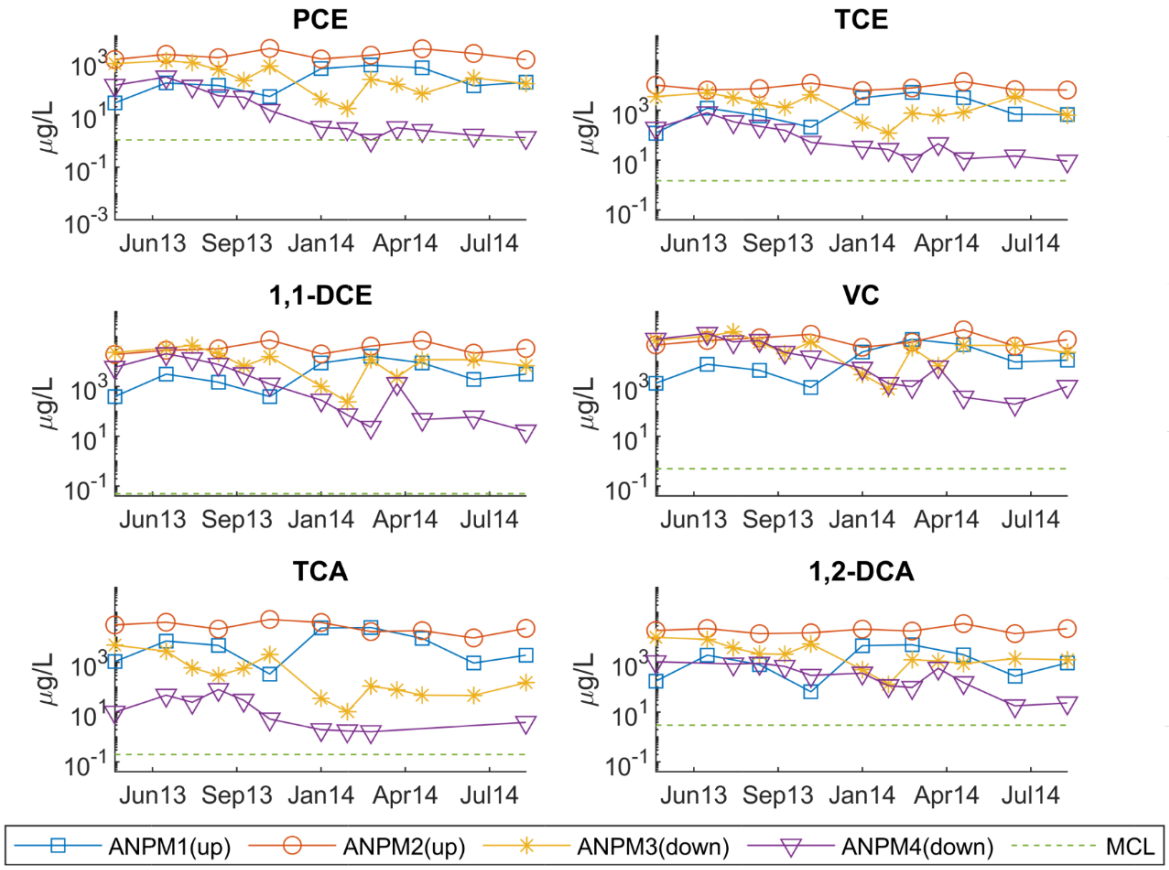

Figure 2.4. Variation of concentrations of PCE, TCE, 1,1-DCE, VC, TCA and 1,2-DCA during the anaerobic pilot test.

The variation of environmental parameters, concentrations of major ions and dissolved oxygen at the up- and downgradient piezometers (Figure 2.5) was consistent with the degradation of CAHs. The oxidizing-reduction potential (ORP), expressed in terms of Eh, dropped from near-zero values (i.e., a system close to oxidizing conditions) to much more negative values, suggesting that reducing conditions were established in the aquifer within the anaerobic pilot area. The more pronounced change in ORP at ANPM4 (up to -300mV) agrees well with larger reduction in concentrations (i.e., more efficient degradation) of CAHs at this piezometer compared to the other piezometers (Figure

2.4). Total iron concentrations were also observed to progressively decrease with time, particularly at ANPM4.

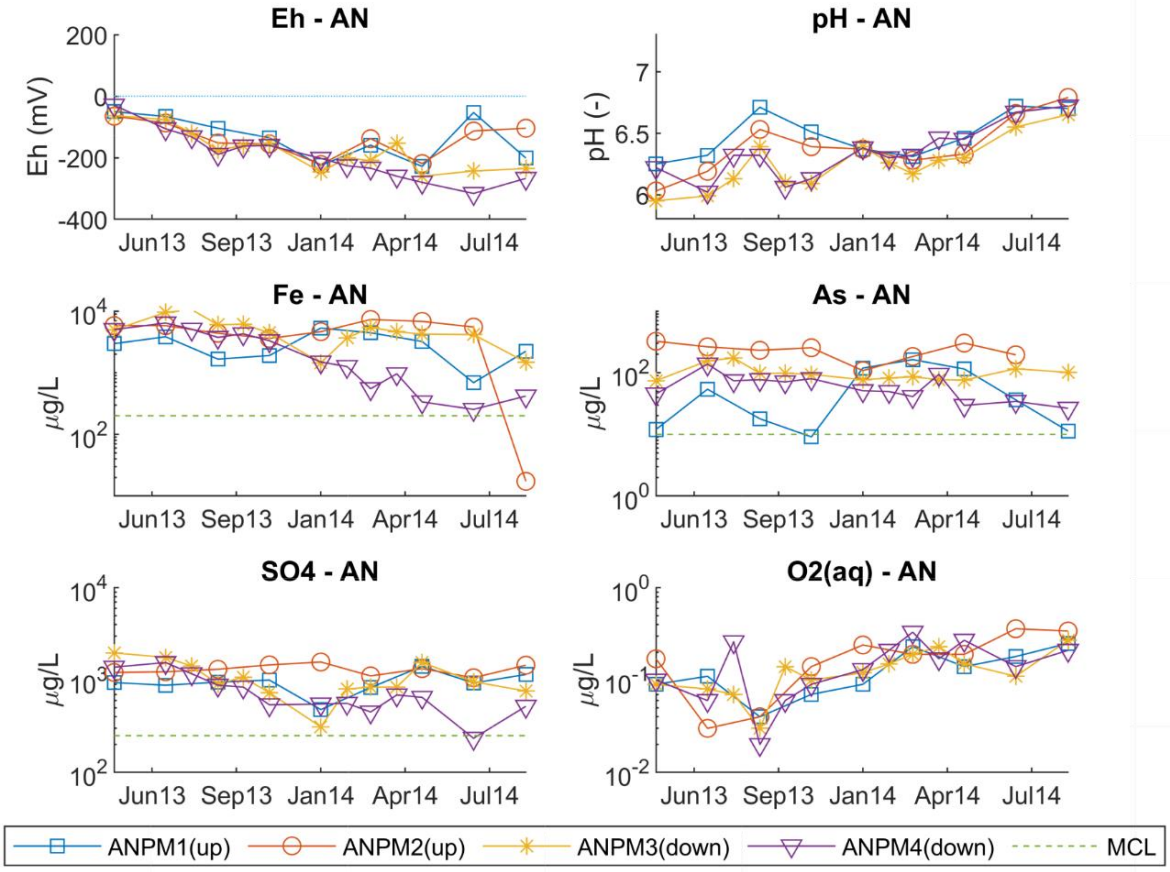

Figure 2.5. Comparison between Eh, pH, total iron (Fe), arsenic (As), sulfate (SO_4) and dissolved oxygen ($O_{2(aq)}$) concentrations measured at upgradient (up) and downgradient (down) piezometers of the anaerobic pilot site.

2.4.2.2 Aerobic biodegradation

The data collected during the pilot test demonstrated that aerobic conditions could provide great reductions of BTEX, MCB and VC concentrations, as well as other monitored contaminants (Figure 2.6). In certain piezometers, the overall reduction of compounds such as benzene, *p*-xylene, MCB and VC was >99%. The reduction led to concentrations well below the MCL. For VC, *in situ* observations at AEPM4 were consistent with the results obtained in the aerobic microcosms (Figure 2.3), while for benzene and MCB *in situ* biodegradation was more effective. The maximum decrease in concentrations was found at AEPM4, one of the two piezometers located upgradient of the injection zone. Of the two piezometers located downgradient of the injection zone, only AEPM2 provided a reduction in concentrations with time. The other piezometers, AEPM1 and AEPM3, did not provide a significant decrease in concentrations with time, as corroborated by the Mann- Kendall test.

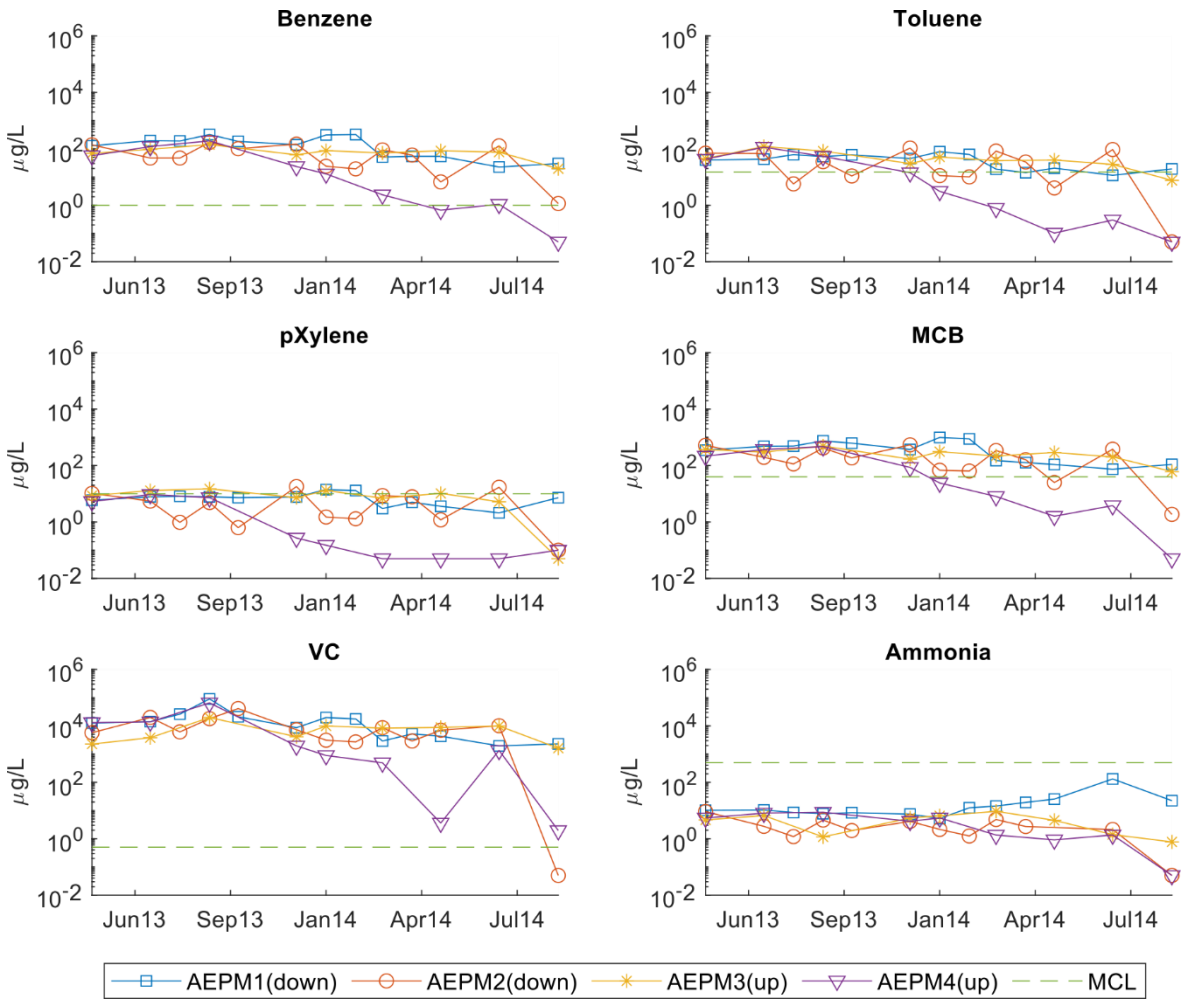

Figure 2.6. Variation of concentrations of benzene, toluene, pXylene, MCB, VC and ammonia during the aerobic pilot test.

At AEPM4, a substantial reduction in the concentrations of metal(loid)s (As, Fe, and Mn) was also reported during the test (Figure 2.7), compared to the initial concentrations before aerobic conditions were established in the pilot area. A steady decrease of As and Fe concentrations was observed until values under the MCL were reached. Similar trends were detected in the early stages of the test performed at AEPM2, although a concentration rebound was observed by the end of the experiment. Concentrations above the MCL were instead maintained in piezometers AEPM1 and AEPM3. At AEPM3 (upgradient of the aerobic pilot site), toluene- and chlorobenzene-degrading bacteria were present in the order of 10^2 most probable number (MPN) g^{-1} soil dry weight (d.w.), whereas benzene-, VC, 1,2-DCA and 1,1-DCA-degrading bacteria were one order lower. At EXTAE2 (downstream of the injection piezometers), the MPN of degrading bacteria increased by one order of magnitude in the presence of all the tested compounds, and by two orders in the presence of toluene. These results indicate that the natural aquifer bacterial community hosts active degrading bacteria which were stimulated by the aerobic treatment.

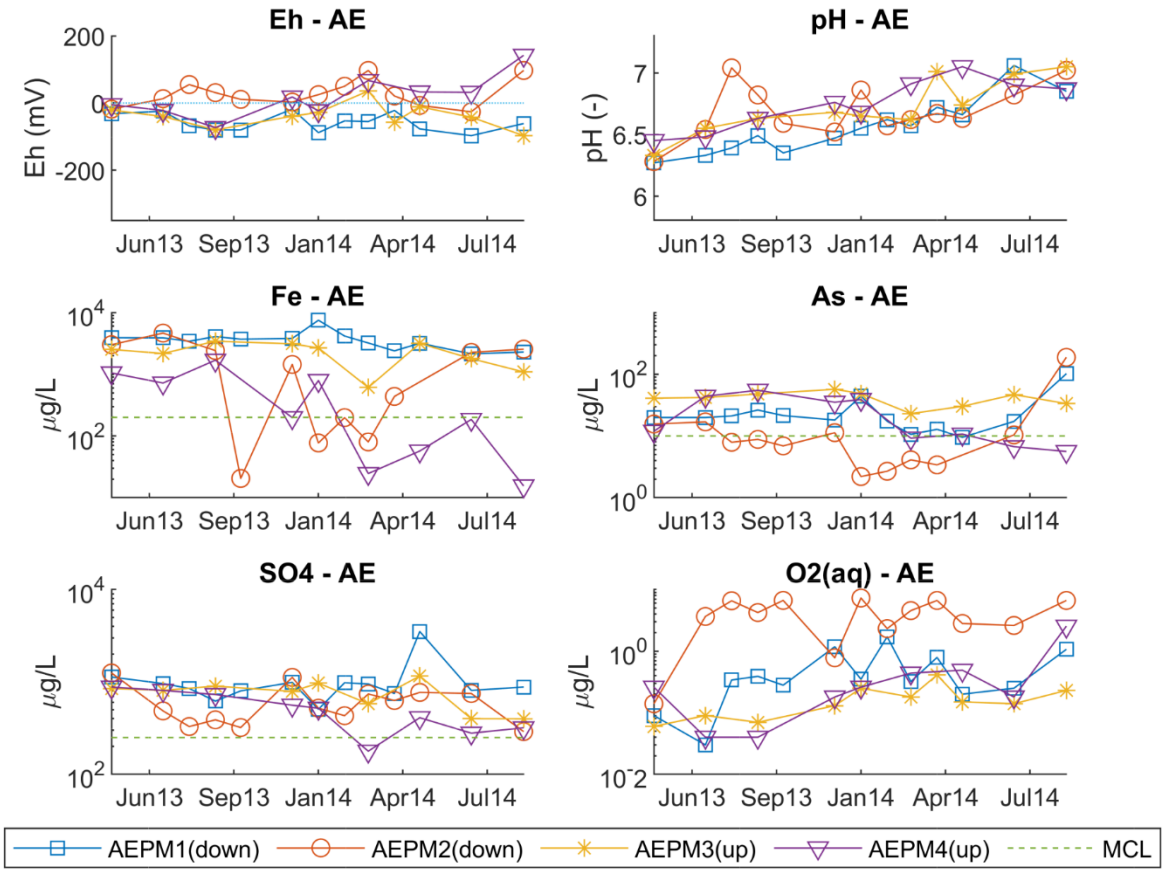

Figure 2.7. Variation of Eh, pH, dissolved oxygen (O2(aq)) and iron (Fe), arsenic (As), sulfate (SO4) concentrations measured at upgradient (up) and downgradient (down) piezometers of the aerobic pilot site.

2.5 Analysis and discussion

2.5.1 Laboratory tests

The analysis of results from unamended anaerobic microcosms confirmed the molecular survey data regarding the poor effectiveness of natural attenuation at the site. TCE, *cis*-1,2-DCE, 1,1-DCE and 1,1,2-TCA were slowly transformed, while the ability of bacteria to dechlorinate *trans*-1,2-DCE, VC, 1,1-DCA and MCB without biostimulation proved to be poor or non-existent. This is a common drawback pointed out in several works at all scales - microcosm and *in situ* (Fennell et al., 2001). This behavior might be associated with the lack of sufficient number of microorganisms in water samples or to the competition of microorganisms for electron donors. The addition of reducing substrates led to a more efficient and faster dechlorination of all CAHs, consistently with observations from other sites (Courbet et al., 2011a; Lendvay et al., 2003). The only exceptions were 1,1-DCA and MCB, which is also in accordance with previous reports (Matteucci et al., 2015b).

Aerobic conditions contributed to the degradation of *cis*-1,2-DCE, 1,1-DCE and VC, which were produced by dechlorination of chloroethenes PCE and TCE. Aerobic conditions were therefore needed to avoid the stall of less-chlorinated compounds in the site. Aerobic conditions were also able to degrade contaminants that were not efficiently transformed under anaerobic conditions, such as

benzene. On the contrary, 1,1-DCA degradation remained limited even under aerobic conditions. As observed in other studies (Kao et al., 2003), oxygen supply was useful to sustain aerobic degradation of contaminants, while the addition of nutrients helped speed up the process.

2.5.2 Pilot biobarriers

At the anaerobic biobarrier, monitored concentrations of CAHs (Figure 2.4) were generally higher in each upgradient piezometer (ANPM1 and ANPM2) compared to the respective downgradient piezometer (ANPM4 and ANPM3, respectively). The gap between upgradient and downgradient concentrations for each contaminant became increasingly larger with time. Lack of statistically significant (negative or positive) trends in PCE, TCE, 1,1-DCE, *cis*- and *trans*-1,2-DCE and VC concentrations with time was also observed in piezometers ANPM1 and ANPM2 (upgradient of the injection wells). The discrepancies between up- and downgradient piezometers can be explained considering that the soil surrounding the upstream piezometers did not receive the hydrogen-releasing substrate that promotes microbial activity. This agrees well with the hypothesis that the compounds dissolved in groundwater upgradient of the injection wells were less prone to undergo biodegradation than the compounds found downgradient of the wells.

The decrease of PCE and TCE concentrations to values near the MCL (1.1 µg L^{-1} and 1.5 µg L^{-1}, respectively) in the piezometers downgradient of the injection wells (ANPM3 and ANPM4) proved the degradation efficiency of the ISB with respect to the higher chlorinated ethenes. The accumulation of DCE and VC, instead, was consistent with the fact that anaerobic conditions were not as favorable for less chlorinated ethenes dechlorination. This further demonstrated the need to create a sequential anaerobic/aerobic ISB system to remove both high- and less-chlorinated compounds.

2.5.3 Role of redox changes

The injection of water dosed with reducing substrate in the anaerobic pilot site generated a drop in Eh values, which were critical to interpret the variation in observed concentrations.

For instance, the more pronounced drop in concentrations of CAHs at ANPM4 (Figure 2.4) can be explained considering the larger drop in Eh (i.e., more reducing conditions) at this piezometer compared to the others (Figure 2.5). Reducing conditions are achieved via fermentation of the organic substrate carried out by microorganisms, which leads to hydrogen and small organic acids production. Hydrogen acts as an electron donor in anaerobic microbial activities that first consume oxygen dissolved in groundwaters. After depletion of dissolved oxygen, anaerobic microbes use nitrate as a terminal electron acceptor, followed by manganese (IV), iron (III), sulfate, and finally carbon dioxide (methanogenesis) leading to more and more reducing conditions in the aquifer.

The strong decrease of sulfate concentrations may indicate that sulfate reducing conditions have been reached, suggesting that anaerobic dechlorination can take place efficiently. The reduction of sulfates is coupled to a decrease in iron concentrations in groundwater, possibly as the result of (chemical or microbiological mediated) precipitation of iron sulfides, which is a common occurrence

during *in situ* anaerobic bioremediation of chlorinated hydrocarbons (such as enhanced OHR) due to availability of both free sulfide and Fe^{2+} (He et al., 2015; Hyun and Hayes, 2009). The occurrence of this process is also supported by another fact: if the free sulfides produced by sulfate reduction were not removed from groundwater, they would inhibit biotic OHR, which is instead an ongoing process.

In particular, sulfate reduction operated by sulfate reducing bacteria increases pH (Luptakova et al., 2013; Mukwevho et al., 2019), giving a possible explanation for the positive trend observed for pH values. At the same time, iron sulfides may also cause abiotic dechlorination of CAHs, contributing to the overall degradation taking place *in situ* (e.g., Jeong and Hayes, 2007; Tobiszewski and Namieśnik, 2012; He *et al.*, 2015).

No trends for As concentrations were statistically detected. However, under reducing conditions, As precipitation during microbial sulfate reduction appears to be important in determining its mobilization or immobilization (Kirk et al., 2004). Sulfides produced by sulfate reduction can form minerals that remove As from solution (Moore et al., 1988; Rittle et al., 1995). These include pure As sulfides (e.g., orpiment and realgar) (Burton *et al.*, 2014) or Fe(II) sulfides (e.g., troilite and pyrite) (Bostick et al., 2003; Bostick and Fendorf, 2003). The As removal capability of Fe(II) sulfides is directly linked to the mineral types (Burton et al., 2014; O'Day et al., 2004) and the interactions between As and those kinds of sulfide minerals that potentially form in aquifers as well as mechanisms responsible for *in situ* As immobilization have yet to be understood (Kirk et al., 2010; Pi et al., 2017).

2.5.4 Anaerobic degradation of benzene and MCB

The efficiency of anaerobic degradation for benzene and MCB was surprising, although not completely unexpected. Anaerobic biodegradation of benzene and other aromatic hydrocarbons has been reported under nitrate-, iron-, manganese-, sulfate-reducing and methanogenic conditions. Comprehensive reviews on this topic are provided by, e.g., Foght (2008) and Haritash and Kaushik (2009). *In situ* anaerobic degradation has also been observed for chlorobenzenes (e.g. MCB), which can be achieved via OHR under both methanogenic and sulfate-reducing conditions (Liang et al., 2011). Although the transformation of MCB to benzene in a methanogenic enrichment culture on river sediments has been documented in the past (Nowak et al., 1996), PHCs degradation is normally better achieved under aerobic conditions.

2.5.5 Aerobic biodegradation

As for the degradation of aromatic hydrocarbons as well as VC, the results suggested that an aerobic biobarrier was needed downstream of the anaerobic one (Figure 2.6). A general reduction in contaminant concentrations was observed mainly at one piezometer upgradient of the pilot barrier (AEPM4) and at one piezometer downgradient of the barrier (AEPM2). This may suggest that the flow field in the aerobic area is not directed as expected. This could be explained by the presence of soil heterogeneities, possibly combined with the intense pumping activity of air and water injection

wells, which creates local increase in groundwater levels that could cause diverging radial flow conditions. A reduction in K due to biomass growth or generation of biogenic gases may also potentially lead to preferential flow of groundwater in the subsurface.

The simultaneous decrease in VC, PHCs and ammonia concentrations (in particular at piezometers AEPM4 and AEPM2 -Figure 2.6) suggested that co-metabolic aerobic oxidation by hydrocarbon-oxidizing bacteria is ongoing. These bacteria use dioxygenase or monooxygenase enzymes to initiate the biodegradation process of growth substrates ("auxiliary substrates"), such as ammonium and aromatic pollutants (Dolinová et al., 2017b; Frascari et al., 2015; Tiehm and Schmidt, 2011), which are present in high concentrations in the site. As oxygenases have a very broad substrate range, they could fortuitously oxidize chloroethenes, yielding unstable chlorinated epoxides that subsequently break down spontaneously. Co-metabolic degradation has been shown for all chloroethenes but it is more efficient for the less chlorinated (i.e. less oxidized) ones (e.g., Mattes *et al.*, 2010). Moreover, aerobic metabolic oxidation of VC might also take place at the site in microaerophilic (*i.e.,* oxygen 0.5-1.8 mg L^{-1}) conditions (Singh et al., 2004) by VC/ethenetrophic bacteria (Liu et al., 2017). The substantial reduction of the concentrations of metal(loid)s (As, Fe, and Mn) at the aerobic barrier, previously present in groundwater under anaerobic conditions, was an expected result of the injection of oxygen. The injection of oxidants is a well-known method for *in situ* treatment of metal-contaminated groundwaters. The oxidation of iron and manganese triggers the precipitation of Fe(III)-(hydr)oxides and Mn(IV)-oxides and arsenic can be removed from solution both by surface adsorption and coprecipitation with these minerals.

2.5.6 Scaling effects in bioremediation rates

The comparison between laboratory and pilot-scale experiments suggests that bioremediation was generally slower in the field than in the laboratory. For instance, in Figure 2.4 we noted that after the injection of the reducing substrate, about four months were needed for the bioremediation to take place in the pilot test site. In comparison, we observed a much quicker activation within the microcosms under equivalent anaerobic conditions. Such "scaling effects" in bioremediation agree well with previously documented experience from other sites (e.g. Sturman *et al.*, 1995). Hydrogeological and biochemical heterogeneities are likely the strongest controls of scaling effects, affecting subsurface flow and transport and biochemical reactions in many ways.

Physical heterogeneities, associated to the variation of hydraulic parameters such as K, control the transport rate and consequently the pore-scale residence time of groundwater. Small variations in K can lead to preferential paths and solute transport channeling (e.g. Bianchi and Pedretti, 2017), a situation which is severely exacerbated in the proximity of pumping wells (D. Pedretti et al., 2013; Pedretti, 2020), where flow and transport tend to be stratified. Transport channeling determines a variation in the pore water residence time. When biostimulation is performed by pumping liquid solutions into the aquifer wells, the resulting distribution of such reactive liquids in a heterogeneous

aquifer could result in a non-homogeneous distribution of reactants. In turn, this could lead to a non-homogeneous biodegradation in the site and the formation of apparent scale effects of biochemical reactions. Microcosms experiments are instead performed in more homogeneous closed systems, at stable temperature and with an even distribution of biostimulating compounds in the porewater. Microcosms are also often performed for very long residence times (e.g. Aulenta *et al.* 2006).
Even though little information was available to quantify physical heterogeneity in the study area, Dalla Libera *et al.* (2020, 2021) reported strong textural and compositional variations at a relatively small (i.e. metric) scale in a site located only few km away from the one investigated in this study. Hence, such spatial variations may indeed be occurring in our study area. From a biochemical perspective, investigations are ongoing to disentangle the spatial variability of natural substrate and the distribution and types of microbiological communities.

2.5.7 Limitation of the study and future developments

The multi-scale activities described in this work were fundamental to obtain the environmental permits for the construction of the full-scale ISB system. Such a system was set up a few years after the end of these experiments (i.e., after 2014) and is currently being monitored. Critical aspects currently being evaluated involve “secondary contamination”, created by toxic intermediates of sequential bioremediation chains (e.g., VC accumulation) and compound-specific isotope analysis, which is expected to provide a better assessment of biodegradation of chloroethenes and give further information on the efficiency of the ISB system. These results will be presented in chapter 3.
We also foresee the setup of a model for the interpretation of combined multiscale observations and evaluate the effectiveness of the full-scale ISB system (see chapter 4). Models are fundamental tools that can assist decision makers in predicting the behavior of a bioremediation system integrating evolving scales (Sturman et al., 1995). Models have also proven scaling-up ability, which can be useful to resolve the apparent scale dependency of parameters (e.g., kinetic rates) estimated from multiscale tests. We believe that a sound model-based analysis could be highly beneficial to break down the several non-technical barriers limiting the development of a full-scale bioremediation facility. In countries such as Italy, regulatory acceptance of *in situ* remediation techniques remains complicated. For instance, administrations remain skeptical, if not reluctant, towards the (re)injection of water and nutrients into polluted aquifers. Therefore, we expect that properly developed models based on solid experimental results could contribute to increase the acceptance of ISBs by administrations.

2.6 Summary and conclusion

This work analyzed the results from a combination of multi-scale analyses that were propaedeutic for the creation of Italy’s largest *in situ* sequential bioremediation (ISB) system. Monitored experiments including microcosms and *in situ* pilot scale biobarriers suggested that natural biodegradation

and a single anaerobic biobarrier were insufficient solutions to fully degrade CAHs and PHCs. Sequential anaerobic-aerobic bioremediation barriers and biostimulation increased the effectiveness of the bioremediation products, as key contaminants achieved concentrations below the Maximum Contaminant Level (MCL) set by the Italian law. This included the less-chlorinated products (e.g., VC) forming from the degradation of highly chlorinated compounds (e.g., PCE). Specific conclusions achieved from this study are presented as follows.

In the microcosms:

- Natural attenuation was observed as an effective degradation method only for certain compounds, such as chloroethenes degradation under anaerobic conditions. This is consistent with initial microbiological molecular surveys that detected the onsite presence of the OHR bacteria *Dehalobacter restrictus* and *Dehalococcoides ethenogenes*. In unamended microcosms, significant biodegradation of TCE, *cis*-1,2-DCE and 1,1-DCE was achieved after 9 months, although concentrations remained much higher (several tens of µg L^{-1}) than the MCL. Moreover, an accumulation of the more toxic daughter product VC (up to 7000 µg L^{-1}) was observed.
- Biostimulation in the microcosms had a strong control on degradation kinetics. In the amended anaerobic microcosms, TCE, 1,1-DCE and *cis*-1,2-DCE concentrations dropped from several hundreds or thousands of µg L^{-1} to values under 5 µg L^{-1} within 2 months, i.e., at a much faster rate than in the unamended microcosms. Biostimulation was effective also on VC, as its concentrations were reduced from 4000 µg L^{-1} to less than 5 µg L^{-1} in only 4 months.
- Aerobic microcosms showed a decrease of hydrocarbon concentrations regardless of the addition of nutrients. As for CAHs, the most important result was achieved for VC, which was efficiently degraded within 7 months with the addition of nutrients (concentrations dropped from almost 40’000 µg L^{-1} to about 10 µg L^{-1}). Noteworthy results were also achieved for *cis*-1,2-DCE, whose concentrations dropped from more than 8000 µg L^{-1} to less than 1000 µg L^{-1} in 7 months with the addition of nutrients.

In the pilot biobarriers:

- The anaerobic tests showed consistent results compared to the anaerobic microcosms. An efficient degradation was observed for chloroethenes. PCE concentrations were reduced almost by 100%, reaching values below the Italian MCL. A significant reduction of TCE, 1,1-DCE and VC concentrations was observed, although concentrations never dropped below the corresponding MCLs. In particular, VC concentrations decreased from about 132000 µg L^{-1} to about 190 µg L^{-1}, i.e., up to three orders of magnitude.
- The aerobic pilot test demonstrated the efficiency of *in situ* aerobic degradation of PHCs. Remarkably, VC concentrations were reduced from about 65000 µg L^{-1} to about 2 µg L^{-1}. The aerobic barrier also helped degrading benzene and MCB; in certain piezometers, concentrations of these compounds were reduced from about 200 µg L^{-1} and about 500 µg L^{-1},

respectively, to < 1 µg L^{-1}. In-situ biodegradation of benzene and MCB was more effective than in the microcosms.

3 Assessing a Large-Scale Sequential In Situ Chloroethene Bioremediation System Using Compound-Specific Isotope Analysis (CSIA) and Geochemical Modeling

3.1 Introduction

The laboratory and field studies reported in Chapter 2 proved the feasibility of sequential anaerobic-aerobic bioremediation in the site which led to the construction of the full-scale (almost 800m long in total) sequential bioremediation system (SBS).

Despite having been idealized several years ago, only a few documented operational-scale SBSs have been presented so far (Tiehm and Schmidt, 2011). From a hydrogeological perspective, this may be partly linked to two reasons.

Lack of model-based analyses of SBSs. Mathematical models are particularly important to provide quantitative support for decision makers (Antelmi et al., 2021; Casasso et al., 2020; Ciampi et al., 2019; Van Breukelen et al., 2017; Varisco et al., 2021; Zheng and Bennett, 2002). As the usefulness of mathematical tools was already demonstrated for single ISBs (Barajas-Rodriguez et al., 2019; Liu et al., 2021; Van Breukelen et al., 2017, 2005), we maintain that such models could also be fundamental for the correct design and implementation of SBSs. While coupled biogeochemical and hydrogeological modeling was traditionally computationally prohibitive, we highlight that modern workstations have considerably alleviated the computational burden and multiple open-source codes are now available (Steefel et al., 2015) to efficiently reproduce the main processes involved in an ISB system. Moreover, in most bioremediation studies, one-dimensional (1D) reactive transport models (RTMs) are utilized, i.e., solute transport models that couple 1D flow dynamics and geochemical processes (Steefel et al., 2015). Such models are useful to identify geochemical processes that occur along individual flow paths (Appelo and Postma 2004), limiting the computational demand compared with more challenging multidimensional models.

Lack of studies applying compound-specific isotope analysis (CSIA) to SBSs. In the presence of organic compounds like tetrachloroethene that undergo parent–daughter reaction chains, transformation reactions produce an enrichment of heavy isotopes in the parent compound and the formation of isotopically lighter products (Pooley et al., 2009). The combined use of compound-specific carbon isotope analysis (C-CSIA) and concentration data can provide a more complete and precise evaluation of the biodegradation processes occurring at a site than the analysis of concentration data alone (Van Breukelen et al. 2005; Courbet et al. 2011a). Therefore, the use of CSIA could be highly valuable for the evaluation of SBSs. For instance, it could help to detect the occurrence of anaerobic or aerobic degradation; evaluate potentially interfering mechanisms, such as the mixing of waters undergoing different degradation pathways; or provide constraints for the development of mathematical models (Van Breukelen et al., 2005).

In this chapter the results of multiyear monitoring of the SBS introduced in Chapter 1 and 2 are reported and analyzed. The aim of the following work was to improve the current state-of-the-art regarding the use of advanced characterization and modeling tools, mainly through the evaluation of concentration time series, CSIA data and RTM to gain insight into the effectiveness of the SBS, identifying processes and quantifying reaction rates occurring at the site.

The contents of this chapter has been published in Casiraghi et al. (2022b) and the work is complemented by supplementary material (SM3), deposited in the online repository.

3.2 Materials and Methods

3.2.1 Background information

The first characterization and monitoring that led to the installation of the ISB started in 2014 when microbiological laboratory analyses and in situ biodegradation tests were carried out. These investigations are described in detail in Chapter 2 (Casiraghi et al., n.d.) and unpublished reports, from which we extracted the following key information.

1. Initial microbiological molecular surveys detected the presence of organohalide-respiring bacteria *Dehalobacter restrictus* and *Dehalococcoides ethenogenes* on site, demonstrating the potential of the site to sustain RD of chloroethenes. *Dehalobacter restrictus* is known to dechlorinate highly chlorinated compounds, such as PCE and TCE (Christof Holliger et al., 1998). *Dehalococcoides ethenogenes* can also transform less chlorinated compounds, such as DCE and VC to ethene (Christof Holliger et al., 1998).
2. However, anaerobic and aerobic microcosms suggested that natural biodegradation was insufficient to achieve a reduction in concentrations of PCE and its degradation products below the Italian MCL. The addition of reducing substrates in anaerobic microcosms and nutrients containing N and P in aerobic microcosms showed that stimulated biodegradation was much more effective, leading to concentrations that were generally below the MCL.
3. Pilot-scale in situ biodegradation tests confirmed the laboratory results. On-site tests demonstrated that a sequential anaerobic and aerobic treatment could attain a high degradation efficiency of all chloroethenes under biostimulated conditions in the field. For the most chlorinated compounds, such as PCE and TCE, the concentrations dropped to values close to the MCLs.
4. At the end of the experimental activities, further microbiological analyses detected the presence of “aerobic bacteria” that were able to degrade toluene, chlorobenzene, benzene and VC. These bacteria were found within and outside the aerobic pilot site, suggesting that natural aerobic biodegradation of organic compounds could also occur in other parts of the site. Moreover, the abundance of such bacteria was higher inside the pilot site, demonstrating the efficiency of the aerobic treatment in stimulating aerobic degradation.

Based on the successful results from the experimental analyses, an operational scale ISB was set up in 2016 (Figure 3.1). The ISB is composed of two biobarriers, each consisting of numerous injection and extraction wells arranged in rows. Each set of wells covers a linear distance of about 400 m. Hydrogeologically, the two barriers are arranged sequentially according to their position related to the source (i.e., the landfill).

The “anaerobic” (AN) barrier (red in Figure 3.1) consists of 20 injection wells and 19 extraction wells and is located close to the landfill. The wells run parallel to the landfill and serve for the extraction of groundwaters and their reinjection in the aquifer after the addition of molasses as a biostimulating

compound. The fermentation of the carbohydrates in the molasses produces hydrogen (Lee et al., 2004), which acts as an electron donor in anaerobic microbial activities. Dissolved oxygen is the first terminal electron acceptor (TEA) to be consumed, followed by nitrate, manganese (IV), iron (III), sulfate and carbon dioxide. This process of TEA consumption leads to progressively more reducing conditions in the aquifer, promoting the RD of chloroethenes, which is most efficient under sulfate reducing and methanogenic conditions (Bouwer et al., 1994). The rate of water recirculation of the whole barrier is about 3.8 m^3h^{-1} and the rate of substrate injection is $2.9 \cdot x\ 10^{-3}$ m^3h^{-1}.

The “aerobic” (AE) barrier (green color in Figure 3.1) is located hydraulically downgradient of the AN barrier and runs parallel to the ALRC. It consists of 39 pumping wells (19 for water extraction and 20 for water reinjection) and 60 air-sparging wells. The extracted water is dosed with an organic substrate and then reinjected through the injection wells. The average distance between neighboring wells is approximately 10 m. For each air-sparging well, the average injected air flow rate is 2.04 $m^3 h^{-1}$, for a total of $1.22 \cdot x\ 10^3$ $m^3 h^{-1}$ along the whole barrier. The rate of water recirculation of the whole barrier is about 2.8 $m^3 h^{-1}$.

The bioremediation system is coupled to a pump-and-treat (P&T) system located downgradient of the AE barrier and parallel to the ARCL. The goal of the P&T is to abate the residual contaminant concentrations that the ISB system did not manage to bring under the MCL.

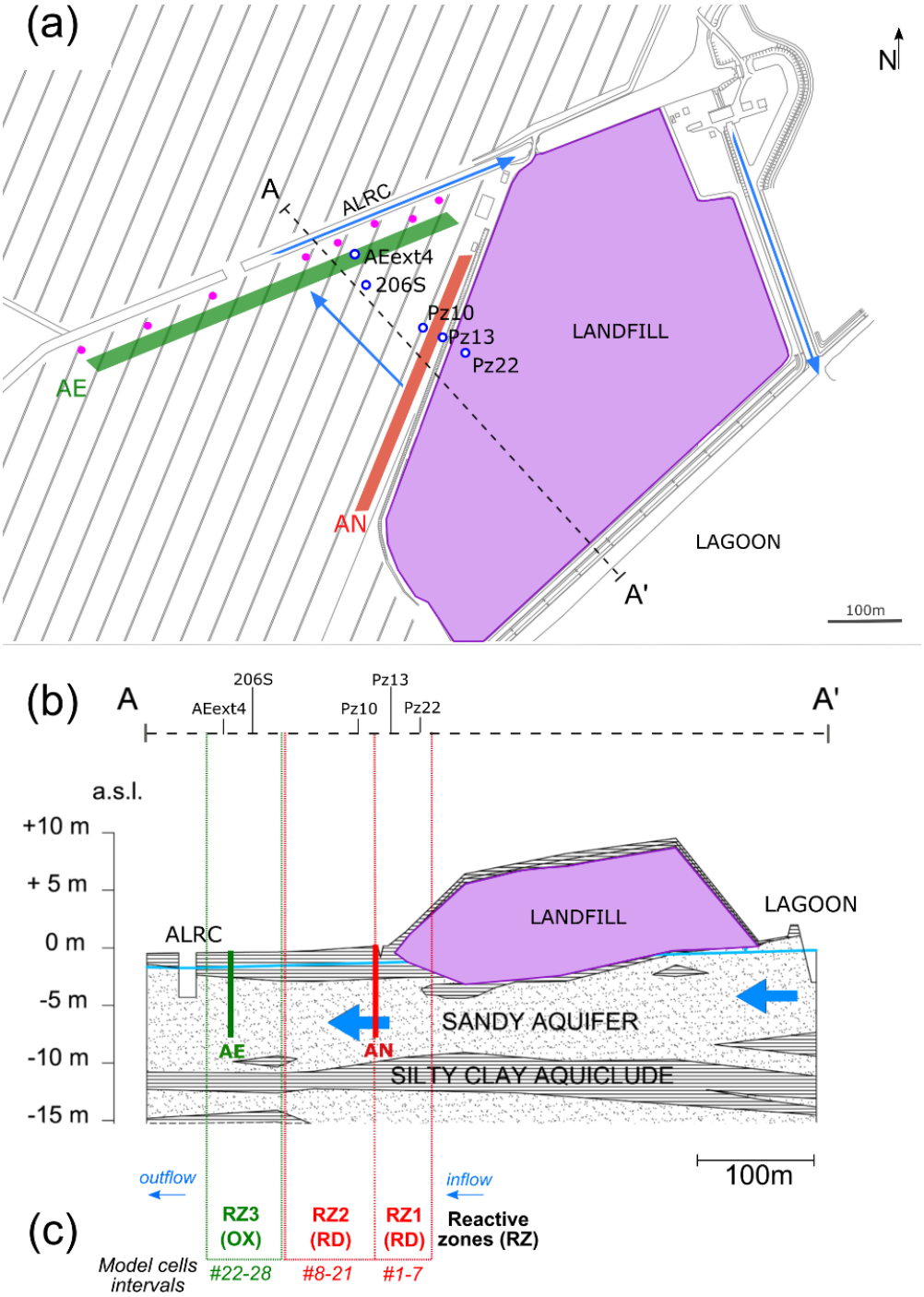

Figure 3.1. (**a**) Map of the study area, showing the landfill (lilac area) and the position of the ISB systems (AN—anaerobic barrier, AE—aerobic barrier) and the five boreholes utilized in the analysis. The wells of the P&T system are represented as purple dots. (**b**) Schematic geological cross-section of the study area (corresponding to the A–A' trace indicated in (**a**)), highlighting the top aquifer (first 10–12 m from the ground surface). The vertical axis represents the topographic elevation above sea level (a.s.l.). The blue arrows indicate the groundwater flow direction, which was oriented from the lagoon in the southeast to the agricultural land reclamation canal (ALRC) in the northwest. (**c**) Conceptual scheme of the PHREEQC model, highlighting the three reactive zones defined by the corresponding cell intervals. In RZ1 and RZ2, reactions were mainly controlled by reductive dechlorination (RD), while in RZ3, oxidation (OX) prevailed.

3.2.2 Hydrochemical and Isotopic Analyses

Our research focused on the monitoring activities performed bimonthly from May 2016 to January 2022 (for a total of 33 sampling campaigns) on five boreholes (Pz22, Pz13, Pz10, 206S and AEext4 in Figure 3.1) lying along a hypothesized aquifer flow path (parallel to the blue arrow in Figure 3.1a) crossing both barriers, which was determined through the interpretation of the aquifer hydraulic heads distribution in the site. These specific boreholes were selected due to their positions relative to the barriers (upgradient and downgradient), which were expected (according to the rationale of the ISB system) to affect the concentrations and isotopic compositions of chloroethenes through stimulation of different degradation processes. Specifically:

- Pz22 was close to the landfill and far upgradient of the AN and AE barriers. Hence, chloroethenes concentrations and isotopic compositions at Pz22 should be representative of the source conditions.
- Pz13 was located at a distance d = 30 m from Pz22, immediately upgradient of the AN barrier and far upgradient of the AE barrier. Hence, chloroethenes at Pz13 should be mainly affected by natural degradation.
- Pz10 was located at d = 60 m from Pz22, immediately downgradient of the AN barrier, but upgradient of the AE barrier. Chloroethenes at Pz10 should therefore be affected by anaerobic biostimulation and no aerobic biostimulation was expected here.
- 206S was located at d = 164 m from Pz22, further downgradient of the AN barrier and immediately upgradient of the AE one. Here, the transition from RD to OX of chloroethenes took place.
- AEext4 was located at d = 200 m from Pz22, downgradient of the AE barrier and upgradient of the P&T wells. Chloroethenes at AEext4 should be mainly affected by OX.

At these boreholes, environmental parameters, such as pH, Eh, electric conductivity and temperature, were measured through a multiparametric probe. Chemical parameters were estimated in the laboratory through standardized methods. Nitrate and sulfate (SO_4) were determined with the APAT CNR IRSA 4020 Man 29 2003 method. Nitrate concentrations remained below the detection limits for almost the totality of the sampling campaigns (data not reported). Ammonium (NH_4) was determined with the APAT CNR IRSA 4030 A1 Man 29 2003 method. Iron (Fe) and manganese (Mn) were determined with the EPA 6020B 2014 method. Determination of contaminant concentrations was carried out by a laboratory that specialized in environmental analysis with headspace gas chromatography/mass spectrometry (GC/MS) using EPA reference methods 5021A 2014 and 8260D 2018.

In January and May 2021, carbon-compound-specific isotope analysis (C-CSIA) was carried out to determine the isotopic composition (expressed as $\delta^{13}C$) of PCE, TCE, *cis*-DCE and VC. In January, the analyses were conducted on groundwater samples collected at Pz22, Pz13, 206S and AEext4. In May, the analyses were repeated on the same piezometers and also carried out at Pz10. For each

sampling point, three 40 mL vials were filled without a headspace and sealed with Teflon-lined caps. Sodium azide (NaN_3) was added to each vial as a preservative. The analyses were conducted at the Isotope Tracer Technologies Europe (Milan, Italy) laboratory by ITEX/SPME gas chromatograph/isotope ratio mass spectrometry system (GC/IRMS). Laboratory standards referenced against the international standard Vienna Pee Dee Belemnite were used for the $\delta^{13}C$ determination.

3.2.3 Geochemical Model

We implemented a one-dimensional (1D) advective–dispersive–reactive transport model to analyze the degradation of chloroethenes in the field, focusing on the control of the two biobarriers on the different degradation rates and isotope fractionation. To this end, we set up a model that was able to reproduce both the concentrations and $\delta^{13}C$ of the chloroethenes measured in the five selected boreholes. The simulations were conducted using PHREEQC version 3 (Parkhurst and Appelo, 2013), which is a widely adopted computer code that can reproduce all the required physical and biochemical processes that occur in typical bioremediation systems (e.g., (Antelmi et al., 2021; Van Breukelen et al., 2005).

3.2.3.1 Reaction Network

Our model assumed that sequential RD can occur for the entire reaction chain PCE→TCE→*cis*-DCE→VC, while oxidation (OX) is limited to *cis*-DCE and VC. Such assumptions are in agreement with the literature since clear evidence of RD was provided for all chloroethenes, while OX was extensively documented only for *cis*-DCE and VC, but rarely for TCE and PCE (Dolinová et al., 2017a). For a generic species "x", first-order degradation kinetics of the form

$$Rate_x = k_x C_x \quad (3.1)$$

were adopted for both RD and OX. In Equation 3.1, $Rate$ is the degradation rate which represents the variation of concentration with time [M L^{-3} T^{-1}], k is the kinetic rate constant [T^{-1}] and C is the concentration [M L^{-3}]. During RD, one mole of the parent product (e.g., PCE) becomes one mole of the daughter product (e.g., TCE). The final products of *cis*-DCE and VC oxidation (CO_2 and Cl^-) were not included in the model.

To simulate carbon isotope fractionation, a bulk isotope model (Van Breukelen et al., 2005) was adopted. For each compound of the degradation chain, couples of "light" and "heavy" C isotope species were defined (i.e., "light" PCE and "heavy" PCE, "light" TCE and "heavy" TCE, etc.). Degradation rates were defined for all "heavy" and "light" species for each step of the reaction network. For instance, in the case of PCE, the degradation rate of the most abundant "light" species, namely, $PCE(l)$, was equal to

$$Rate_{PCE(l)} = k_{PCE}\, C_{PCE(l)} \quad (3.2)$$

where K_{PCE} is the first-order degradation constant for PCE and $C_{PCE(l)}$ is the concentration of $PCE(l)$. For the "heavy" species, namely, $PCE(h)$, the degradation rate was defined such that

$$Rate_{PCE(h)} = \alpha k_{PCE}\, C_{PCE(h)} \quad (3.3)$$

where α is the bulk fractionation factor of the reaction step [-] and $C_{PCE(h)}$ is the concentration of $PCE(h)$. The scalar factor α (fractionation factor) accounts for the slower reaction rate of the heavy species compared with the light one, which is usually expressed as an isotopic enrichment factor (ε) as follows:

$$\varepsilon = 1000(\alpha - 1) \quad (3.4)$$

The concentration of each of the two isotope species is then recalculated over a specified time interval by multiplying each of the degradation rate expressions (Equations 3.2 and 3.3) by the interval length. The interval is imposed by the user and is calculated based on the distance traveled by water and its velocity.

The isotopic composition of the species is then computed using

$$\delta^{13}\mathrm{C_{PCE}} = \left(\frac{R_{PCE}}{R_{standard}} - 1\right) \times 1000 \quad (3.5)$$

where $\delta^{13}\mathrm{C}$ is the "delta" notation conventionally used to specify isotopic compositions [‰], R_{PCE} is the ratio between $PCE(h)$ and $PCE(l)$, and $R_{standard}$ is the ratio between ^{13}C and ^{12}C in the standard, which is known (Craig, 1957).

The whole approach (Equations 3.2–3.5) was repeated to compute the $\delta^{13}\mathrm{C}$ of the other "daughter" compounds formed from the dechlorination of PCE. The minimum, mean and maximum k and ε values for each compound obtained through a literature review are shown in Table 3.1. k_{RD} values were obtained from the compilation of Tillotson and Borden (2017), who considered bioremediation under monitored natural attenuation (MNA) field conditions. k_{OX} values were obtained from the compilation of Suarez and Rifai (1999). ε_{OX} and k_{OX} for PCE and TCE were not considered in this study. ε values were obtained from two databases (Antelmi et al., 2021) [4,34]. Further information can be found in the Supplementary Materials.

Table 3.1. Statistics of the enrichment factors (ε) and first-order degradation constants (k) obtained through a literature review. All ε values are expressed as "per mille" (‰).

	PCE	TCE	*cis*-DCE	VC
		Reductive Dechlorination (RD)		
$\boldsymbol{\varepsilon_{RD}}$ min (‰)	−7.12	−16.40	−30.50	−28.80
$\boldsymbol{\varepsilon_{RD}}$ mean (‰)	−4.51	−11.65	−21.43	−24.52
$\boldsymbol{\varepsilon_{RD}}$ max (‰)	−1.60	−3.30	−14.90	−19.90
$\boldsymbol{k_{RD}}$ min (y^{-1})	0.00	0.00	0.00	0.00
$\boldsymbol{k_{RD}}$ mean (y^{-1})	1.07	1.10	1.82	2.20
$\boldsymbol{k_{RD}}$ max (y^{-1})	29.00	8.40	28.00	3.00
		Oxidation (OX)		
$\boldsymbol{\varepsilon_{OX}}$ min (‰)			−19.90	−8.20
$\boldsymbol{\varepsilon_{OX}}$ mean (‰)			−7.99	−6.06
$\boldsymbol{\varepsilon_{OX}}$ max (‰)			−0.90	−3.20
$\boldsymbol{k_{OX}}$ min (y^{-1})			102.57	15.70
$\boldsymbol{k_{OX}}$ mean (y^{-1})			323.03	43.80
$\boldsymbol{k_{OX}}$ max (y^{-1})			715.40	204.40

3.2.3.2 *Reactive Transport Model*

The reaction network described above was embedded into a 1D transport model, which reproduced an L = 224 m long flow path, discretized into 28 regular cells that were 8 m wide. L covers the linear distance between the piezometers Pz22 (close to the landfill) and AEext4 (close to the ARLC), crossing the AN and AE biobarriers. The total simulation time was set to approximately 11 years in order to reach steady-state conditions. A summary of the model parameters is reported in Table 3.2.

Table 3.2. PHREEQC model input parameters. TOC: total organic carbon.

Parameter	Value	Unit
Domain length (L)	224	m
Tracer velocity (v_{nr})	0.45	m d^{-1}
Averaged chloroethene velocity (v_r)	0.10	m d^{-1}
Longitudinal dispersivity (α_L)	22.4	m
Cell length (ΔX)	8	m
Number of cells	28	-
Shifts	50	-
Time step length	80	d
Equivalent simulation time	4000	d
Cell numbers for reactive zone 1	1–7	-
Cell numbers for reactive zone 2	8–21	-
Cell numbers for reactive zone 3	22–28	-
Flow inlet/outlet boundary conditions	Constant flux	-
Bulk density (ρ_b)	1.6	g cm^{-3}
Porosity (ϕ)	0.25	-
Fraction of organic carbon (f_{oc})	10% of TOC	-

Aquifer properties were considered homogeneous in the modeled domain. The advective velocity for a conservative (i.e., a non-reactive) tracer (v_{nr}) was set to $v_{nr} = 0.45$ m d^{-1}. This value was derived from the already-interpreted results of a fluorescein dye tracer test performed at the site and reported in technical documents provided by the site's owner. The tracer test velocity agreed with the $v_{nr} = 0.37 - 0.48$ m d^{-1} obtained through the monitored groundwater head levels, assuming a

hydraulic conductivity K = 14 m d^{-1} (obtained from slug tests performed on the site) and a porosity ϕ = 0.25 (typical value obtained from the literature for this type of aquifer (Domenico and Schwartz, 1998). Following (Gelhar et al., 1992), we set a coefficient of longitudinal dispersivity $\alpha_L = 0.1L$, resulting in $\alpha_L = 22.4$ m. Compared with a conservative tracer, the advective velocity of the reactive chloroethenes (v_r) was reduced by the effect of sorption on the porous medium. Thus, the pore water velocity in the model was set as the retarded velocity v_r and computed using

$$v_r = \frac{v_{nr}}{\bar{\beta}} \tag{3.6}$$

where $\bar{\beta}$ is the average retardation factor calculated from the species-specific retardation factors β_x, which are in turn calculated using (e.g., Freeze and Cherry, 1979)

$$\beta_x = 1 + \frac{\rho_b}{\phi} K'_{d(x)} \tag{3.7}$$

where ρ_b is the bulk density of the soil [M L^{-3}] and K'_d is the distribution coefficient of the species x. The term K'_d can be calculated using

$$K'_d = f_{oc} k_{oc} \tag{3.8}$$

where f_{oc} is the fraction of organic carbon [-] and the species-specific k_{oc} is the partition coefficient between organic carbon and water [L^3 M^{-1}]. We used representative values for ρ_b and ϕ for silty sands and sandy silts, while we set $f_{oc} = 1\%$, which was a value obtained by considering one-tenth of the total organic carbon (TOC) measured in samples collected in the field and estimated as TOC = 10% (*v/v*). Typical values for k_{oc} were obtained from the Italian reference database for environmental health risk analysis (ISS-INAIL). The resulting k_{oc} and β values are listed in Table 3.3.

Table 3.3. Representative value of the partition coefficient between organic carbon and water (k_{oc}) and retardation factors (β) for chloroethenes. $\bar{\beta}$ is the average retardation factor.

Chloroethene	k_{oc} (cm^3 g^{-1})	β	$\bar{\beta}$
PCE	94.94	7.08	4.47
TCE	60.70	4.88	
cis-DCE	39.60	3.53	
VC	21.73	2.39	

As direct information regarding the composition of the landfill was missing, the flow and solute input boundary condition was calculated from the groundwater composition at Pz22, i.e., the closest piezometer to the landfill (Figure 3.1). The source released a constant concentration of “light” and “heavy” PCE, TCE, *cis*-DCE and VC. The model concentrations of light and heavy species for each chloroethene are reported in Table 3.4. These values were calculated from the total concentrations and carbon isotopic ratios measured at Pz22 in May 2021, which are also reported in Table 3.4 and the “Results” section.

Table 3.4. Concentrations and isotopic compositions used to model the plume source in the PHREEQC model.

Compound	Concentrations (µM)	$\delta^{13}C$ (‰)
PCE tot	34.982	
PCE(l)	34.615	−58.2 ± 0.7
PCE(h)	0.367	
TCE tot	228.137	
TCE(l)	225.726	−49.7 ± 0.3
TCE(h)	2.411	
cis-DCE tot	194.845	
cis-DCE(l)	192.767	−40.3 ± 0.2
cis-DCE(h)	2.078	
VC tot	1568.000	
VC(l)	1551.135	−32.7 ± 0.1
VC(h)	16.865	

The model assumed three different "reactive zones" (RZs; Figure 3.1c) by considering the different biodegradation processes and the corresponding degradation kinetics expected in the different portions of the flow path. Specifically, we defined the following:

- Reactive zone 1 (RZ1), including model cells 1–7 and parametrized by k_{RD1} and ε_{RD1}. It represented the portion of the flow path immediately upgradient of the AN barrier, from Pz22 to between Pz13 and Pz10, where the AN barrier was located. Here, only natural RD was expected to take place without stimulation by the AN barrier.
- Reactive zone 2 (RZ2), including cells 8–21 and parametrized by k_{RD2} and ε_{RD2}. It represented the portion of the flow path located between the AN and AE barriers until just upgradient of the piezometer 206S. Stimulated RD was expected to take place in this section of the flow path.
- Reaction zone 3 (RZ3), including cells 22–28 and parametrized by k_{OX} and ε_{OX}. It represented the last portion of the flow path extending from 206S to the end of the transect, which included the AE barrier and piezometer AEext4 just downgradient of it. OX was expected to be largely stimulated by the AE barrier, while RD was not expected to be as efficient as in the upgradient zones.

3.2.3.3 Model Calibration

Model calibration was carried out with a trial-and-error approach using the results of the May 2021 campaign, which provided a complete dataset for both concentrations and isotopic data. The weighted root-mean-square error ($wRMSE$) between the simulated and observed values was used as the error metric to obtain the best-fitting model parameters. For each species, $wRMSE$ was calculated using

$$wRMSE = \frac{1}{N}\sqrt{\sum_{i=1}^{N}\left[w_i\left(Y_{obs_i} - Y_{sim_i}\right)\right]^2} \quad (3.9)$$

where Y_{obs} is either the observed concentration or $\delta^{13}C$, Y_{sim} is either the simulated concentration or $\delta^{13}C$, w is an observation-specific weight and N is the number of observations $(i = 1, \dots, N)$.

A total of 16 parameters were estimated during the calibration. Specifically, we estimated the three RD parameters (k_{RD1}, k_{RD2}, ε_{RD}) for each of the four considered species (PCE, TCE, *cis*-DCE and VC) and the two OX parameters (k_{OX}, ε_{OX}) for *cis*-DCE and VC.

Two different calibration approaches were used. In the first approach ("Approach 1"), we initially calibrated the degradation rate constants (k_{RD1}, k_{RD2}, k_{OX}) by matching the concentration data. Then, we used the best-fitted k to obtain the enrichment factors ($\varepsilon_{RD1}, \varepsilon_{RD2}, \varepsilon_{OX}$) by matching the isotopic data. In "Approach 1", we assigned a weight w = 1 to all observations by considering that all observations were equally reliable.

Calibrated parameters using "Approach 1" could be affected by two problems. First, no constraints on the best-fit ε were imposed. This may lead to unrealistic enrichment factors when compared with the typical values reported in the literature (Table 3.1). Second, the third reaction zone covered 206S and AEext4. Concentrations at these piezometers may not have exclusively depended on OX processes, but also depended on the RD processes that took place in reactive zones RZ1 and RZ2. As such, the use of concentrations and isotopic compositions at 206s and AEext4 for the estimation of k_{OX} and ε_{OX} were expected to be more uncertain than the use of concentrations and isotopic compositions at the other piezometers for the estimation of $k_{RD1,2}$ and $\varepsilon_{RD1,2}$.

To account for the possible problems with "Approach 1", the second calibration approach ("Approach 2") adopted a different strategy. For the reaction zones RZ1 and RZ2, the degradation rate constants k_{RD} were calibrated by simultaneously matching concentration and isotopic data and prioritizing the minimization of RMSE of isotopic data rather than concentrations. The maximum and minimum ε_{RD} values were constrained within the ranges indicated in Table 3.1. For RZ3, k_{OX} was estimated exclusively using the CSIA data. We fixed ε_{OX} according to the average, minimum and maximum values obtained from the literature. For each ε_{OX} value, we fitted the isotopic data by changing k_{OX} values within the ranges indicated in Table 3.1. To account for the uncertainty in the observations, in "Approach 2", we assigned w = 0.5 to the CSIA data in AExt4 for PCE and TCE, lacking information at 206S, and to *cis*-DCE and VC in RZ3, to account for the more uncertain use of piezometers 206S and AEext4 for the estimation of k_{OX} and ε_{OX}. For all other observations w = 1.

A sensitivity analysis was conducted to evaluate the impact of the variation of α_L and the best-fitted k_{RD2} and ε_{RD} obtained using "Approach 2". The results did not provide further insight into the interpretation of the processes and are reported in the SM3.

3.3 Results

3.3.1 Hydrochemical and Isotopic Analyses

3.3.1.1 Concentration Data

Figure 3.2 shows the statistics, in the form of boxplots, of all concentration time series that were obtained by merging the 33 available monitoring campaigns from May 2016 to January 2022. The time series of the individual sampling campaigns can be found in the Supplementary Materials. All horizontal axes in the plots report the distance from Pz22.

A first key observation was that while RD positively affected the biodegradation of all species, RD was less efficient for *cis*-DCE and VC than for PCE and TCE. Upgradient of the AN barrier (i.e., from Pz22 and Pz13), Figure 3.2shows that the concentrations of PCE remained constant with a median value close to 6000 µg L^{-1}, while an increase in concentrations was observed for TCE, *cis*-DCE and VC. Across the AN barrier (i.e., between Pz13 and Pz10), the PCE and TCE concentrations dropped from 6300 µg L^{-1} to 470 µg L^{-1} (i.e., decreased by 92.6%) and from 50,500 µg L^{-1} to 1500 µg L^{-1} (i.e., a decrease of 97.1%), respectively. Furthermore, the *cis*-DCE and VC concentrations considerably decreased from 36,000 µg L^{-1} to 9000 µg L^{-1} (i.e., 75%) and from 149,000 µg L^{-1} to 55,000 µg L^{-1} (i.e., 73.1%), respectively.

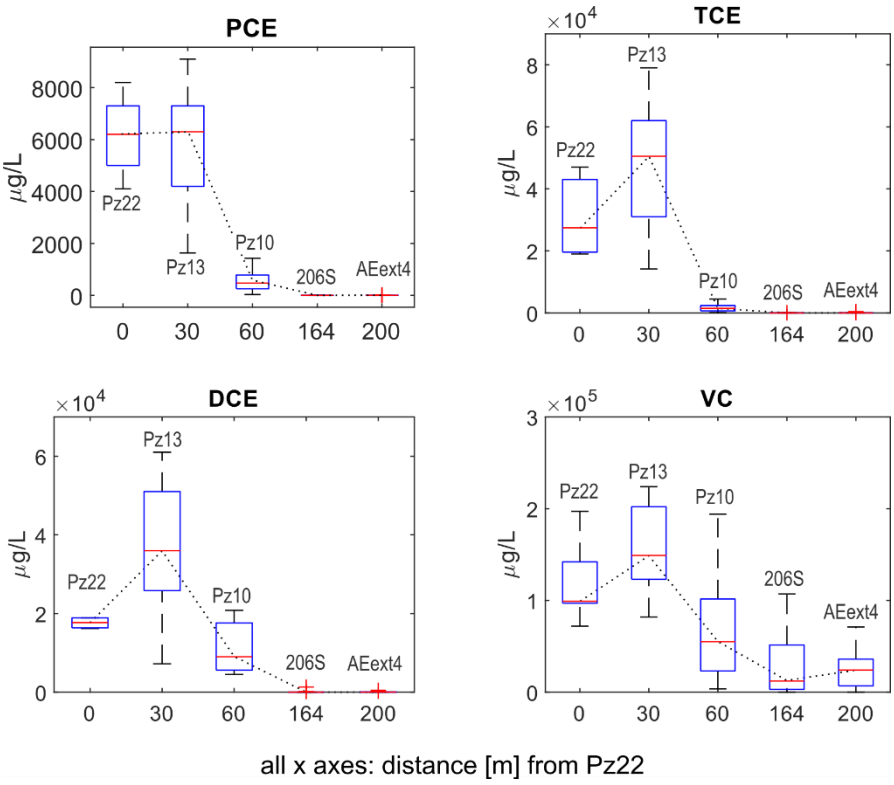

Figure 3.2**.** Evolution of the PCE, TCE, DCE and VC concentrations along the transect from Pz22 to AEext4 for all available sampling campaigns. The dotted black line connects the median values (red marks) of the different boxplots.

Moving downgradient of the AN barrier and approaching the AE barrier, the overall degradation efficiency jumped to >99.9% for PCE, TCE and *cis*-DCE and to 84–91.8% for VC. At 206S, we observed further decreases in PCE to 0.80 µg L^{-1}, TCE to 2.80 µg L^{-1}, *cis*-DCE to 0.71 µg L^{-1} and VC to 12,200 µg L^{-1}. At AEext4, we found median values of 1.39 µg L^{-1} for PCE, 11.00 µg L^{-1} for TCE, 7.55 µg L^{-1} for *cis*-DCE and 24,050 µg L^{-1} for VC. This meant that the SBS was highly beneficial for the removal of contaminant mass from the aquifer.

3.3.1.2 Environmental Parameters

Trends of chloroethene concentrations were consistent with the variations in Eh, iron, manganese, sulfate and ammonium concentrations measured in the boreholes. Statistics for Eh, iron, manganese, sulfate and ammonium concentrations are shown as boxplots in Figure 3.3. The individual time series for each monitoring campaign can be found in the Supplementary Materials. Data for pH, electrical conductivity and temperature were not reported, as no spatiotemporal trends or remarkable seasonal variations were observed for these parameters.

Upgradient of the AN barrier (from Pz22 to Pz13), the Eh value decreased from −139 mV to −181 mV, while at Pz10, just downgradient of the AN barrier, a value as low as −255 mV was reached as a consequence of the injection of the reducing substrate. The decrease in Eh between Pz22 and Pz13 suggested that while the injection rates at the AN barrier were very modest, the resulting radially divergent flow could have forced injected solute to move locally upgradient and against the mean natural gradient of the aquifer.

Between Pz22 and Pz13, we observed an increase in median concentrations of Fe (from 5500 µg L^{-1} to 11,800 µg L^{-1}) and Mn (from 935 µg L^{-1} to 1360 µg L^{-1}). This trend was consistent with the decrease in Eh, which could mobilize Fe and Mn by dissolving iron- and manganese hydroxides. The decrease in Fe and Mn concentrations from Pz13 to Pz10 (from 11,800 µg L^{-1} to 4255 µg L^{-1} for Fe and from 1360 µg L^{-1} to 686 µg L^{-1} for Mn) could be explained by the precipitation of Fe and Mn sulfides due to the presence of hydrogen sulfide produced by sulfate reduction (Christensen et al., 2000; D'Affonseca et al., 2011; He et al., 2015; Hyun and Hayes, 2009), as observed for Eh < −200 mV in similar geological settings (Dalla Libera et al., 2018). Indeed, SO_4 concentrations remained relatively stable between Pz22 and Pz13, while they decreased significantly between Pz13 and Pz10, reaching a value as low as 602 mg L^{-1}. This further confirmed that sulfate-reducing conditions were reached at the AN barrier.

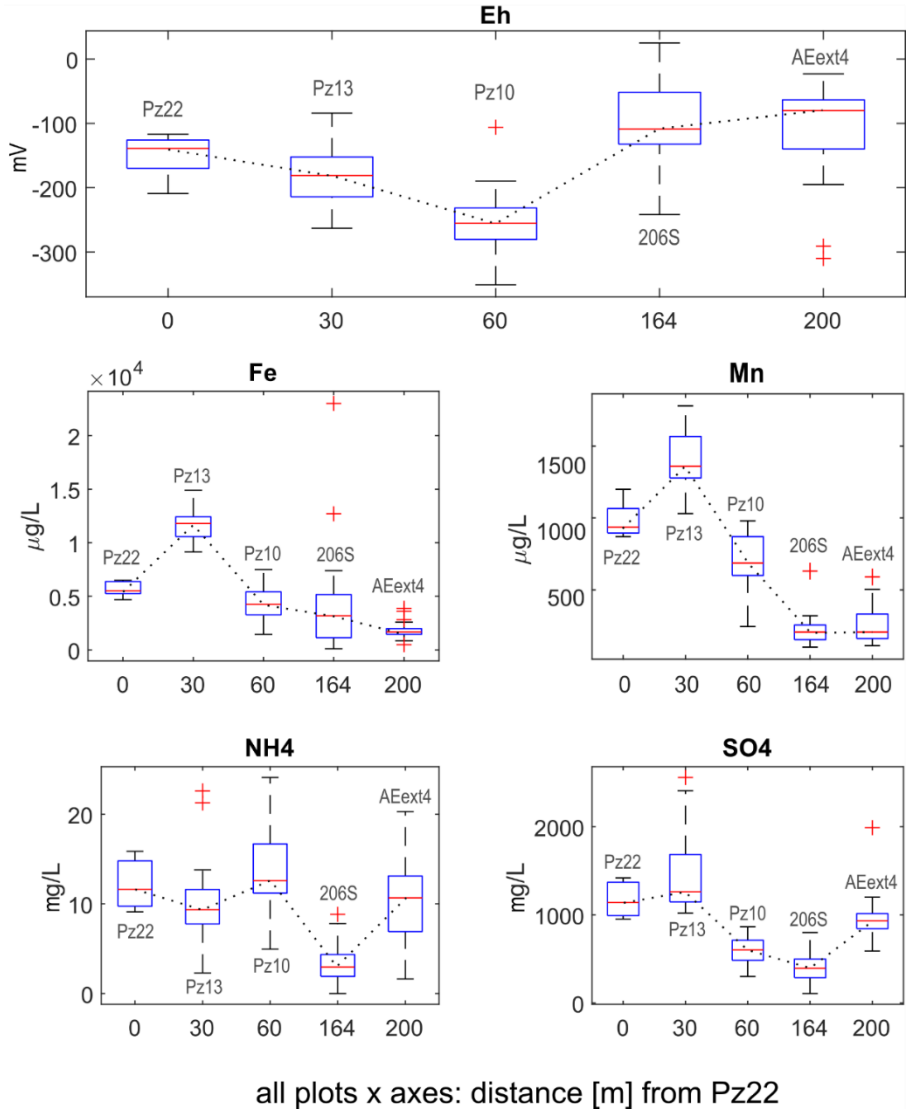

Figure 3.3**.** Evolution of the oxidizing–reduction potential (expressed as Eh), iron, manganese, ammonium and sulfate concentrations along the transect from Pz22 to AEext4 for all available sampling campaigns. The dotted black line connects the median values (red marks) of the different boxplots.

Approaching the AE barrier, the Eh switched back to more oxidizing conditions (−109 mV in 206S and −80 mV in AEext4). Consistently, at 206S and AEext4, iron (3180 µg L^{-1} and 1670 µg L^{-1}, respectively) and manganese (206 µg L^{-1} in both piezometers) concentrations decreased compared with upgradient piezometers. In contrast, SO_4 concentrations were not as easily correlated with Eh variations in 206S. In fact, from Pz10 to 206S, SO_4 decreased while Eh increased. In contrast, from 206S to AEext4, SO_4 increased from 395 mg L^{-1} to 931 mg L^{-1}, while Eh increased slightly. This latter trend could be due to sulfide oxidation due to more oxidizing conditions created at the AE barrier. This should have caused an increase in Fe and Mn concentrations as well, which may have been counterbalanced by the precipitation of Fe and Mn oxides/hydroxides, which are more stable compared with sulfides for Eh > −100 mV (Dalla Libera et al., 2018).

The behavior of NH_4 was more complex than the other species, yet it was still consistent with the general behavior of the SBS. In all boreholes, ammonium concentrations were well above the

analytical detection limit (0.1 mg L^{-1}), which was expected for an aquifer with a high TOC (10% (*v*/*v*)). Upgradient from the AN barrier, from Pz22 to Pz13, the ammonium concentrations decreased from 11.62 mg L^{-1} to 9.35 mg L^{-1}, probably due to the decrease in the natural organic matter content in sediments caused by its progressive consumption during reductive processes, as observed in adjacent sites (Slater et al., 2001). Concentrations of NH_4 increased again to 12.6 mg L^{-1} as a result of the injection of the reducing organic substrate at the AN barrier. The concentrations showed a significant drop at 206S (2.96 mg L^{-1}), consistent with the increasing distance from the injection wells and the associated lower availability of ammonium-producing substrate From 206S to AEext4; the concentrations then increased again (10.67 mg L^{-1}) due to the injection of nutrients (P and N) at the AE barrier.

3.3.1.3 C-CSIA Data

The C-CSIAs carried out in January and May 2021 were critical for providing key information regarding the biodegradation processes that occurred in the SBS. The results are reported in Table 3.5. PCE and TCE isotopic signatures could not be determined in piezometer 206S, as the concentrations of these two compounds were below the detection limit for isotope analysis. Moreover, concentration data at Pz22 were not available for January 2021.

For each compound, the variation in $\delta^{13}C$ along the flow path in January and May 2021 is displayed in Figure 3.4.

Table 3.5. Results from the C-CSIAs from samples collected in January and May 2021. * b.d.l.—below detection limit. The standard deviation of the concentration data was 35%.

	Pz22		**Pz13**		**Pz10**		**206s**		**AEext4**	
	Conc (µg L^{-1})	**$\delta^{13}C$ (‰)**	**Conc (µg L^{-1})**	**$\delta^{13}C$ (‰)**	**Conc (µg L^{-1})**	**$\delta^{13}C$ (‰)**	**Conc (µg L^{-1})**	**$\delta^{13}C$ (‰)**	**Conc (µg L^{-1})**	**$\delta^{13}C$ (‰)**
January 2021										
PCE	/	−58.2 ± 0.7	/	/	1340	−55.2 ± 0.5	0.091	b.d.l. *	1.94	−42.3 ± 0.1
TCE	/	−49.7 ± 0.3	/	/	2250	−47.3 ± 0.1	0.41	b.d.l. *	8.1	−38.8 ± 0.6
cis-DCE	/	−40.3 ± 0.2	/	/	17,600	−37.8 ± 0.2	0.71	−26.4 ± 0.4	232	−11.5 ± 0.5
VC	/	−32.7 ± 0.1	/	/	108,000	−32.9 ± 0.2	5200	−24.4 ± 0.1	8000	−23.2 ± 0.1
May 2021										
PCE	5800	−57.2 ± 0.3	3200	−55.7 ± 0.1	1410	−55.8 ± 0.4	0.054	/	0.94	−23.0 ± 0.5
TCE	30,000	−49.4 ± 0.2	20,700	−49.3 ± 0.3	4400	−47.4 ± 0.4	0.122	/	3.00	−32.1 ± 0.7
cis-DCE	18,900	−40.6 ± 0.5	30,600	−46.7 ± 0.1	17,800	−38.9 ± 0.5	0.5	−31.6 ± 0.8	490	−18.7 ± 0.5
VC	98,000	−32.4 ± 0.3	125,000	−33.1 ± 0.2	121,000	−33.2 ± 0.1	590	−42.5 ± 0.2	5800	−28.0 ± 0.1

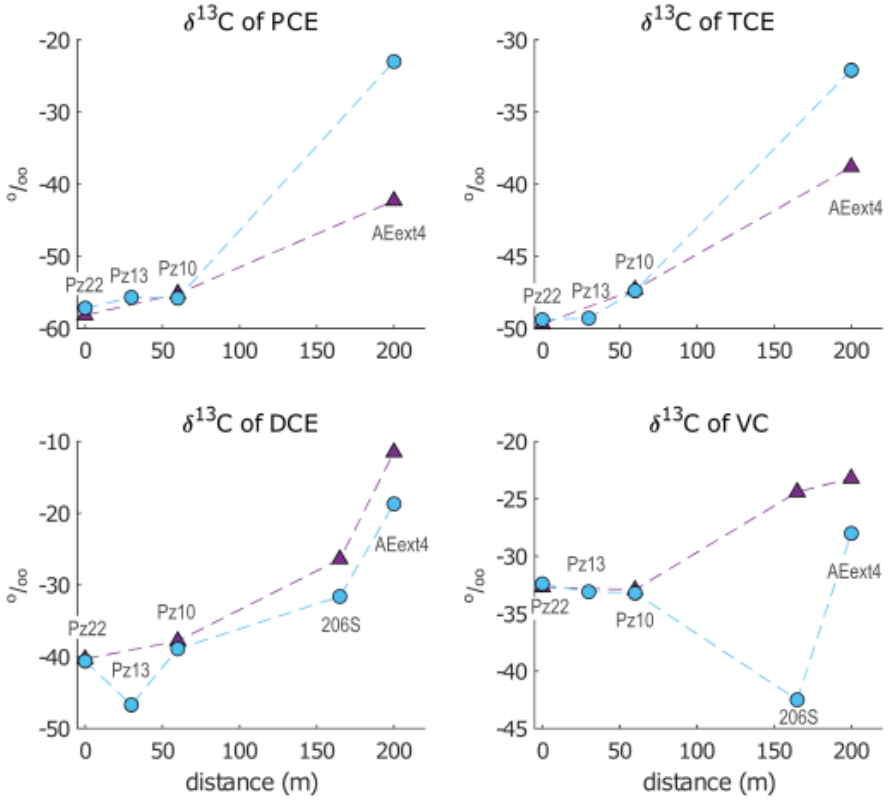

Figure 3.4**.** Evolution of isotopic signatures for PCE, TCE, *cis*-DCE and VC in January 2021 (purple triangles) and May 2021 (blue circles) from Pz22.

The results revealed a general progressive increase in $\delta^{13}C$ for all chloroethenes from Pz22 to AEext4 in both sampling campaigns, which was consistent with the isotopic enrichment caused by degradation processes. In fact, during degradation, microbes tend to favor isotopically lighter molecules (containing ^{12}C) rather than heavier molecules containing one or more heavy atoms (^{13}C). This leads to an enrichment of heavier molecules in the remaining contaminant, which translates into an increase of its $\delta^{13}C$.

The isotopic enrichment produced along the AN barrier from Pz22 to Pz10 was similar in both sampling campaigns for all compounds. Instead, higher temporal variations in isotopic compositions were observed downgradient of Pz10.

Isotopic shifts ($\Delta^{13}C$) were calculated for each compound as the difference between $\delta^{13}C$ in the downgradient piezometer and $\delta^{13}C$ in the respective upgradient piezometer. All isotopic shifts can be found in Table S3.4 (SM3). The isotopic enrichment of PCE and TCE from Pz10 to AEext4 was higher in May ($\Delta^{13}C_{PCE}$ = 32.8‰ and $\Delta^{13}C_{TCE}$ = 15.3‰) compared with January ($\Delta^{13}C_{PCE}$ = 12.9‰ and $\Delta^{13}C_{TCE}$ = 8.5‰). Opposite behavior was observed for *cis*-DCE, as a slightly higher enrichment was measured in January from Pz10 to 206S ($\Delta^{13}C_{DCE}$ = 11.4‰) and from 206S to AEext4 ($\Delta^{13}C_{DCE}$ = 14.9‰) than in May ($\Delta^{13}C_{DCE}$ = 7.4‰ from Pz10 to 206S and $\Delta^{13}C_{DCE}$ = 12.9‰ from 206S to AEext4). For VC, the isotopic composition also increased monotonically from Pz22 to AEext4 in the January dataset. In contrast, in May, we found a negative isotopic shift from Pz10 to 206S ($\Delta^{13}C_{VC}$

= −9.3‰), followed by a significant enrichment from 206S to AEext4 ($\Delta^{13}C_{VC}$ = 14.5‰). However, the final isotopic composition in AEext4 in May ($\delta^{13}C$ = −28.0‰) did not reach values as high as in January ($\delta^{13}C$ = −23.2‰). The unexpected drop in $\delta^{13}C_{VC}$ measured in May 2021 points to a likely intervention of processes different from biodegradation on the isotopic signature of VC, such as volatilization, dilution or mixing of multiple flow paths, as addressed in the “Discussion” section.

Overall, steady behavior was observed at the AN barrier between January and May, while significant differences were detected in the AE area. This points to major stability of the microbial activity in the AN zone compared with the AE zone, possibly due to the intervention of physical processes linked to the activity of the AE barrier, e.g., a local variation in air injection rates (possibly due to temporary malfunctioning of the AS wells). This is also in line with the hypothesis of the intervention of volatilization on the isotopic signature of VC in May since a higher injection rate of AS wells could lead to its volatilization.

3.3.2 Geochemical Model

The calibration process using both methods resulted in an excellent matching between observed and simulated concentration and isotopic data. However, the use of "Approach 1" generated best-fitted degradation constants falling within the ranges indicated in Table 3.1, but the enrichment factors were not consistent with literature values. In contrast, the use of "Approach 2" resulted in more consistency between enrichment factors obtained in the literature and those obtained from the model at the expense of a slightly poorer matching between measured and calculated concentrations.

3.3.2.1 Approach 1

A summary of the fitted ε and k values and the corresponding RMSEs for the concentration and CSIA data are reported in Table 3.6. The results of the concentration and isotopic data simulations are displayed in Figure 3.5.

Table 3.6. Calibrated k and ε values for the tested scenarios with May 2021 data.

	PCE	**TCE**	***cis*-DCE**	**VC**
Approach 1—Reductive Dechlorination (RD)				
k_{RD1} (y^{-1})	0.84	0.43	0.00	0.00
k_{RD2} (y^{-1})	2.70	11.00	2.15	0.48
ε_{RD} (‰)	−9.4	−3.6	−6.2	−2.0
Approach 1—Oxidation (OX)				
k_{OX} (y^{-1})	-	-	50	50
ε_{OX} (‰)	-	-	−2.2	−1.2
wRMSE				
Concentrations	0.07	0.60	16.60	159.50
CSIA	3.89	0.36	1.18	1.67
Approach 2—Reductive dechlorination (RD)				
k_{RD1} (y^{-1})	0.3	0.2	0	0
k_{RD2} (y^{-1})	6.5	2.9	0.6	0
ε_{RD} (‰)	−5.6	−5.7	−16.0	0
Approach 2—Oxidation (OX) *Using the Average [Minimum ÷ Maximum] ε_{OX}*				
k_{OX} (y^{-1})	-	-	4.7 [0.7 ÷ 155]	2.9 [1.7 ÷ 12.6]
ε_{OX} (‰)	-	-	−7.99 [−19.9 ÷ −0.9]	−6.06 [−8.2 ÷ −3.2]
wRMSE (average ε_{OX})				
Concentrations	1.10	13.14	24.08	157.76
CSIA	1.88	0.13	1.12	0.80

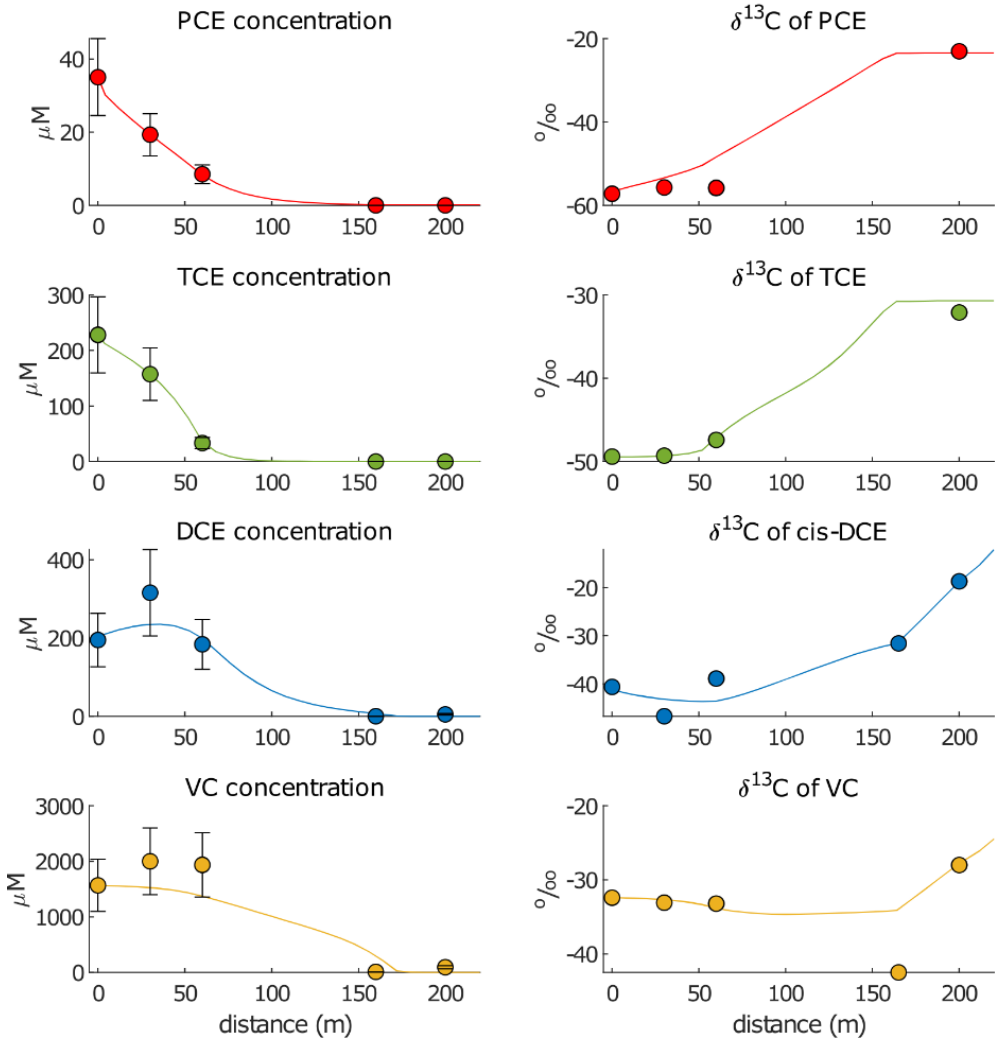

Figure 3.5**.** Simulated (lines) and observed (dots) chloroethenes concentrations and isotopic compositions using the first calibration ("Approach 1").

The best-fitted RD degradation constants for each reaction zone (RZ) were k_{RD1} = 0.84 y^{-1} and k_{RD2} = 2.70 y^{-1} for PCE and k_{RD1} = 0.43 y^{-1} and k_{RD2} = 11.00 y^{-1} for TCE. The larger degradation rate constant for TCE in RZ2 was explained by the steep drop in concentrations observed from Pz13 to Pz10 (from approximately 160 µM to approximately 35 µM). For *cis*-DCE, the best-fitting parameters were k_{RD1} = 0 and k_{RD2} = 2.15 y^{-1}. The model reproduced the accumulation of *cis*-DCE at Pz13 and the calculated value still fell within the standard deviation of the observed data. The fitted $k_{RD1} = 0$ was consistent with the lack of *cis*-DCE degradation expected in the anaerobic reaction zone RZ1 upgradient of the AN barrier. A large deviation was present between the observed and simulated concentrations in 206S, as the calculated values were three orders of magnitude higher (6 µM) than the observed values (0.005 µM). For VC, the best-fitted parameters were k_{RD1} = 0 and k_{RD2} = 0.48 y^{-1}. As in the case of *cis*-DCE, the fitted k_{RD1} agreed with the expected lack of VC degradation up-gradient of the AN barrier, and the calculated VC concentrations fell within the standard deviations of observed data for Pz13 and Pz10. However, the calculated concentrations at 206S were close to

400 µM, which was about 40 times higher than the observed concentrations (9.44 µM). The best-fitted OX degradation kinetics k_{OX} were 50 y^{-1} for both *cis*-DCE and VC. Such markedly higher values compared with the RD kinetic rates agreed with the literature data (Table 3.1).

Considering the best-fitted k_{RD} and k_{OX}, the lowest wRMSE were calculated for the PCE and TCE concentrations (equal to 0.07 and 0.60, respectively), for which the concentration data were perfectly reproduced. Higher wRMSE were obtained for DCE (16.60) and VC (159.50) concentrations, for which the model did not allow for accurately reproducing the accumulation of both compounds at Pz13, as well as the observed concentrations in 206S. As for isotopic data, the resulting wRMSEs were the lowest for TCE (0.36), highest for PCE (3.89) and *cis*-DCE and VC fell in between (1.18 and 1.67, respectively). Notwithstanding the general good reproduction of isotopic evolutions, the enrichment factors calculated using "Approach 1" fell outside of the literature ranges, with a few exceptions. The resulting ε_{RD} values were −9.4‰ for PCE (literature range is −7.12 – −1.60‰), −3.6‰ for TCE (literature range is −11.65 – −3.30‰), −6.2‰ for *cis*-DCE (literature range is −30.50 – −14.90‰) and −2.0‰ for VC (literature range is −28.8 – −19.9‰). The resulting ε_{OX} values were −2.2‰ for *cis*-DCE (−7.90 – −0.90‰) and −1.2‰ for VC (−6.06 – −3.20‰). This suggested that "Approach 1" was not useful for estimating the bioremediation parameters.

3.3.2.2 Approach 2

Best-fitted concentration and isotopic data are displayed in Figure 3.6, while the summary of the results can be found in Table 3.6.

For *cis*-DCE, a much lower k_{RD2} (0.6 y^{-1}) was found compared with "Approach 1", while the resulting enrichment factor (−16.0‰) fell within the literature range. The lower k_{RD2} for *cis*-DCE combined with the lower k_{RD1} and higher k_{RD2} of TCE (which generated less production of *cis*-DCE upgradient and more production downgradient of the AN barrier) caused an increase in the concentration peak, which shifted toward Pz10, compared with the concentration peak obtained with "Approach 1".

The very low k_{RD2} for *cis*-DCE was explained by considering that this species is usually hardly degraded through RD. The same holds for VC, for which we obtained $k_{RD1} = k_{RD2} = 0$. The null degradation rate in both zones demonstrated that VC was possibly not degraded at all under anaerobic conditions at the site. The absence of VC concentration abatement from Pz22 to Pz10 was coherent with the small decrease in $\delta^{13}C_{VC}$ between the two points ($\Delta^{13}C$ = −0.8‰), which resulted from the production of VC (from RD of *cis*-DCE) in the absence of its degradation.

For the estimation of the OX degradation rates, Table 3.6 compares the results from the calibration by fixing the average, minimum and maximum enrichment factors values reported in the literature (Table 3.1). We obtained great variability in the best-fitted oxidative rates, namely, k_{OX} = 0.7–155 y^{-1} for *cis*-DCE and k_{OX} = 1.7–12.6 y^{-1} for VC. These ranges agreed with the results obtained using "Approach 1" (k_{OX} = 50 y^{-1}). The much higher OX rate obtained for these compounds compared with

the RD rates further confirmed that aerobic biodegradation of *cis*-DCE and VC was more effective than anaerobic biodegradation.

In this case, overall higher wRMSEs for concentrations were obtained compared with “Approach 1”, even though in “Approach 2”, the weight of observations in RZ3 (206S and AEext4) were halved. Like in “Approach 1”, increases in concentration wRMSEs from PCE to VC were observed, and the lowest and the highest wRMSEs for isotopic data were obtained for TCE (0.13) and PCE (1.88), respectively.

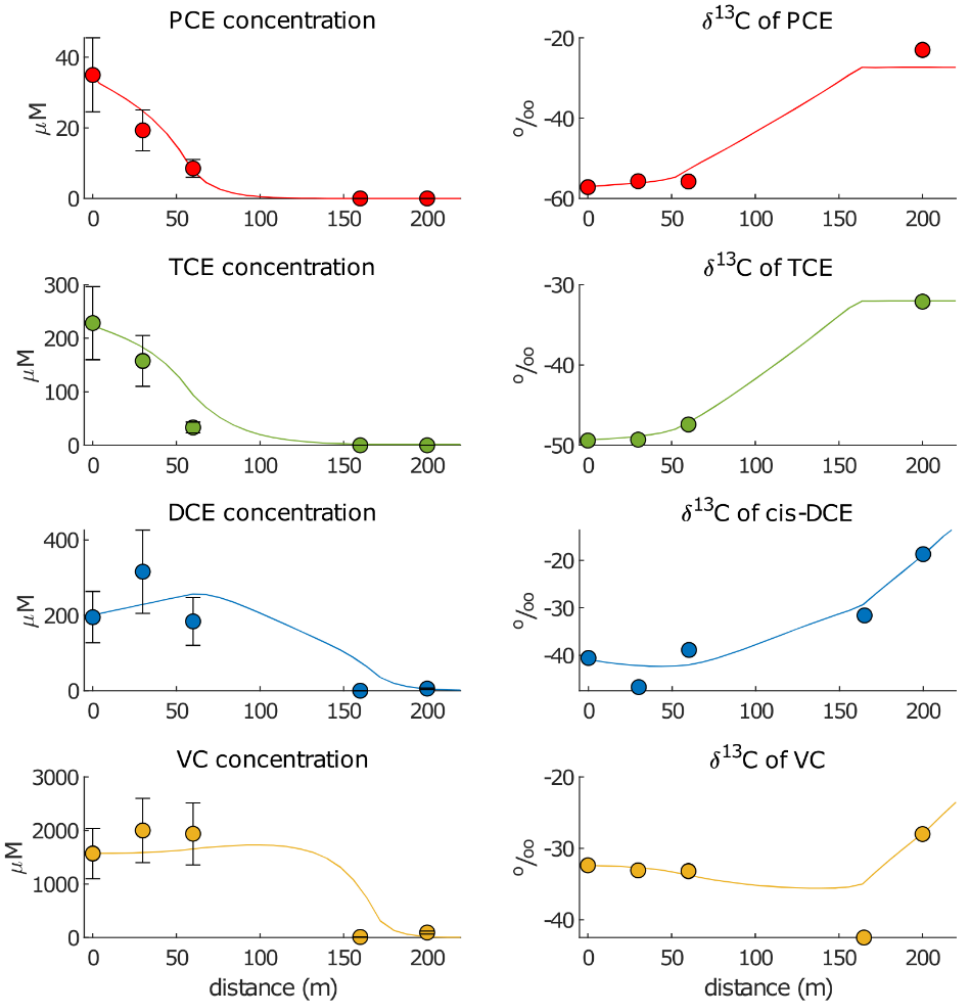

Figure 3.6**.** Simulated (lines) and observed (dots) showing the chloroethene concentrations and isotopic compositions in “Approach 2”.

3.4 Discussion

3.4.1 Interpretation of the Fitted Parameters in "Approach 2"

The combination of C-CSIAs and their RTM-based interpretation provided a novel and unique way to quantify the biodegradation kinetics that occurred in the different parts of the SBS.

The degradation of PCE and TCE occurred both upgradient (reactive zone RZ1) and downgradient (reactive zone RZ2) of the AN barrier. The higher degradation rates in RZ2 (k_{RD2} = 6.5 y^{-1} for PCE and k_{RD2} = 2.9 y^{-1} for TCE) compared with RZ1 (k_{RD1} = 0.3 y^{-1} for PCE and k_{RD1} = 0.2 y^{-1} for TCE) were explained considering the effect of the injected substrate in the AN barrier, proving its effectiveness in biostimulating the RD of higher chlorinated ethenes.

The fact that k_{RD} of PCE was higher than the k_{RD} of TCE was explained by considering that the degradation process tends to slow down for less chlorinated compounds (Cichocka et al., 2007; Hourbron et al., 2000; Liang et al., 2007; Renpenning et al., 2015; Wiegert et al., 2013). Microorganisms such as *Dehalococcoides* and *Dehalobacter* preferentially undertake the RD of higher chlorinated ethenes due to the higher energetic yields associated with their reduction compared with the RD of lesser chlorinated ethenes (Dolinová et al., 2017a; Tiehm and Schmidt, 2011).

Degradation rate constants for PCE and TCE upgradient of the AN barrier (k_{RD1}) were of the same order of magnitude as those reported in Table 3.1, which were obtained from the compilation by (Powell et al., 2014). Note that these authors analyzed biodegradation in sites exclusively undergoing natural attenuation. The similarity of degradation rates between our study and that compilation suggested that dehalogenating bacteria in the study site were able to carry out an important process of degradation of higher chlorinated ethenes even without the addition of substrates. However, given the high contaminant concentrations, the process of natural attenuation was not enough to abate the concentrations of PCE and TCE to under a satisfactory level, as demonstrated by the high concentrations of both compounds at Pz13. Even though the k_{RD2} values were lower than the maximum values observed for natural attenuation at some sites (in particular for PCE, for which a maximum rate of 29.00 y^{-1} was observed), they were still much higher than the mean literature values (Powell et al., 2014).

C-CSIA data showed an important isotopic enrichment of TCE from Pz13 to AEext4. Since CSIA data in the middle borehole 206S for TCE were not available, uncertainties remain about how much of the observed isotopic enrichment was produced upgradient and downgradient of 206S through RD and OX, respectively. While TCE is preferably degraded through RD, a few studies reported its degradation under aerobic conditions (Ryoo et al., 2000; Wang et al., 2019; Zalesak et al., 2017; Zimmermann et al., 2020). However, we believe that TCE OX is much less effective than RD, as no specific aerobic microorganism specialized in TCE degradation has been found to date in the study area. If part of the observed TCE enrichment in AEext4 were produced by OX at the AE barrier, a lower ε_{RD} would be needed for TCE. This would result in a substantially lower calibrated ε_{RD} for TCE

compared with PCE, which is not usually observed, since ε values for RD of chloroethenes by *Dehalococcoides* and *Dehalobacter* tend to decrease from the higher to the lower chlorinated compounds (Cichocka et al., 2007; Hourbron et al., 2000; Liang et al., 2007; Renpenning et al., 2015; Wiegert et al., 2013). The same considerations apply to PCE. In this case, we could safely rule out aerobic degradation since evidence of this process in the literature is scarce (Huang et al., 1999; Tiehm and Schmidt, 2011).

Degradation of *cis*-DCE and VC was more efficient through OX rather than RD, as expected. The literature ε_{OX} values considered for these compounds spanned a huge range, thus the resulting k_{OX} values differed markedly (0.7–155 y^{-1} for *cis*-DCE and 1.7–12.6 y^{-1} for VC). However, even when using the lowest literature values for ε_{OX} (−19.9‰ for *cis*-DCE and −8.3‰ for VC), a certain degree of degradation was produced nonetheless (0.9 y^{-1} and 1.5 y^{-1} for *cis*-DCE and VC, respectively). Moreover, VC degradation through OX was hugely underestimated since $\delta^{13}C_{VC}$ calculated in 206S by the model was higher than the actual value ($\Delta^{13}C$ = 7.5‰). This meant that the calibrated k_{OX} of VC reflected only part of the enrichment produced by OX through the AE barrier from 206S and AEext. Notwithstanding the uncertainty of the ε_{OX} values, the resulting k_{OX} showed that *cis*-DCE and VC degradation at the AE barrier was stimulated much more efficiently than in anaerobic conditions. However, the k_{OX} ranges for these two compounds comprised much lower values compared with the literature values (Table 3.1).

The slight increase in concentrations observed from 206S to AEext4 for all compounds could not be reproduced considering that only oxidation was active between these two piezometers, and thus, no daughter compound was produced via RD from 206S onward. This suggested that RD may continue even after the onset of OX at 206S. This would allow for producing TCE, *cis*-DCE and VC via RD, even at the AE barrier. However, the concentrations of PCE and TCE were not high enough to produce the increase observed for *cis*-DCE and VC concentrations, which would be even higher than observed, since *cis*-DCE and VC were simultaneously being degraded via oxidative pathways. Moreover, the same increase was observed for PCE, which is the parent compound. Thus, a more likely explanation might be that 206S did not lie perfectly on the hypothesized flow path.

3.4.2 Limitations and Future Developments

Although the use of C-CSIA and RTM was demonstrated to be critical to disentangle the processes that occurred at the site, the model could not reproduce the entire behavior of VC isotopic data. For instance, the model did not correctly simulate the marked drop in $\delta^{13}C$ observed in May 2021 at 206S (d = 164 m) (Figure 4). Future developments are envisioned to improve the understanding of the processes occurring at the study site and obtain more robust modeling tools that are able to make predictions about the fate of contaminants. Specifically, future studies shall consider the following limiting factors of the present work.

Processes not included in the reactive model. Our model assumed that biodegradation was the sole process that altered the chloroethene concentrations and isotopic composition. However, other processes, such as volatilization (Poulson and Drever, 1999), could remove organic compounds from the aquifer and cause isotopic fractionation. Volatilization alters the isotopic fingerprint, reducing the $\delta^{13}C$ value while decreasing the concentrations of polluted groundwater. Since air sparging takes place at the AE barrier, volatilization could be invoked to explain the drop in VC concentration coupled with the huge decrease in $\delta^{13}C_{VC}$ observed from Pz10 to 206S. However, to the best of our knowledge, $\delta^{13}C$ depletion during volatilization was only demonstrated for TCE (Chapelle et al., 1996; Jeannottat and Hunkeler, 2012; Kouznetsova et al., 2010) and dichloromethane (Jeannottat and Hunkeler, 2012), but never for VC.

Use of first-order degradation rates. Our kinetic constants were calculated using a first-order model for which the rates depended linearly on the k value and the compound concentration (Equation 3.1). While the model provided excellent fitting of the observed data, there are many factors that could nonlinearly influence the degradation rates along a flow path. One of them is the presence of alternative terminal electron acceptors (TEAs), which can compete with chloroethenes for hydrogen produced by the fermentation of the organic substrate injected and the organic matter naturally present in the site (Maillard et al., 2003; Yu and Semprini, 2004). Iron and sulfate are the most important TEAs to consider since they are present in very high concentrations at the study site (Huang et al., 1999; Jeannottat and Hunkeler, 2012; Poulson and Drever, 1999). The first-order model did not consider the so-called “Haldane inhibition”, i.e., the inhibition of chloroethene RD due to its own concentration (Amos et al., 2007; Cupples et al., 2004; Widdowson, 2004; Yu and Semprini, 2004). It also ignores the competition with higher chlorinated ethenes. In fact, higher chlorinated solvents are preferentially used as a source of energy, inhibiting the degradation of lesser chlorinated compounds (Abe et al., 2009; Cupples et al., 2004; van Warmerdam et al., 1995; Yu et al., 2005; Yu and Semprini, 2004).

Use of a one-dimensional reactive transport model. Our 1D reactive transport model assumed that the flow path perfectly crossed the five boreholes analyzed in this work. However, this remained an approximation of the more complex and multidimensional real-life aquifer system. Such a system is composed of multiple flow paths due to the presence of multiple boundary conditions (such as the multiple pumping wells injection and extracting air and water to the soil), and the ubiquitous presence of soil heterogeneity. For instance, concentrations and isotopic data at 206S may be affected by the mixing of different flow paths. This could explain the slight increase in concentrations observed from 206S to AEext4, which could not be reproduced by considering a single flow path, as discussed in Section 4.5.1.

Support from other isotopes. Our study was based on C-CSIA, which is widely adopted to study biodegradation processes in complex aquifers. However, other isotopes could be adopted to achieve a better comprehension of degradation processes, as well as a better assessment of the ISB

efficiency. In this sense, the acquisition of chlorine CSIA data (Abe et al., 2009; van Warmerdam et al., 1995; Zimmermann et al., 2020) could provide further information regarding the degradation pathways, as well as provide an additional constraint on the calibrated model parameters.

3.5 Summary and conclusion

Compound-specific carbon isotope analysis (C-CSIA) data and geochemical models were used to evaluate the efficiency of an 800 m-long SBS in Italy. This system was installed for the clean-up of a solute plume that originated from a former landfill in Northern Italy. The combination of these different tools and methodologies is novel and helped to disentangle the complex, nonlinear processes that occurred at different parts of the contaminated aquifer. Specifically, it helped with evaluating and quantifying natural biodegradation and anaerobic and aerobic biostimulation enhancing reductive dechlorination (RD) and oxidation (OX).

The combined use of concentration and CSIA data, which were interpreted using a properly calibrated geochemical model, was critical to identifying the relative impact of the different processes taking place in the different portions of the analyzed flow path. The following conclusions were drawn from this study.

The temporal trends of the observed concentrations suggested that the SBS was highly effective at degrading chloroethenes. The median values of PCE, TCE and *cis*-DCE dropped by >99% and VC dropped by >80%. The sequential effects of anaerobic and aerobic biostimulation were consistent with the trends in Eh and redox-sensitive species (Fe, Mn, SO_4^{2-}, NH_4^+).

Natural biodegradation of PCE and TCE took place upgradient of the AN barrier. Here, first-order degradation rate constants that measured the efficiency of the RD (k_{RD}) were k_{RD1} = 0.3 y^{-1} and k_{RD1} = 0.2 y^{-1}, respectively. Although this demonstrated the ability of the indigenous microbial populations to carry out RD without the addition of stimulating substrates, natural biodegradation was inefficient at producing a significant reduction in PCE and TCE concentrations. The resulting reaction rate constants estimated from boreholes downgradient of the AN barrier (k_{RD2}) were higher (k_{RD2} = 6.5 y^{-1} for PCE and k_{RD2} = 2.9 y^{-1} for TCE) compared with those obtained upgradient of the AN barrier. This suggested that biostimulation was required to make RD effective for the degradation of higher chlorinated compounds. Nonetheless, the very low or null estimated k_{RD2} for *cis*-DCE and VC (k_{RD2} = 0.6 y^{-1} and k_{RD2} = 0, respectively) indicated that RD was insufficient to complete the dechlorination process, further supporting the need for the SBS.

The degradation of *cis*-DCE and VC was better accomplished through OX, which was stimulated by the AE barrier. Indeed, first-order degradation rate constants measuring the efficiency of the OX (k_{OX}) were much higher (k_{OX} = 0.7–155 y^{-1} for *cis*-DCE and k_{OX} = 1.7–12.6 y^{-1} for VC) than the RD rates estimated for these species.

4 Multidimensional Reactive Transport Modeling of Sequential Bioremediation and pump-and-treat in a heterogeneous aquifer affected by chloroethenes

4.1 Introduction

Laboratory analyses and field-scale piloting tests suggested that a sequential bioremediation system (SBS) stimulating reductive dechlorination (RD) and oxidation (OX) is an effective way to remove tetrachloroethene (PCE) and its breakdown products from the site (Casiraghi et al., 2022a). The actual occurrence of chloroethenes biodegradation was further investigated through a modeling analysis based on concentration and C-CSIA data acquired in selected piezometers along a specific groundwater flow path (Casiraghi et al., 2022b). The 1D model developed using the code PHREEQC (Parkhurst and Appelo, 2013) was able to reproduce the field observations, and indicated that anaerobic and aerobic biodegradation were actually being stimulated by the biobarriers.

Although Casiraghi et al. 2022b's model helped elucidating the occurrence of biodegradation processes taking place at different distances from each biobarrier, the 1D model could be used to make "upscaled" predictions of the fate of the contaminant plume at the bulk aquifer scale. For instance, the model could not be used to compute the sitewide mass loadings of chloroethenes exfiltrating along the entire outflow boundary (i.e. the ALRC). Moreover, the 1D model did not simulate the pump-and-treat (P&T) system, which is currently active and coupled to the bioremediation for the aquifer cleanup. As P&T systems entail higher operational costs than bioremediation, decision makers are interested in studying the potential effects of deactivating the P&T system on the cleanup operation.

A new model able to make such predictions would be highly desired to assist decision makers when making optimal decisions about the site management and operations. To this end, this chapter introduces the development and use of a two-dimensional (2D) reactive transport model (RTM) that extends the predictive capabilities of the 1D model. The 2D RTM was created using RT3D (Clement, 1999; Clement et al., 1998), a code that can simulate multispecies reactive transport in groundwater. RT3D was chosen for this study as it efficiently couples the widely adopted MODFLOW groundwater flow model (Harbaugh and McDonald, 1996) with the multispecies transport code MT3DMS (Zheng and Wang, 1999). Compared to the latter code, RT3D extends its capabilities by accommodating user-specific kinetics and sorption processes of sequential chains of first order "parent-daughters" reactions, such as those controlling the transformation of PCE into its less chlorinated byproducts.

The overarching aim of this chapter was to propose a general methodology that can be readily reproduced in virtually any other site where chloroethenes are affecting the groundwater resources. Specifically, our approach can be used to optimize aquifer cleanup operations involving sequential bioremediations and/or P&T systems, rendering them more cost effective. For what concerns the

case study, the model analysis was developed for two specific goals. The first goal was the estimation of the total chloroethenes loadings (L) exfiltrating at the ALRC canal, by computing the discharge rates (Q) at different positions of the downstream boundary and the corresponding aqueous concentrations (C) of the different species. The second goal was to incorporate the P&T system into the model and evaluate the effect of its deactivation on the biodegradation efficiency and resulting contaminant loadings. The aim was to point out the relative contribution of the P&T in the system and, eventually, determine if the P&T operations could be safely terminated or should be continued.

Since selecting the adequate model parametrization to set up a RTM is always complex, a highlighted aspect of this study was the comparison between the model results obtained with a heterogeneous (i.e., spatial variable) distributions of the aquifer parameters compared to a more parsimonious modelling approach embedding homogeneous (i.e., spatially constant) parametrization. Specifically, we compared models with heterogeneous first-order kinetic rate constants (k) controlling the time-dependent degradation of each chloroethene species and analyzed how a different parsimoniousness in the model parametrization can lead to different model outcomes, and thus to different courses of action in the site.

This work is complemented by supplementary material (SM4), deposited in the online repository.

4.2 Materials and methods

4.2.1 Background

The degradation of chloroethenes is strongly controlled by the aquifer redox conditions. Reductive dechlorination (RD) tends to be more effective on more chlorinated compounds (PCE, TCE) than on less chlorinated ones (DCE, VC), which are usually better degraded via oxidation (OX) under aerobic conditions. In the previous chapters, we showed that the study area is naturally characterized by weakly reducing conditions, which generate a slow natural attenuation of PCE and TCE and virtually no attenuation of DCE and VC. Bioremediation is stimulated by the two biobarriers, which sequentially (i.e., along the main groundwater gradient) enhance RD and OX. Along the mean aquifer hydraulic gradient, three general “reaction zones” (RZs) can be envisioned:

1) A first reactive zone (RZ1), upgradient of the anaerobic (AN) barrier, is characterized by non-stimulated reducing conditions. Natural attenuation occurs through RD, whose rates are lower than in the downgradient adjacent zone. In this zone, OX is considered negligible.
2) A second reactive zone (RZ2), located between the AN and AE barrier, is affected by biostimulation induced by the AN barrier. Enhanced RD occurs at higher rates than in RZ1. As in RZ2, OX is considered negligible in this zone, too.
3) A third reaction zone (RZ3), located in proximity of the ALRC, is characterized by strongly oxidizing conditions induced by the AE barrier. Here OX is expected to be active on DCE and VC. Conversely, RD is considered negligible.

In Casiraghi et al (2022b), zone-specific first-order kinetic rate constants (k) were used to parametrize the PHREEQC 1D model, which aimed at reproducing one of the multiple flow paths of the three-dimensional aquifer flow field. Such path was assumed to follow the mean groundwater flow direction between the landfill (model inflow boundary) and the canal (outflow boundary). Data collected in piezometers lying on this flow path were used as calibration targets for the PHREEQC model.

The main limitations of the 1D model were that (1) the geometry of the hypothesized flow path was not derived from a rigorous, calibrated flow model, but on a semi-qualitative estimation of the aquifer streamlines obtained using measured piezometric levels and interpolated maps. Another limitation was that (2) the 1D model did not consider spatial variation (transversal to the main groundwater direction) of the hydrogeological characteristics of the aquifer. As already acknowledged in Casiraghi et al. (2022b), maps of concentrations and diagrams of environmental parameters (e.g., the oxidizing-reducing potential, ORP) variations along different flow paths displayed in Figure 4.1 and in S4.4 (SM4) show well-defined heterogeneous patterns. Heterogeneity is controlled by the spatially variable composition of the contaminant source (i.e., the landfill leachate) as well as by biodegradation processes. Microbiological content is heterogeneous in the aquifer, as well. By analyzing groundwater samples collected in the site, Casiraghi et al. (2022b) and Bertolini et al. (2021)

determined variable relative abundance of *phyla* among different microbial communities and variable amount (number of cells or gene copies per liter) of bacteria. Microbial heterogeneity can influence the relative variation in concentrations of the difference chloroethenes species, as bacteria are the main catalyzers of the biodegradation reactions of organic compounds. Additional information related to microbiological analyses performed in the site has been reported as Supplementary Material (SM4).

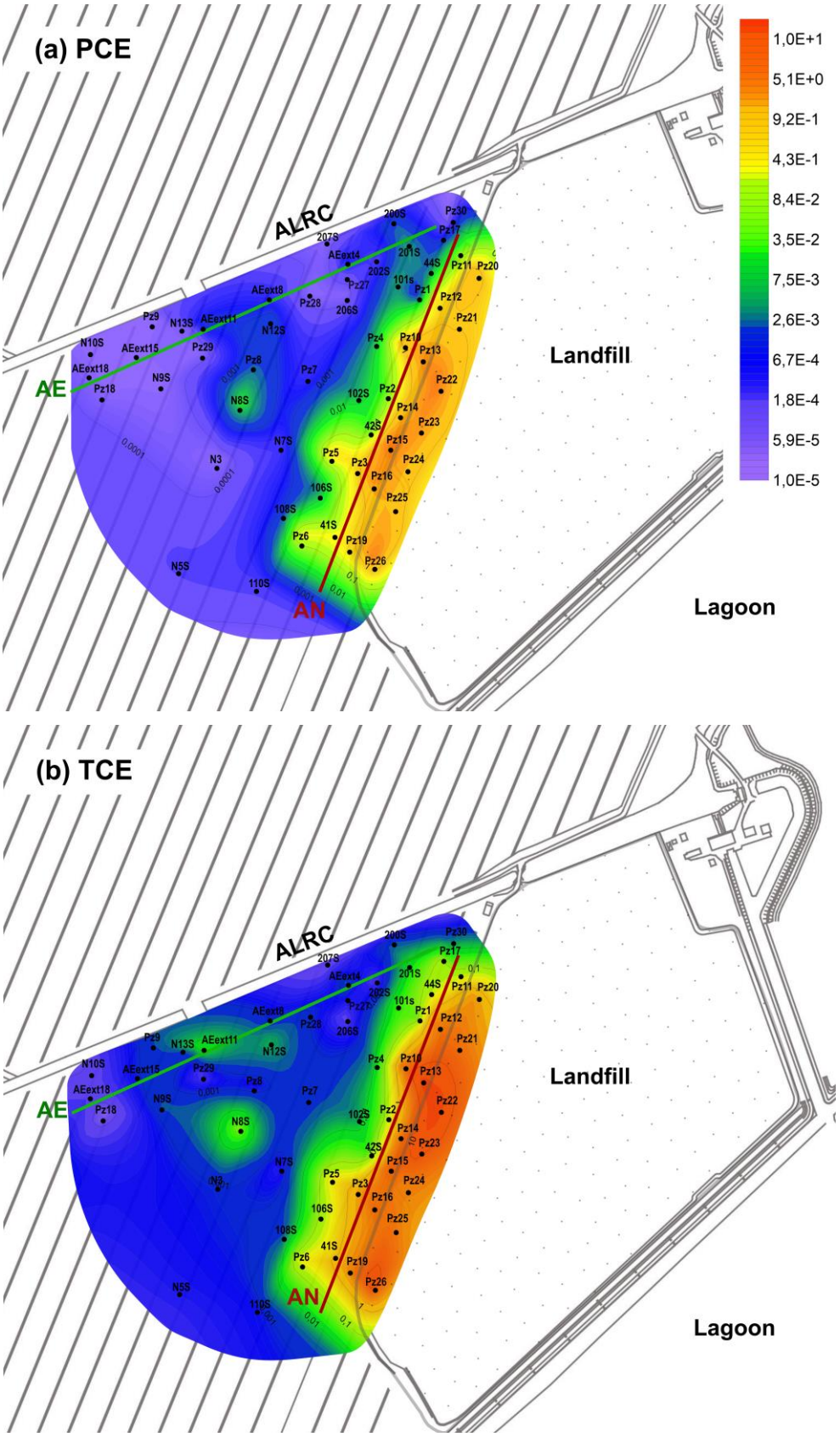

Figure 4.1. Maps of chloroethenes concentrations: (a) PCE; (b) TCE; (c) DCE; (D) VC. AN = anaerobic barrier; AE = aerobic barrier.

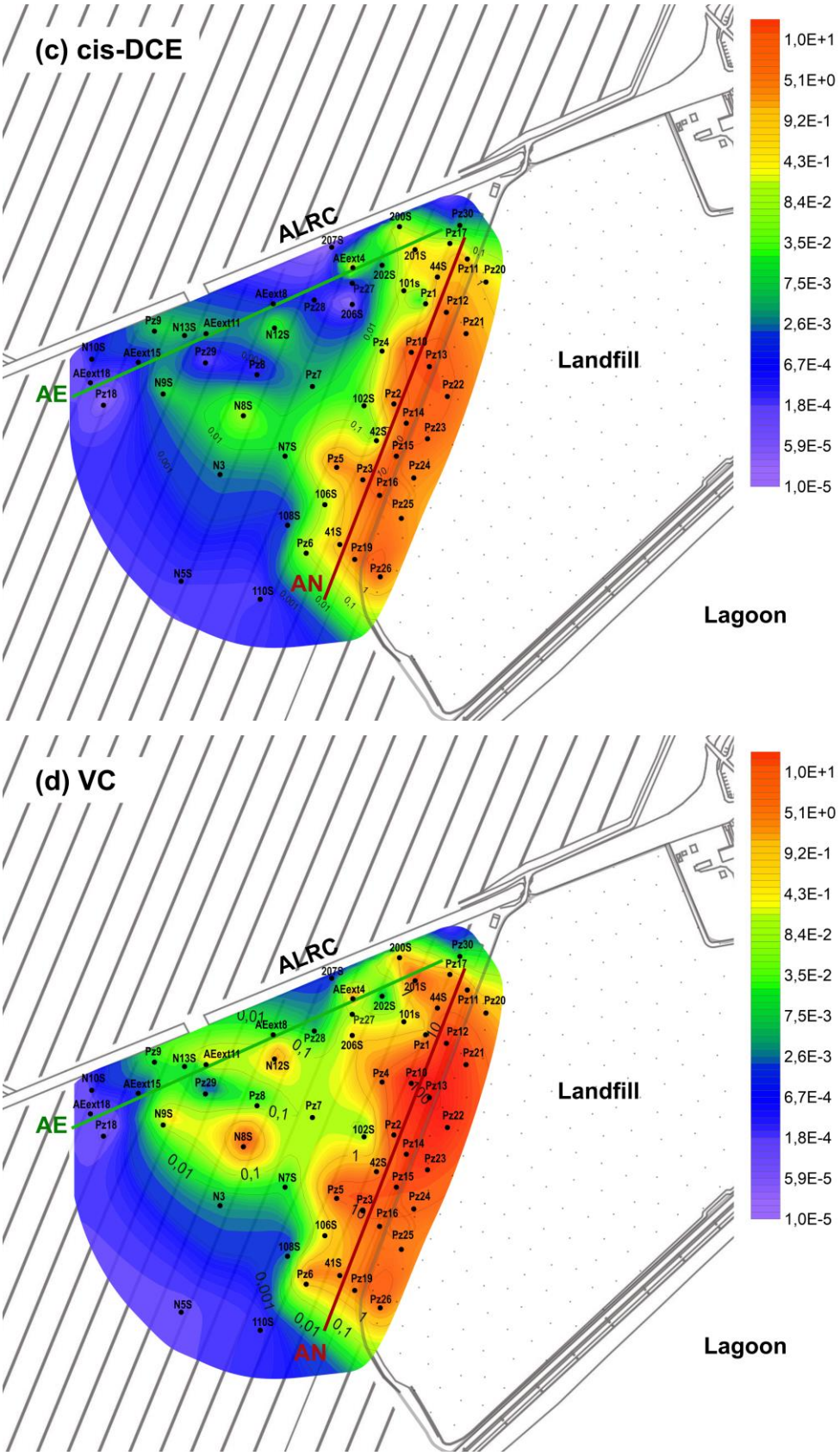

Figure 4.1. (continues) Maps of chloroethenes concentrations: (a) PCE; (b) TCE; (c) DCE; (D) VC. AN = anaerobic barrier; AE=aerobic barrier.

4.2.2 Model setup

To account for the multidimensional nature of the flow field, the existence of a P&T system and the impact of hydrogeological and biochemical heterogeneities, a new 2D reactive transport model (RTM) was developed. The model was set up in two stages. First, we set up and calibrated a flow model using the code MODFLOW (Harbaugh, 2005). Then, the geochemical transport was resolved using the code RT3D (Clement, 1997). RT3D adopts an operator splitting approach to couple the seepage rates (q) calculated by MODFLOW with the multicomponent reactive modules. Among such modules, RT3D embeds a module for the anaerobic and aerobic biodegradation of PCE/TCE/DCE/VC through first-order biodegradation kinetics. Species-dependent sorption parameters can also be included. The model was built using the graphical user interface Processing Modflow 8 (https://www.simcore.com).

The groundwater model simulated an area of about 630000 m^2, discretized in regular cells of 180 columns and 140 rows, with cells dimension Δx=Δy=5m. In the vertical direction, a single layer was assumed, rendering the model a "quasi-three-dimensional" model. Each cell has a top elevation of 0 m above sea level (a.s.l.) and a bottom elevation of -10 m a.s.l., according to the average aquifer thickness of about ten meters. The layer property was set to automatically switch between confined and unconfined conditions depending on the local pressure status. This setup was consistent with the discontinuous presence of silty materials acting as aquitards in adjacent sites with similar geological contexts (Beretta and Terrenghi, 2017; Dalla Libera et al., 2021, 2020).

The model was developed assuming steady-state conditions, considering May 2021 as the reference simulated period.

The boundary conditions and parameters were set up as follows. The lagoon acted as inflow boundary and was modelled using prescribed head (1st kind, Dirichlet) boundary condition (MODFLOW's CHD package). To account for the effects of tidal fluctuations, we set the hydraulic head (h) at the lagoon boundary to a constant h=0.45 m, which corresponds to the mean sea level measured in May 2021 at the mareograph closest to the site. The outflow ALRC canal was simulated as a head-dependent (3rd kind, Cauchy) boundary condition (RIV package). The ALRC head was set to h=-2.2 m, which corresponds to the mean head level measured in a borehole located inside the canal. The elevation (z) of riverbed bottom was estimated as z=-4m, while the river width (w) was set to w=-3m. The P&T wells were simulated using prescribed flux (2nd kind, Neumann) boundary condition (WEL package). The pumping rates (Q_w) used in in the model are reported in

Table 4.2. A prescribed-flux condition was used to simulate the recharge rates (r_c) associated to precipitation (RCH package).

The conductance of the ALRC bottom sediments (C_r), the aquifer horizontal hydraulic conductivity (K) and r_c were estimated through inverse calibration. The flow model calibration was performed using the code PEST (Doherty et al., 1994). Calibration targets were head observations measured in May 2021 at nineteen boreholes in the site. Specifically, since multiple readings were available at

each borehole, the median value of the observations was used as calibration target. For K, we considered an initial (i.e. pre-calibrated) value K=10 m d^{-1}, consistent with the nature of the aquifer material (medium-size sands embedded in a silty matrix). Since one of the main goals of this work was to isolate the impact of heterogeneous reaction rates occurring in the site, an effective (isotropic and homogeneous) K was considered. For the riverbed conductance, initial values of C_r were assumed one order of magnitude lower than the initial K. The range of calibration for r_c varied between 4 and 10% of the mean daily precipitation (P) registered in May 2021, which was P = 4×10^{-3} m d^{-1}.

Table 4.1. MODFLOW and RT3D model input parameters. * indicates the calibrated values.

Parameter	**Value**	**Unit**
Flow simulation time	Steady state	
Transport simulation time	8000	d
Grid spacing (columns, **Δ**x × rows, **Δ**y)	5 × 5	m
Model length	700	m
Model width	900	m
Number of layers	1	
Number of cells	25200	
Number of active cells	20527	
Aquifer type	Confined/unconfined	-
Aquifer top elevation	0	m a.s.l.
Aquifer bottom elevation	-10	m a.s.l.
Horizontal hydraulic conductivity* (K)	15	m d^{-1}
Aquifer recharge (r_c)*	0.00016	m d^{-1}
Porosity (ϕ)	0.25	-
Longitudinal dispersivity (α_L)	25	m
Transversal horizontal dispersivity (α_{Th})	2.5	m
Bulk density (ρ_b)	1.6	g cm^{-3}

Table 4.2. MODFLOW model Boundary Conditions (BCs).

Element		**BC**	**Parameter**	**Value**	**Unit**
Lagoon		Constant head	Hydraulic head	0.45	m
Outflow canal		Constant head	Hydraulic head	0.46	m
ALRC		River	Head in the river Conductance*	-2.0 15.8	m m^2 d^{-1}
P&T extraction wells	P1	Constant flux	Pumping rate	-60	m^3 d^{-1}
	P2			-24	
	P3			-30	
	P4			-19	
	P5			-24	
	P6			-50	
	P7			-39	
	P8			-32	

The reactive transport model was parametrized as follows. As the starting time of the contamination is unknown, the total transport simulation time was set to 30 years, a sufficiently large value to reach

steady-state transport conditions. The pore velocity (v) is calculated by RT3D dividing the MODFLOW seepage rates (q) by an effective porosity (ϕ) we set equal to ϕ = 0.25, according to the typical literature value for sandy aquifers (e.g. Domenico and Schwartz, 1998). The longitudinal dispersivity (α_L) was equal to $\alpha_L = 25$ m while the transversal dispersivity (α_{Th}) was set to α_{Th}=2.5 m, following the classic ratio $\alpha_L/\alpha_{Th} = 10$ reported in the compilation by Gelhar et al. (1992). The value of the longitudinal dispersivity is similar to the one used for the 1D-model by (Casiraghi et al., 2022a) and satisfies the stability condition defined by the Péclet numbers. Since RT3D does not allow species-dependent diffusion coefficients, a single, effective molecular diffusivity coefficients (D_m) was set as D_m=7.5 x 10^{-5} m^2 d^{-1}, which corresponds to the average diffusion coefficient ($\overline{D_m}$) of the different chloroethenes species (Clapp et al., 2004), as reported in Table 4.3. Linear equilibrium isotherms were assumed to compute solute sorption on the soil matrix and the resulting solute retardation (R). The adopted species-dependent distribution coefficients (K'_D) are reported in Table 4.3 for each chloroethene.

Table 4.3. RT3D model input parameters. K'_D is the species-specific distribution coefficient (m^3 kg^{-1}), β is the species-specific retardation factor, D_m is the species-specific molecular diffusivity coefficient and $\overline{D_m}$ is the average molecular diffusivity coefficient (m^2 d^{-1}).

Chloroethene	K'_D	β	D_m	$\overline{D_m}$
PCE	9.5 x 10^{-4}	7.08	6.2 x 10^{-5}	7.5 x 10^{-5}
TCE	6.07 x10^{-4}	4.88	6.9 x 10^{-5}	
cis-DCE	3.96 x 10^{-4}	3.53	7.8 x 10^{-5}	
VC	2.17 x 10^{-4}	2.39	9.2 x 10^{-5}	

The transport boundary conditions were set as follows. At the inflow boundary (the landfill), prescribed concentration was set up in the cells located along a line parallel to the landfill downgradient boundary. This line crosses the piezometers located in the landfill (Pz20, Pz21, Pz22, Pz23, Pz24, Pz25 and Pz26), which provide the species concentrations in the intercepted cells. The concentration in the other source cells were mapped using a deterministic (natural neighbor) interpolation between pairs of observations. The outflow boundary condition was set up at the ALRC as a free exit mass flux boundary condition, which allows solutes to exit by both advective and dispersive fluxes.

The parameters controlling the timescales of the anaerobic and aerobic biodegradation were obtained by calibration. In RT3D, reaction kinetics defining the rate of change in concentration of a species can be written as (Clement, 1999)

$$\frac{dC_{PCE}}{dt} = -\frac{K_{PCE}^{RD}\ C_{PCE}}{R_{PCE}} \tag{4.1}$$

$$\frac{dC_{TCE}}{dt} = \frac{Y_{PCE\rightarrow TCE}\,K_{PCE}^{RD}\,C_{PCE} - K_{RD}^{TCE}C_{TCE} - K_{TCE}^{OX}\,C_{TCE}}{R_{TCE}} \tag{4.2}$$

$$\frac{dC_{DCE}}{dt} = \frac{Y_{TCE\rightarrow DCE}\,K_{TCE}^{RD}\,C_{TCE} - K_{RD}^{DCE}C_{DCE} - K_{DCE}^{OX}C_{DCE}}{R_{TCE}} \tag{4.3}$$

$$\frac{dC_{VC}}{dt} = \frac{Y_{DCE\rightarrow VC}\,K_{DCE}^{RD}\,C_{DCE} - K_{VC}^{RD}C_{VC} - K_{VC}^{OX}C_{VC}}{R_{VC}} \tag{4.4}$$

In equations 4.1-4.4, C is the concentration of each species, [mg L^{-1}], t is the time [d], K_{RD} and K_{Ox} are the first-order kinetic rate constants for RD and OX, respectively [d^{-1}] and Y represents the stoichiometric yield values [d^{-1}]. The latter are estimated from the reaction stoichiometry and molecular weights. The values can be found in the RT3D manual (Clement, 1999, p.35). The reader is referred to the manual for the other equations not reported here.

One goal of this study was to evaluate the implication of the spatial heterogeneities in biodegradation rates. In RT3D, a different value of k_{RD} and k_{OX} can be assigned to each model cell, but deterministically imposing cell-specific reaction rates is almost never possible due to the limited sites characterization and scaling effects in the measurements (stochastic methods may be indeed invoked, as discussed later). We thus considered and analyzed two possible spatial distributions of the first-order degradation constants.

The first distribution accounts for three reactive zones, as defined in the previous section. Each zone is parameterized by a single, homogeneous k_{RD1}, k_{RD2} and k_{OX}, which corresponds to RZ1, RZ2 and RZ3, respectively (Figure 4.2a). The same analysis carried out in Chapter 3 (Casiraghi et al., 2022b) on contaminants concentrations and environmental parameters along the investigated flow path, was extended to the whole site area, corroborating the subdivision in three RZs adopted in the previous study. The complete analysis can be found in the SM4.

The second distribution accounts for a division of the flow systems into a finite number of “transects” (T), each one corresponding to a specific flow path between the landfill to the ALRC. Initially, we identified one transect for each piezometer located in the landfill (i.e., at the source), for a total of seven transects (sequentially labelled from T1 to T7), as depicted in Figure 4.2b. This decision was made to maximize the use of the concentration at the landfill piezometers to parametrize the source of each flow path and to replicate (and extend) the modeling approach developed in our previous study. The transect considered in the 1D model in Casiraghi et al. (2022b) corresponds to T3 in the 2D model.

The model area to be assigned to each transect was determined through forward and backward particle-tracking simulations carried out with PMPATH, which permitted to identify observation points located along the same streamtube. Similar to the previous "homogeneous" model approach, such transects resulted internally divided into the three aforementioned reactive zones RZ1, RZ2 and RZ3. In this "heterogeneous" model, for each n^{th} transect (n=1,…,N) RZ-specific first-order degradation rate constants were assigned, such that in each transect $k_{RD1} \rightarrow k_{RD1}(n)$, $k_{RD2} \rightarrow k_{RD2}(n)$ and $k_{OX} \rightarrow k_{OX}(n)$. The concentration measured at the piezometers contained in each transect were used to calibrate these transect-specific kinetic rates.

There are no landfill piezometers in the south-westernmost part of the site (i.e., in the proximity of piezometers Pz6, 108S, 110S, N5S, N8S, N3, N9S; Figure 4.2b). However, the AE barrier also extends in this portion of the site, and therefore it is important to simulate biodegradation in this area, too. As such, the south-westernmost part of the site was split into two further transects (T8 and T9). Unlike transects, no distinction between RZ1 and RZ2 was made in T8 and T9. In other words, no subdivision between biostimulated and natural RD was simulated, due to the absence of the AN barrier in this part of the site.

Inverse calibration was not implemented in Processing Modflow 8 to calibrate RT3D models. Therefore, the RTM calibration was performed using a semi-automatic approach, by which we minimized the root mean square error (RMSE) between simulated and observed concentrations using the two different (homogeneous and heterogeneous) configurations. Initial values for k_{RD1}, k_{RD2} and k_{OX} were set equal to those obtained in the 1D model (Chapter 3) and then manually modified until the calculated RMSE for each species was minimized. The results are shown in Table S4.3 and Figure 4.6.

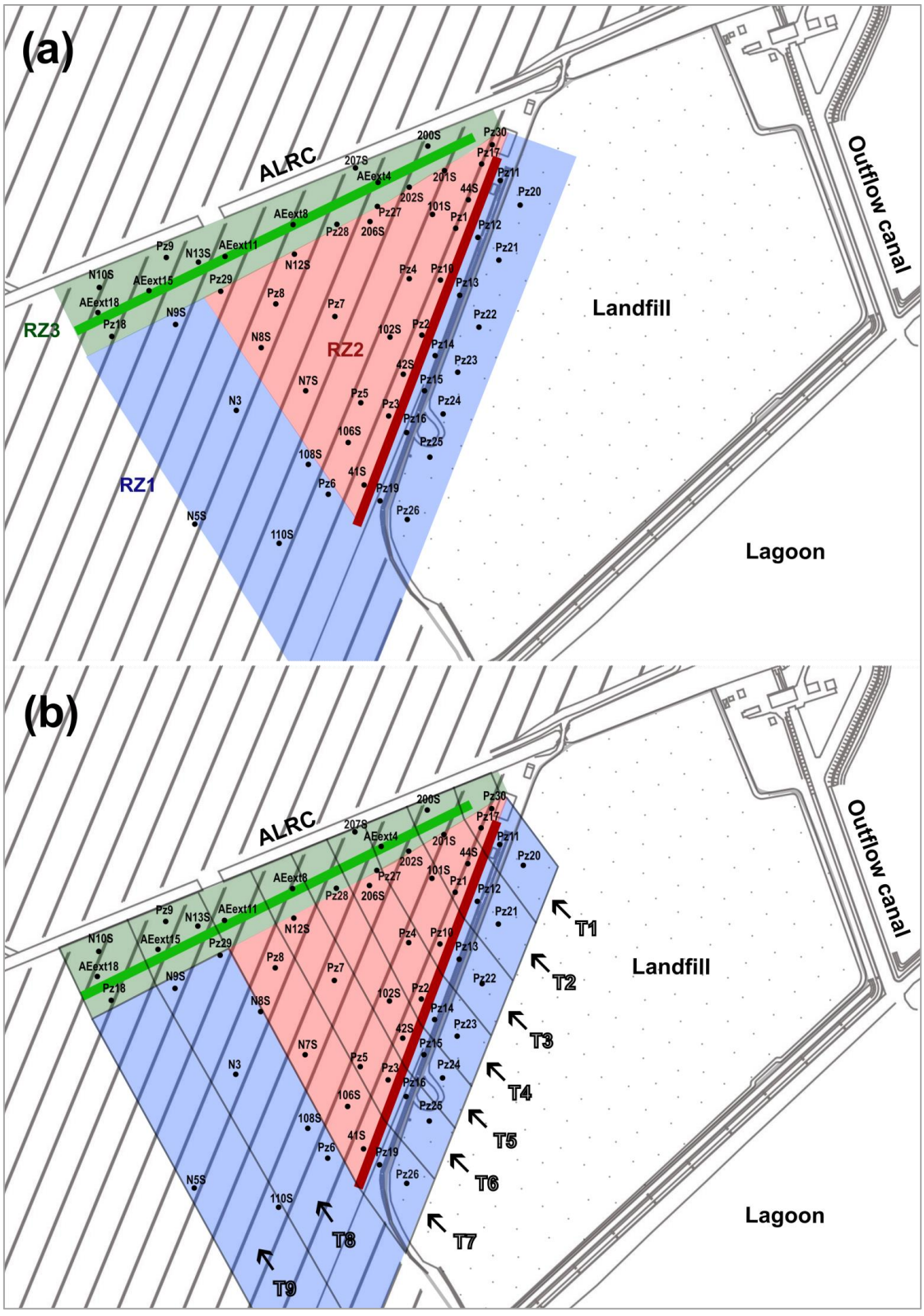

Figure 4.2 (a) Reactive Zones (RZ) in the homogeneous model. RZ1: natural RD (blue); RZ2: biostimulated RD (red); RZ3: oxidation (green).the red and green lines represent the AN barrier and AE barrier, respectively. (b) Heterogeneous model area subdivision. Reactive Zones (RZ) as in the homogeneous model. The red and green lines represent the AN barrier and AE barrier, respectively. Tn identifies a specific transect, where n=1,…,9.

4.2.3 Model-derived indicators

Damköhler numbers (Da) and contaminant loadings were calculated to compare the results obtained from the two different model configurations.

Da is a dimensionless indicator that relates the chemical reaction timescale to the transport or residence timescale. The Da can be computed as

$$Da = k\, C_0^{n-1}\, \tau \qquad (4.5)$$

where k is the kinetic degradation rate (i.e. k_{RD1}, k_{RD2} or k_{OX} in our study), n is the reaction order, C_0 is the initial concentration and τ is a characteristic transport time. A large Da ($>> 0$) indicates that the contaminants degradation dominates over their transport (i.e. more contaminants are removed chemically than they are transported away), while the contrary is true for $Da \rightarrow 0$. Since we adopted first-order kinetics (n=1), Equation 4.5 reduces to

$$Da = k\tau \qquad (4.6)$$

In an advective dominated system, such as the studied aquifer, the characteristic time τ can be calculated as $\tau = d\beta v^{-1}$, where β [-] is the compound-specific retardation factor, d [m] is the length of a portion of aquifer (e.g., the distance from the inflow to the outflow boundaries of a streamtube) with mean pore water velocity v [m d^{-1}]. We used, the particle tracking code PMPATH (Chiang and Kinzelbach, 2003) to compute τ directly, by tracking the travel time of a particle (i.e. a tracer) from the inflow to the outflow boundary. In this way, the Da could be easily calculated for each transect of the flow system, allowing to compare the relative efficiency of biodegradation in the different sectors of the aquifer.

The second indicator was the contaminant loading (L). Daily L were calculated for each chloroethene species and each transect, as follows. We stored the concentration (C) computed by RT3D in each cell of the outflow boundary and multiplied them by the corresponding discharge rates (Q) computed by MODFLOW. For each transect, daily loadings at the outflow boundary (L_{ALRC}) were calculated as

$$L_{ALRC}(n) = \sum_{i=1}^{N_C^{ALRC}(n)} C_i(\mathrm{n})\, Q_i(n) \qquad (4.7)$$

where $N_C^{ALRC}(n)$ denotes the total number of cells in the outflow boundary (the ALRC) within the n^{th} transect.

Another goal of this work was to evaluate the relative importance and the effects of the P&T on the aquifer cleanup. Specifically, we used the model to suggest whether the P&T could be safely terminated (in favor of a reduction in cleanups costs) or if it should be continued (to ensure a lower risk of the plume spreading). To this end, we compared the two indicators (Da and L) calculated from the simulation of different scenarios: a first scenario (called “P&T on”) in which the P&T was active, as in the current real-life situation; a second scenario (called “P&T off”), in which the P&T was turned off. To evaluate the effect of the P&T deactivation, for each transect the difference (ΔL_{ALRC}) between

the loadings from the “P&T off” and the “P&T on” scenario were computed and reported as a percentage, as

$$\Delta L_{ALRC} = \frac{L^{OFF} - L^{ON}}{L^{ON}} \times 100 \qquad (4.8)$$

Positive ΔL_{ALRC} mean that the P&T is succeeding in abating the contaminant loading. Negative ΔL_{ALRC} mean that the contaminant loading is decreasing without the P&T wells. In other words, a negative difference means that the presence of the P&T system is hampering the aquifer bioremediation. The higher ΔL_{ALRC}, the higher the contaminant loadings reaching the ALRC without P&T compared to the loadings exiting the system with an active P&T system.

Since the transects length d varies significantly within the second reactive zone (RZ2), we computed L also at the downgradient boundary of RZ2 (Figure 4.2). Our aim was to single out and quantify the relative efficiency of the anaerobic treatment and estimate how a possible P&T deactivation may affect the RD process. Similar to the calculation at the ALRC, for each transect, daily loadings at the RZ2-RZ3 boundary ($L_{RZ2,3}$) were calculated as

$$L_{RZ2,3}(n) = \sum_{i=1}^{N_C^{RZ2,3}(n)} C_i(\mathrm{n})\, Q_i(n) \qquad (4.9)$$

where $N_C^{RZ2,3}$ denotes the total number of cells along the RZ2-RZ3 boundary within the transect. The difference between the computed loadings with and without the P&T systems ($\Delta L_{RZ2,3}$) was calculated as in Eq. 4.8.

4.3 Results and analysis

4.3.1 Calibrated flow and reactive transport model

A good match between observed and calculated head levels was obtained (Table S4.2 and Figure S4.9 n SM4). Best-fitted parameters were K =15 m d^{-1}, r_c=1.6×10^{-4} m d^{-1} and C_r=15.8 m d^{-1}. The resulting hydraulic conductivity is consistent with the values adopted in the 1D model (K = 14 m d^{-1}), while the recharge rates are in line with the previous model analyses in adjacent areas (Beretta and Terrenghi, 2017; Dalla Libera et al., 2021). The model was fairly sensitive to small variations of K (Figure S4.10 in SM4), which supports the reliability of the calibrated parameters. The spatial distribution of groundwater heads resulting from the calibrated MODFLOW model is mapped in Figure 4.3.

The different transect length and the P&T status (i.e. “on” or “off”) controlled the water residence time (τ) in each transect. The calibration was carried out assuming and active P&T, as in the current real-life situation. When the P&T was “on”, τ calculated considering the whole length of each transect varied between a minimum time of $\tau \approx 360$ d in T1 to a maximum of $\tau \approx 2200$ d in T9. In the simulated scenario with deactivated P&T (“P&T off”), τ was slightly reduced and varied between a minimum time of $\tau \approx 300$ d in T1 to a maximum of $\tau \approx 2100$ d in T9.

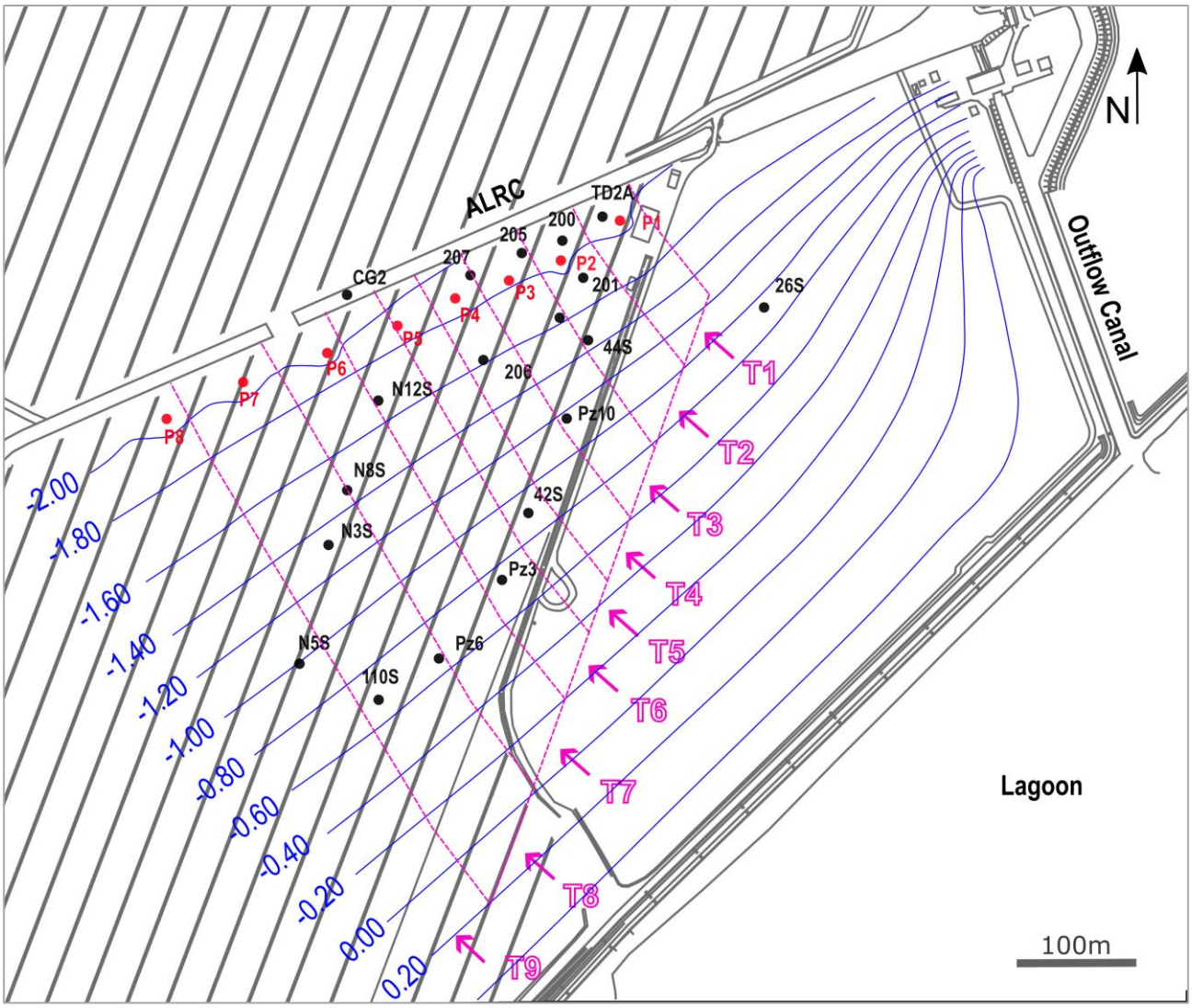

Figure 4.3. Groundwater contours (m a.s.l.) calculated by the groundwater flow model in the "P&T on" scenario.

The calibration of the transport model was also satisfactory (Figure 4.4). For all species, we obtained linear regression coefficients (R^2) above R^2=0.78. The match between observed and simulated concentrations was higher for the heterogeneous model than for the homogeneous model. This is consistent with its higher number of fitting parameters (i.e., the kinetic rates, k) in the heterogeneous model than in the homogeneous model. This allows more flexibility to fit the observed data at the expense of a more complex spatially variable parametrization.

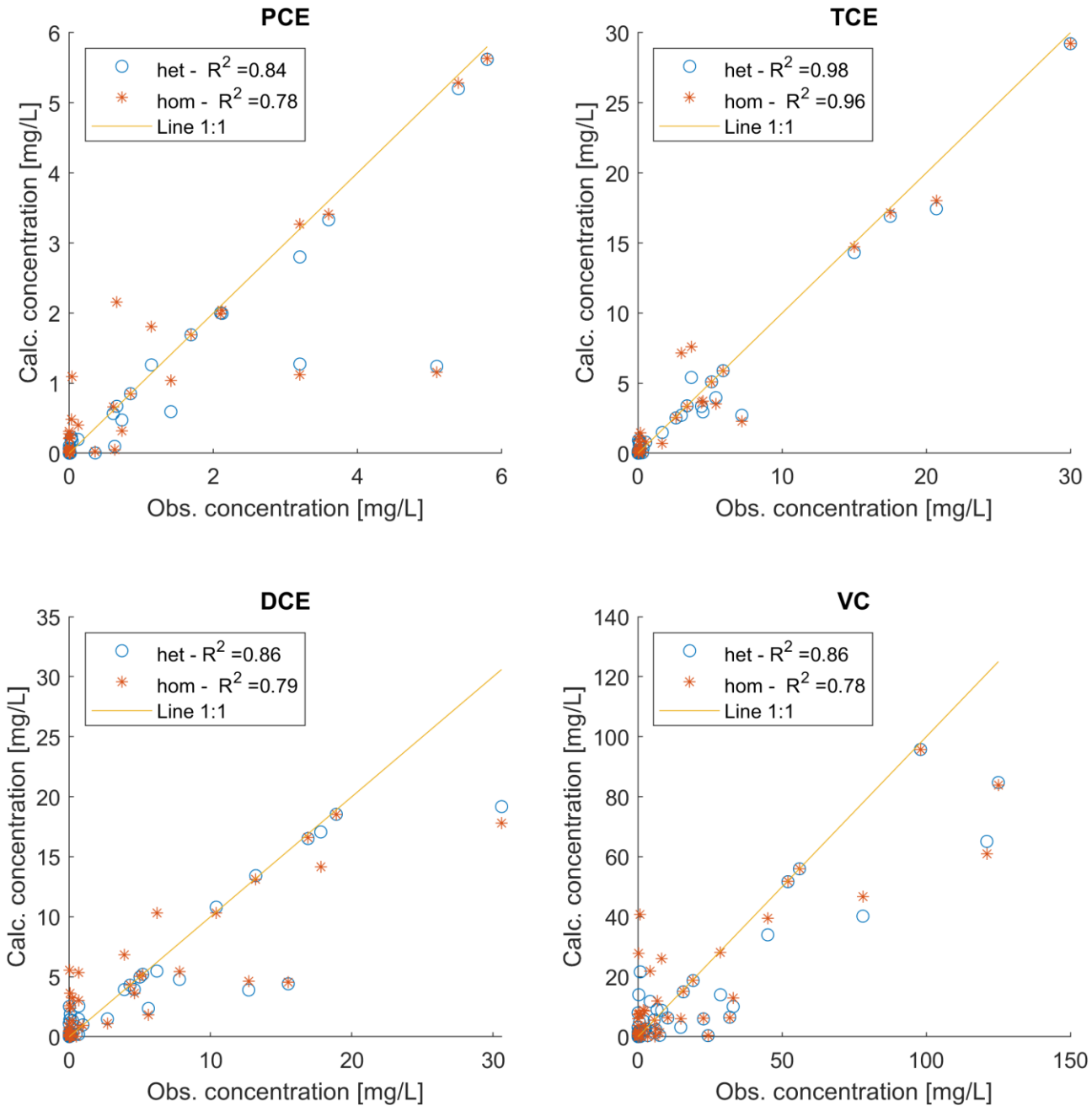

Figure 4.4. Scatter diagrams comparing the observed ("Obs") and the calculated ("Calc") concentrations [mg L^{-1}] using the heterogeneous ("het") and the homogeneous ("hom") model configurations. The goodness-of-fit is expressed through the linear regression coefficient (R^2) between calculated and observed data.

The estimated kinetic rates (k) for the different reactive zones (RZ1, RZ2 and RZ3) were consistent with our previous 1D model (Casiraghi et al., 2022b) and remark the role of the anaerobic and aerobic barriers in enhancing biostimulation. The full set of results is reported in the SM4 (Table S4.3). We found that the kinetic degradation rates in RZ1, which describe natural attenuation (i.e. k_{RD1}), tend to be much lower than those obtained in RZ2 describing biostimulated RD (i.e. k_{RD2}). This is true for each chloroethene species. Both k_{RD1} and k_{RD2} are higher for PCE and TCE than for DCE and VC, indicating that RD is more effective for the more chlorinated compounds. On the contrary, k_{OX} tends to be higher than k_{RD2} for DCE and VC, which confirm that less chlorinated ethenes prefer

oxidative degradation pathways to reducing ones. This proves that the conceptual model developed for the 1D model also works for the new 2D model.

A strong difference was pinpointed among the estimated k values of the heterogeneous model in the different transects (T1 to T9), as graphically shown in Figure 4.5. In this figure, the vertical axes of each subplot report k in logarithmic scales, to maximize the difference among the estimated values. Since in some cases the best-fitted kinetic value was $k = 0$ (Table S4.3), such values were plotted using small colored bars to graphically display null values on log scales. The horizontal axes display the number of transect (n). The red line in each subplot is the kinetic rate obtained from the calibration of the homogeneous model.

For PCE, transect T1 shows the highest rates in RZ1 (k_{RD1} = 0.09 d^{-1}) and RZ2 (k_{RD2} = 0.7 d^{-1}). A general negative trend from T1 to T9 is observed, particularly in RZ2, where a minimum value was found in T9 (k_{RD2}=2 x 10^{-3} d^{-1}). Similar conclusions can be drawn for TCE: maximum rates were observed in T1 in both RZ1 (k_{RD1} = 0.03 d^{-1}) and RZ2 (k_{RD2} = 0.5 d^{-1}), but the negative trend from T1 to T9 was only observed in RZ2, where rates dropped to k_{RD2} = 3 x 10^{-3} d^{-1} in T8 and T9. For both PCE and TCE, k_{RD2} were always higher than k_{RD1}, proving the efficiency of the AN barrier in stimulating RD of higher chlorinated ethenes along its whole length.

For DCE and VC k_{RD1} were always null with the only exception of T7 (k_{RD1} = 18 x 10^{-3} d^{-1} and 0.01 d^{-1}, respectively), meaning that natural RD was active only in a small portion of RZ1. DCE and VC rates in RZ2 were always higher compared to their rates in RZ1 (with the only exception of T7 where k_{RD1} = 18 x 10^{-3} d^{-1} and k_{RD2} = 11 x 10^{-3} d^{-1}) but resulted generally lower than PCE and TCE rates. Maximum rates were observed in T1 for DCE (k_{RD2}= 0.13 d^{-1}) and in T5 for VC (k_{RD2} = 0.05 d^{-1}). The kinetic rates k_{OX} were always null for PCE and TCE since no degradation of these two compounds via oxidative pathways was assumed. For DCE and VC, k_{OX} varies between 8 x 10^{-3} d^{-1}-0.2 d^{-1} and 0.02 d^{-1} -0.12 d^{-1}, respectively.

Recalling that T3 overlaps with the streamtube simulated using the 1D model by Casiraghi et al (2022b), we compared the calibrated degradation rates obtained in T3 with the rates found in the 1D model. In both models, the kinetic rates in the RZ2 are higher than RZ1. However, k_{RD1} and k_{RD2} values were up to one order of magnitude higher in the RT3D model than in the 1D model. Instead, k_{OX} values in the RT3D model remained more similar to the values obtained in the 1D model.

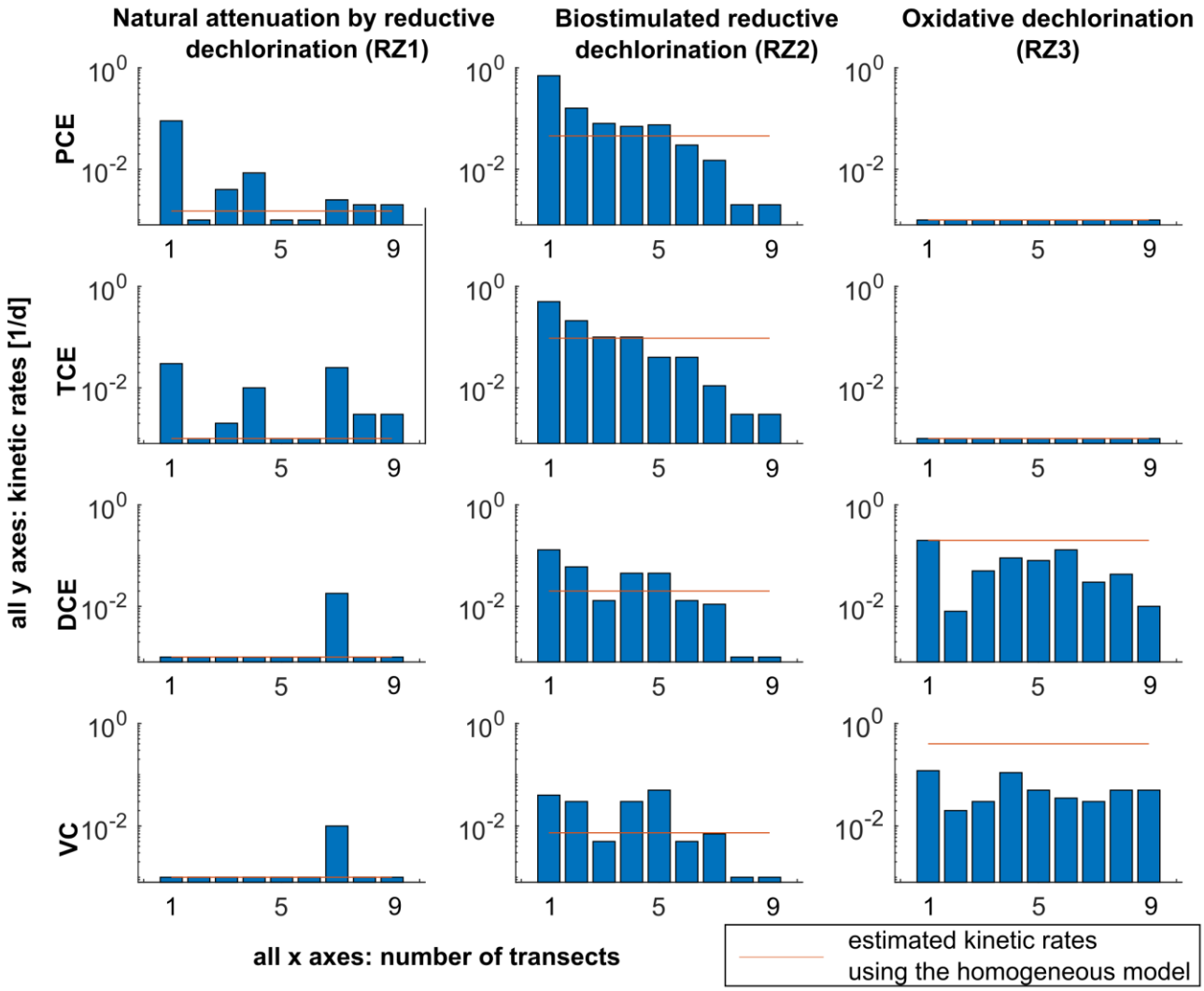

Figure 4.5. Graphical summary of the estimated kinetic rates, k [d^{-1}], obtained from the calibrated transport model. The blue bars show the kinetic rates for each transect, while the red line corresponds to rates obtained from the calibration of the homogeneous model.

In Figure 4.5 the behavior of the heterogeneous model and the behavior of the homogeneous model were compared. For PCE and TCE, k_{RD1} values in the heterogeneous model showed strong fluctuations in RZ1. Some transects have higher k_{RD1} than the homogeneous model, while others have an opposite behavior. For PCE, rates vary between k_{RD1}=1.5 x 10^{-3} d^{-1} and k_{RD2}=46 x 10^{-3} d^{-1} without a clear pattern. Even if in RZ2 the data show a more defined trend, comparing the mean behavior of the transects with that of homogeneous model remains difficult. Therefore, for each reactive zone and species, the arithmetic mean and the 50% percentile (p50) of the cumulative distribution of the kinetic rates were computed as "effective" heterogenous rates (k_{eff}) to be compared with the homogeneous model rates (k_{hom}). The results are plotted in Figure 4.6. In the top plot (a), it could be noticed that the effective rates (vertical axis) never exceed a value of k_{eff}=0.15 d^{-1}, while the rates in the homogeneous model reached much higher values, with a maximum of k_{hom} = 0.4 d^{-1}. The departure between k_{eff} and k_{hom} were particularly remarkable for the oxidative rates of DCE and

VC; specifically, k_{OX} were about four times higher for VC and two times higher for DCE. In the sub-plot (b), which limits the axes to k=0.15, homogeneous and effective heterogeneous rates tended to be more similar (i.e., $k_{hom}/k_{eff} \rightarrow 1$). Being more influenced by extreme values, arithmetic mean tends to overestimate the median (p50) values.

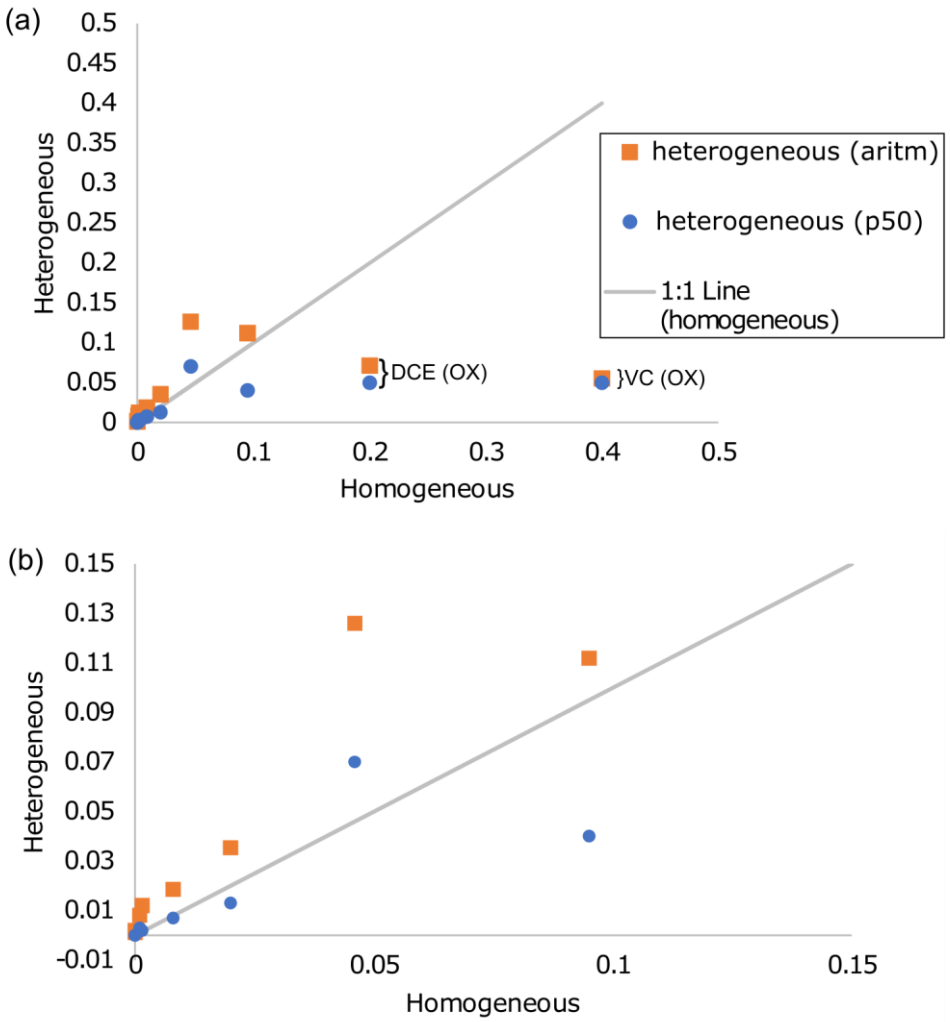

Figure 4.6. Comparison between estimated kinetic rates k [d^{-1}] obtained from the calibration of the homogeneous model (x-axis) and effective kinetic rates calculated for the heterogeneous model using arithmetic averaging (circles) and as the 50% percentile of the data distributions (squares) (y-axes). The 1:1 line highlights the departure of effective heterogeneous rates from the homogeneous rates. In the bottom panel (b) is represented an enlarged plot of the upper panel (a).

4.3.2 Damköhler numbers

Since in the domain the hydraulic conductivity was homogeneous, the pore velocity in each transect differed mainly because of the transect length d. As such, the analysis of Da was particularly useful to evaluate the interplay between the kinetic rates and the residence time of water in RZ2, where transects have significantly different lengths. The full set of calculated *Da* for the different species and scenarios ("P&T on" and "P&T off") is reported in Table 4.4.

In the homogeneous model (Figure 4.7a) it was found a progressive decrease of Da from more to less chlorinated species and an increasing Da trend from the shortest to the longest transects. For the "P&T on" scenario, the range of estimated values were: from Da=16 at T1 to Da=296 at T7 for PCE; from Da =22 at T1 to Da=422 at T7 for TCE; from Da=3 at T1 to Da=64 at T7 for DCE; from Da=1 at T1 to Da =17 at T7 for VC.

The correlation between Da and the number of chlorine atoms in chloroethenes could be explained recalling that RZ2 is controlled by biostimulated RD. Biodegradation is more efficient (higher k_{RD2}) for PCE and TCE than for DCE and VC (lower k_{RD2}). The correlation between Da and d can be explained considering that the kinetic rates k_{RD2} are homogeneous in the model and Da depends uniquely on the residence time of water in the transect, which is mainly a function of d. Shorter transects are characterized by lower residence time than longer transects; in turn, less time is allowed for biodegradation in the shorter transects compared to the longer ones. The low Da values obtained in transects T8 and T9 are explained considering that these transects are not biostimulated by the AN barrier. The kinetic rates associated to RZ2 in T8 and T9 are identical to the rates in RZ1, mimicking the slow natural attenuation process. Switching off the P&T system seems to have a positive effect on the bioremediation system. Examining Figure 4.7b, the Da values in the "P&T off" scenario are slightly higher than in the "P&T on" scenario. This is explained considering that the deactivation of the pumping wells reduces the flow rates and increases the residence time in the transects, thus allowing more time for contaminant mass destruction in the different streamtubes.

A key result from the homogeneous model is that biodegradation seems progressively more dominant over transport from T1 to T7. However, this result is not consistent with the field observations, which indicates that the biodegradation is not linearly correlated with the transect length. For instance, the lowest PCE concentrations were observed in the piezometers included in T1 and T5 (Figure 4.1).

Table 4.4. Damköhler numbers (Da) calculated for the homogeneous and heterogeneous model with and without P&T.

		PCE			TCE			*cis*-DCE			VC		
Homogeneous model													
Transect	P&T	k_{RD2}	*Da*	Δ*Da*	k_{RD2}	*Da*	Δ*Da*	k_{RD2}	*Da*	Δ*Da*	k_{RD2}	*Da*	Δ*Da*
T1	off	0.046	23	7	0.095	32	10	0.02	5	2	0.008	1.34	0.43
	on		16			22			3			0.91	
T2	off	0.046	62	10	0.095	88	14	0.02	13	2	0.008	3.63	0.57
	on		52			74			11			3.06	
T3	off	0.046	101	13	0.095	144	19	0.02	22	3	0.008	5.93	0.76
	on		88			125			19			5.16	
T4	off	0.046	155	16	0.095	220	23	0.02	34	4	0.008	9.08	0.96
	on		138			197			30			8.13	
T5	off	0.046	200	20	0.095	285	29	0.02	43	4	0.008	11.76	1.20
	on		180			256			39			10.56	
T6	off	0.046	238	20	0.095	338	28	0.02	52	4	0.008	13.96	1.15
	on		218			311			47			12.81	
T7	off	0.046	332	36	0.095	473	51	0.02	72	8	0.008	19.50	2.10
	on		296			422			64			17.40	
T8	off	0.0015	10	1	0.001	5	1	0	0	0	0	0	0
	on		9			4			0			0	
T9	off	0.0015	12	1	0.001	6	1	0	0	0	0	0	0
	on		11			5			0			0	
Heterogeneous model													
Transect	P&T	k_{RD2}	*Da*	Δ*Da*	k_{RD2}	*Da*	Δ*Da*	k_{RD2}	*Da*	Δ*Da*	k_{RD2}	*Da*	Δ*Da*
T1	off	0.7	347	112	0.5	171	55	0.13	32	10	0.04	7	2
	on		235			116			22			5	
T2	off	0.16	215	34	0.21	195	31	0.06	40	6	0.03	14	2
	on		181			164			34			11	
T3	off	0.08	176	23	0.1	151	20	0.01	14	2	0.005	4	0
	on		153			132			12			3	
T4	off	0.07	235	25	0.1	232	24	0.05	75	8	0.03	34	4
	on		211			207			68			30	
T5	off	0.075	327	33	0.04	120	12	0.05	98	10	0.05	73	7
	on		293			108			88			66	
T6	off	0.03	155	13	0.04	142	12	0.01	33	3	0.005	9	1
	on		142			131			31			8	
T7	off	0.015	108	12	0.011	55	6	0.01	40	4	0.007	17	2
	on		97			49			35			15	
T8	off	0.002	20	2	0.003	20	2	0	5	1	0	0	0
	on		18			18			4			0	
T9	off	0.002	23	2	0.003	24	2	0	6	1	0	0	0
	on		21			22			5			0	

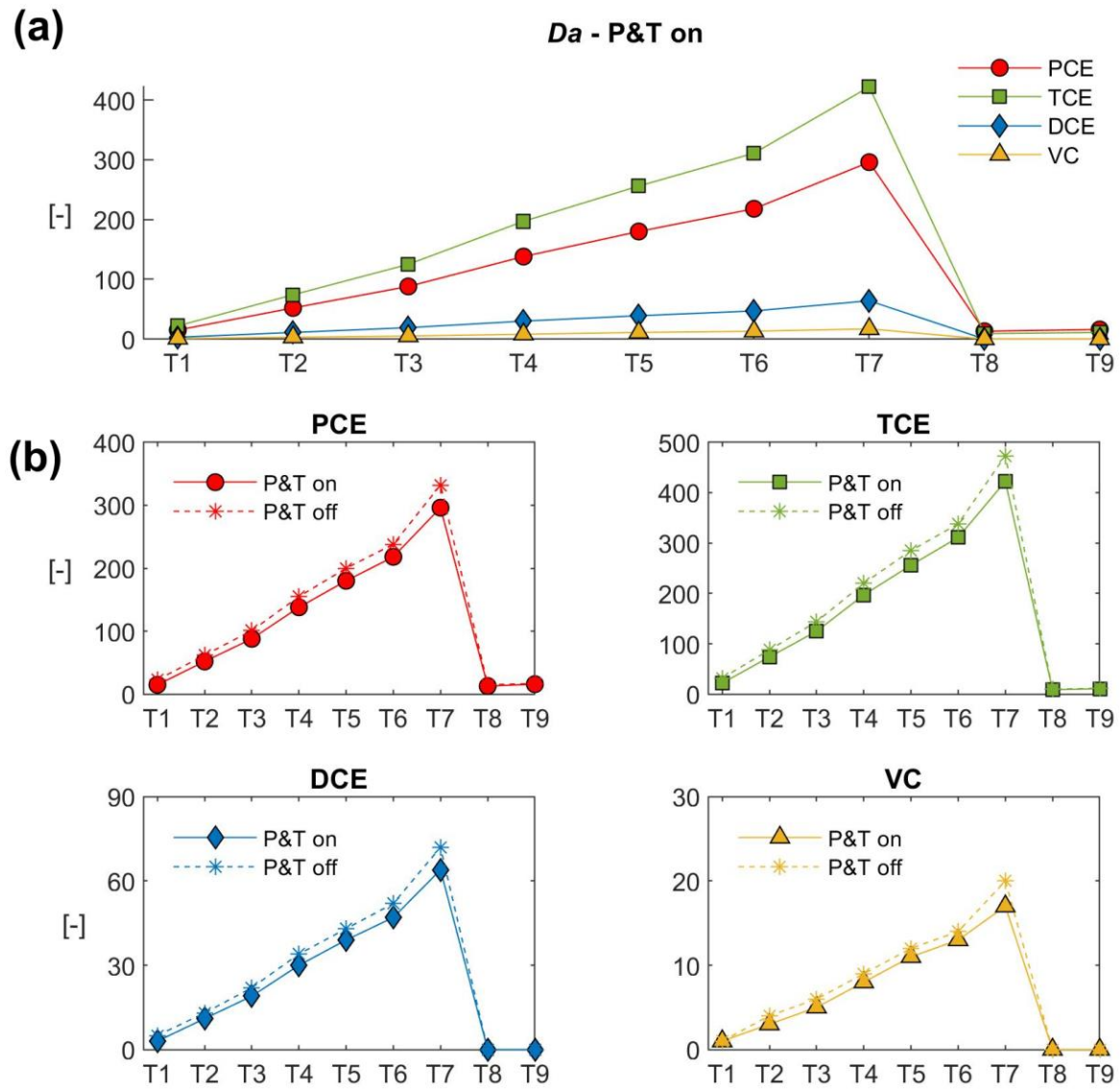

Figure 4.7. (a) Da variation from transects T1 to T9 for each chloroethene in the homogeneous model; (b) Da variation in the homogeneous model from transect T1 to T9 for PCE, TCE, DCE and VC with and without P&T.

The heterogeneous model provides more consistent results than the homogeneous model (Figure 4.8). As in the homogeneous model, Da tends to decrease from PCE to VC in each transect, and for PCE and TCE the large Damköhler numbers ($Da \gg 0$) suggest that biodegradation prevails over transport. No monotonic Da trend from shorter to longer transects was observed in the heterogeneous model. Analyzing the "P&T on" scenario, for PCE the highest Da values were observed in T1 (Da=235) and T5 (Da=293), indicating that biodegradation is more effective in these transects than elsewhere. This result is now consistent with the lowest PCE concentrations observed in the piezometers included in T1 and T5 (Figure 4.1), showing that the heterogeneous distribution of kinetic rates generates a more reliable model configuration than the homogeneous one. As in the homogeneous model, T8 and T9 show the lowest Da, consistent with the slower natural biodegradation rate in the peripheral part of the plume.

Comparing the scenarios with and without P&T, we found an inverse correlation between the difference in Da between "P&T off" and "P&T on" ($\Delta Da = Da_{P\&T\_OFF} - Da_{P\&T\_ON}$) and d. For instance, for PCE we found ΔDa=112 at the shortest T1 transect, ΔDa=12-33 at the intermediate transects T2-T7 and ΔDa=2 at the non-biostimulated T8 and T9.

Similar conclusions can be drawn for TCE, although different values and spatial distribution of Damköhler numbers was calculated. In the "P&T on" scenario, the highest Da values for TCE were observed in T4 (Da=207); at T1 and T5 we found Da=116 and Da=108, respectively. The lowest overall values indicate that biodegradation may not be as efficient for TCE as for PCE (for which Da=235 and Da=293, respectively).

The Da values in the "P&T off" scenario are slightly higher than in the "P&T on" scenario. This result is consistent with that of the homogeneous model, and remarks that biodegradation becomes relatively more effective when the P&T system is switched off and the water residence time is increased. At T1, the effect of the well deactivation on the residence times is the largest (increase of residence time of 32% compared to 8-16% in the other transects).

Another highlighted result is that the maximum Da numbers in the heterogeneous model for DCE and VC are relatively higher than the maximum values in the homogeneous model. The spatial distribution of Da peaks is similar to that of the more chlorinated species; the highest Da found in T4 (Da=68 for DCE and Da=30 for VC) and T5 (Da=88 for DCE and Da=66 for VC).

Overall, the comparison between the homogeneous and heterogeneous model shows that the use of spatially variable kinetic rates provides significantly different results. Given that the heterogeneous model generates more consistent results with the field observations, the use of a model with spatially variable parameterization should provide more accurate predictions than the use of a more parsimonious homogeneous model. The variation of Da values suggests that different processes (associated to, e.g., different distribution of microbial species) may be occurring in the different parts of the aquifer. In terms of "efficiency" of the biodegradation process (epitomized by the different Da values), the heterogeneous model indicates that biodegradation may be in general more efficient in transects T4 and T5 than elsewhere, however with some important exceptions (e.g., TCE in T5 and PCE in T1).

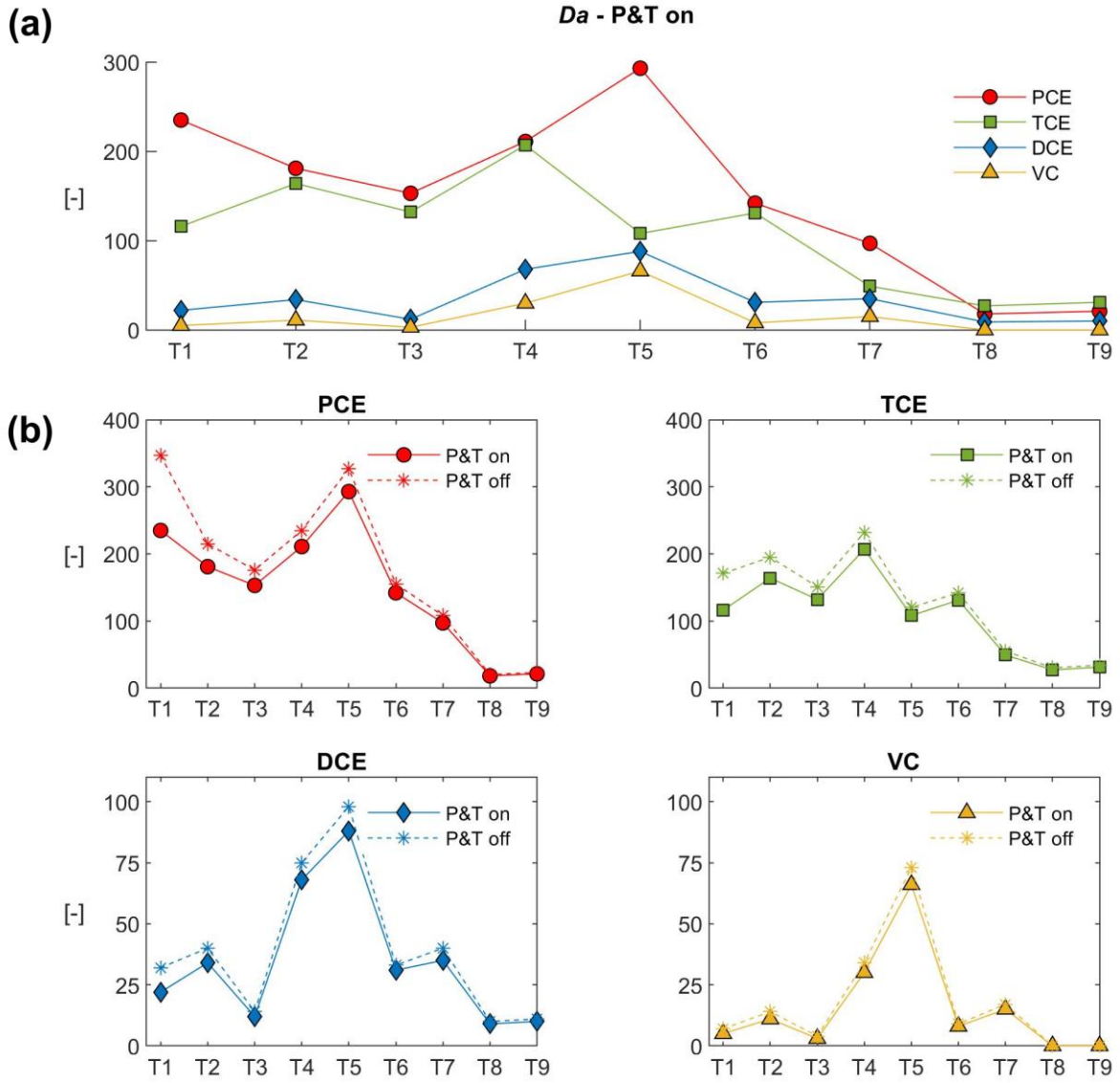

Figure 4.8. (a) Variation of Damköhler numbers (ΔDa) from transect T1 to T9 for each chloroethene in the heterogeneous model, with active pump-and-treat ("P&T on"). (b) Comparison of Da with and without pump-and-treta system ("P&T on" and "P&T off", respectively), by species.

4.3.3 Loadings calculation

4.3.3.1 At the ALRC

While the analysis of Da suggests that switching off the P&T system increases the efficiency of anaerobic biostimulation, the comparison of daily loadings (L) suggests that switching off the P&T to reduce operational costs may not be a straightforward decision. The full list of calculated loadings at the model outflow boundary (L_{ALRC}) is reported in Table 4.5 and Table 4.6.

We found a great difference in calculated loadings between the homogeneous and heterogeneous models (Figure 4.9). Considering both "P&T on" and "P&T off" scenarios, the total PCE and TCE loadings reaching the ALRC are much higher in the homogeneous model (L_{ALRC}=4727.31÷10534.12 mg d^{-1} and L_{ALRC} =5943.24÷12263.08 mg d^{-1}, respectively) than in the heterogeneous model (L_{ALRC}=65.81÷74.62 mg d^{-1} and L_{ALRC}=351.50÷650.69 mg d^{-1}, respectively). For these two compounds, the difference between the two model setups is particularly large in the shortest transects T1-T3 (Figure 4.9). While in the homogeneous model PCE and TCE loadings are way higher than 10^2 mg L^{-1} (L_{ALRC} = 325.12÷8233.43 mg L^{-1}), in the heterogeneous model loadings are consistently lower than 10^2 mg L^{-1} (L_{ALRC} = 4.57÷95.08 mg L^{-1}). Such a remarkable difference can be explained considering that the shortest transects have the lowest residence time (τ). Since in the homogeneous model the kinetic rates k are spatially invariant, the resulting k_{RD1} and k_{RD2} in T1-T3 were too slow to generate sufficient biodegradation to abate PCE and TCE concentrations (Figure 4.5 and Table S4.3 in the SM).

On the contrary, DCE and VC total loadings are way higher in the heterogeneous model (L_{ALRC}=2222.52÷4291.12 mg d^{-1} and L_{ALRC} =8641.13÷25147.73 mg d^{-1}, respectively) compared to the homogeneous model (L_{ALRC}=23.48÷205.06 mg d^{-1} and L_{ALRC} = 7.23÷67.08 mg d^{-1}, respectively), where the loadings are severely underestimated: simulated concentrations were lower than $< 10^{-8}$ mg L^{-1} for DCE in the longest transects T6-T9 and for VC in T5-T9. Since very low concentrations may be prone to numerical oscillation, the loadings in these transects were not calculated and assumed to be negligible in the homogeneous model.

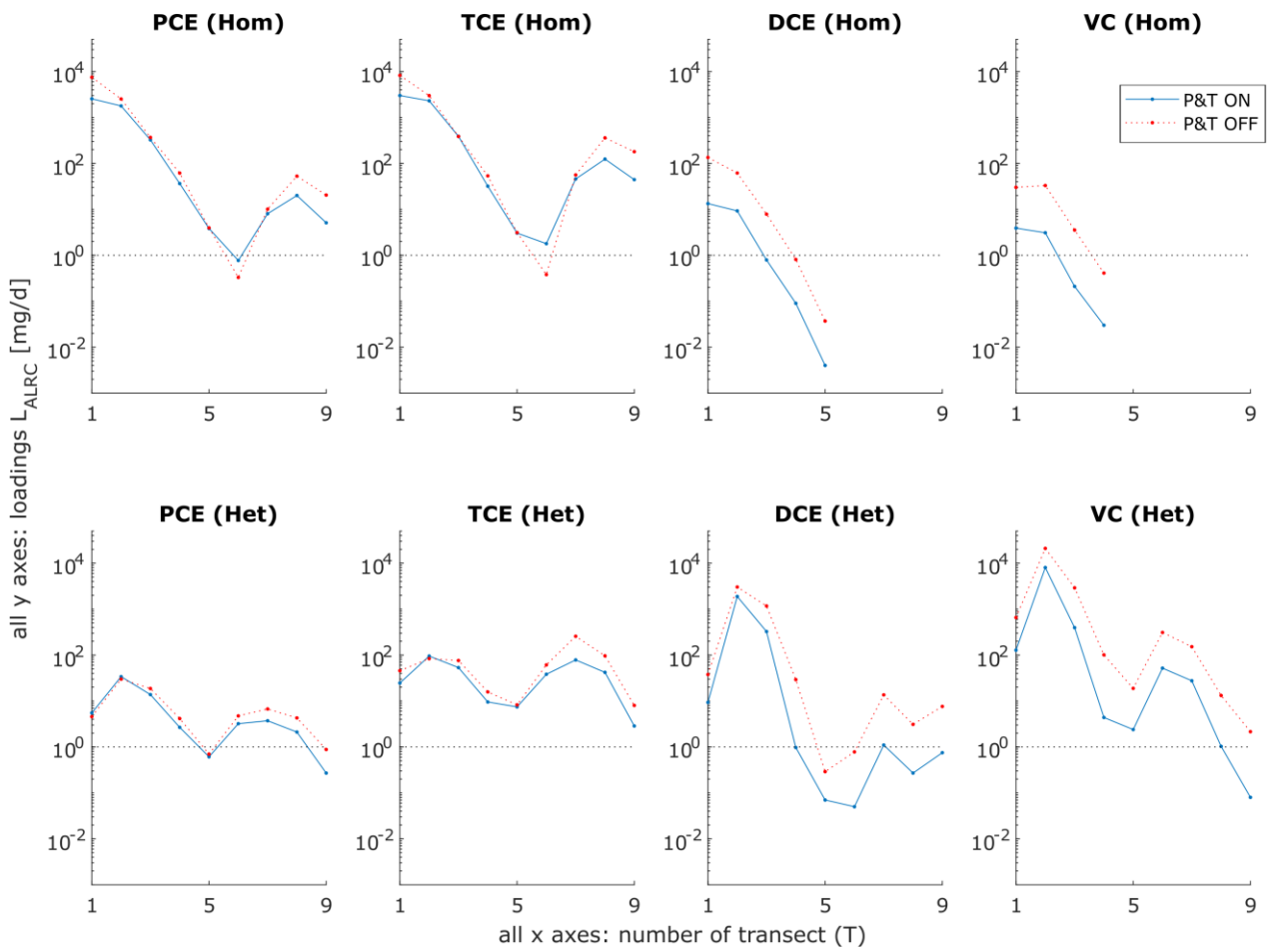

Figure 4.9. Calculated loadings at the outflow model boundary, L_{ALRC} [m d^{-1}] in the homogeneous (hom) and heterogeneous (het) models for the different species. The scenarios with ("P&T on") and without ("P&T off") pump-and-treat wells are compared. For DCE and VC in the homogeneous model, concentrations were too low and likely affected by numerical oscillation, and therefore loadings were not calculated.

In Figure 4.10 loadings variation (%) generated in each transect with the deactivation of the P&T is reported, while the full list of calculated ΔL_{ARLC} and $\sum\Delta L_{ARLC}$ is reported in Table 4.5 and Table 4.6. In general, deactivating the P&T led to a significant increase of contaminant loading at the ALRC, particularly for the less chlorinated species. The difference was much larger in the homogeneous model than in the heterogeneous model. .For PCE, ΔL_{ALRC} in the heterogeneous model was negative only in transects T1 (-17%) and T2 (-12%), while in the remaining transects, ΔL_{ALRC} was always positive and erratic, with fluctuating values ranging between 15% in T5 and 225% in T9. In the homogeneous model, the cumulative loading was calculated as $\sum\Delta L_{ALRC}$ =123%, while in the heterogeneous model the value was limited to $\sum\Delta L_{ALRC}$ =13%. In the homogeneous setup, the very high concentrations in the northeastern part of the site corresponding to T1 and T2 exerted a strong weight on the cumulative variation of PCE loading.

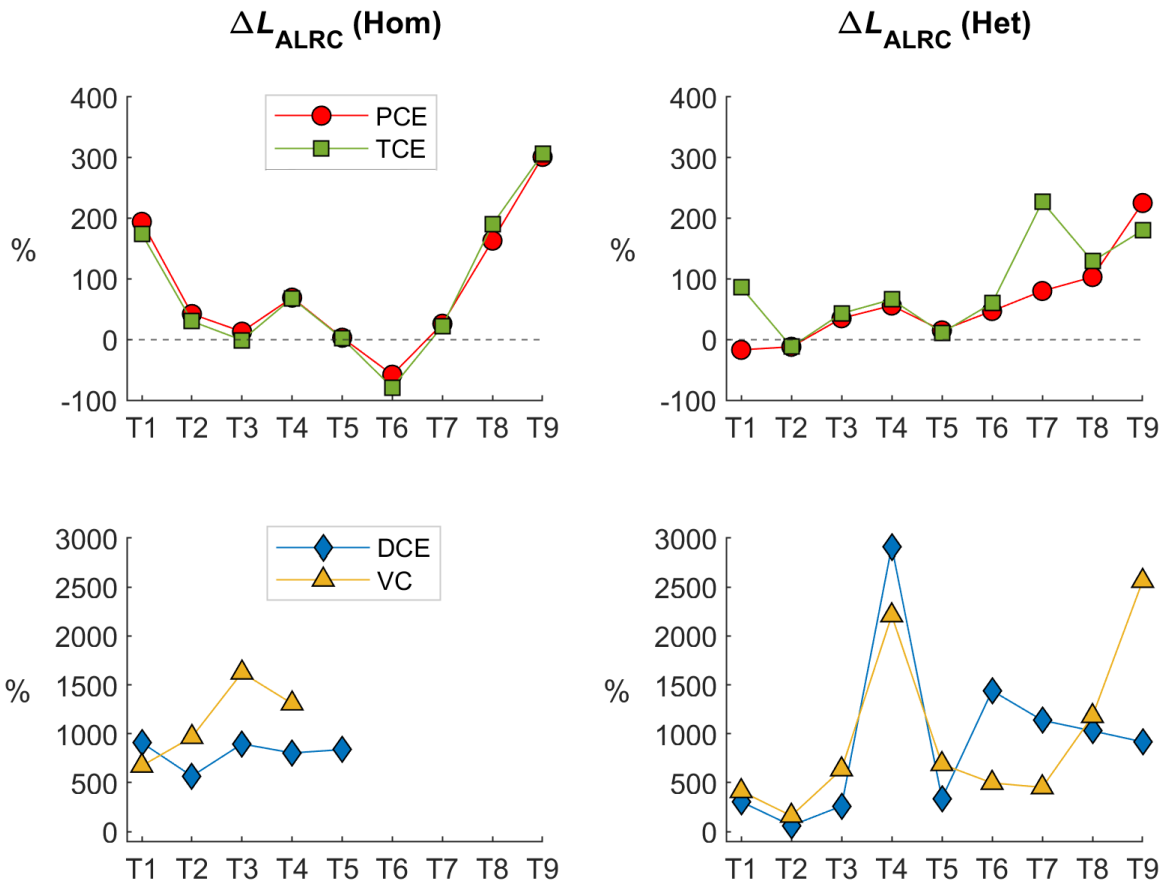

Figure 4.10 . Variation (%) of PCE and TCE (top panels) and DCE and VC (bottom panels) loadings reaching the canal (ΔL_{ALRC}) for each transect in the homogeneous (left panels) and heterogeneous (right panels) models with the deactivation of the P&T system compared to the initial situation with active P&T.

Table 4.5. Contaminant loadings reaching the canal (L_{ALRC}) calculated for each transect (T1-T9) in the homogenous model. Blank cells indicate that concentrations were too low and likely affected by numerical oscillation, and therefore not used for the loadings calculation.

		T1	**T2**	**T3**	**T4**	**T5**	**T6**	**T7**	**T8**	**T9**	$\sum \Delta L_{ALRC}$
						PCE					
L_{ALRC} **[mg d^{-1}]**	P&T on -	2546.05	1781.95	325.12	36.41	3.83	0.77	8.03	20.04	5.10	4727.31
	P&T off -	7488.31	2528.15	368.45	61.57	3.96	0.33	10.10	52.79	20.45	10534.12
	Δ L_{ALRC} (off-on)	4942.26	746.20	43.32	25.16	0.13	-0.44	2.07	32.74	15.36	5806.80
	Δ L_{ALRC} (%)	194%	42%	13%	69%	3%	-58%	26%	163%	301%	123%
						TCE					
L_{ALRC} **[mg d^{-1}]**	P&T on -	3001.07	2303.27	387.90	31.95	3.04	1.79	45.85	124.04	44.33	5943.24
	P&T off -	8233.43	2990.96	385.76	53.54	3.12	0.38	56.09	359.68	180.13	12263.08
	Δ L_{ALRC}	5232.36	687.69	-2.14	21.59	0.07	-1.41	10.24	235.64	135.80	6319.84
	Δ L_{ALRC} (%)	174%	30%	-1%	68%	2%	-79%	22%	190%	306%	106%
						cis-DCE					
L_{ALRC} **[mg d^{-1}]**	P&T on -	13.35	9.25	0.79	0.09	0.004					23.48
	P&T off -	134.63	61.68	7.85	0.81	0.037					205.06
	Δ L_{ALRC}	121.27	52.43	7.07	0.72	0.033					181.58
	Δ L_{ALRC} (%)	908%	567%	896%	804%	838%					773%
						VC					
L_{ALRC} **[mg d^{-1}]**	P&T on -	3.90	3.09	0.21	0.03						7.23
	P&T off -	30.14	32.98	3.54	0.41						67.08
	Δ L_{ALRC}	26.24	29.88	3.34	0.38						59.84
	Δ L_{ALRC} (%)	672%	966%	1624%	1308%						827%

Table 4.6. Contaminant loadings reaching the canal (L_{ALRC}) calculated for each transect (T1-T9) in the heterogenous model.

		T1	T2	T3	T4	T5	T6	T7	T8	T9	$\sum \Delta L_{ALRC}$
							PCE				
L_{ALRC} [mg d^{-1}]	P&T on -	5.50	33.92	13.79	2.67	0.61	3.21	3.72	2.11	0.27	65.81
	P&T off -	4.57	29.91	18.69	4.15	0.70	4.74	6.71	4.28	0.88	74.62
	Δ L_{ALRC}	-0.93	-4.02	4.89	1.49	0.09	1.53	2.99	2.17	0.61	8.81
	Δ L_{ALRC} (%)	-17%	-12%	35%	56%	15%	47%	80%	103%	225%	13%
							TCE				
L_{ALRC} [mg d^{-1}]	P&T on -	24.63	95.08	53.32	9.52	7.44	38.26	78.34	42.04	2.86	351.50
	P&T off -	45.73	83.52	76.02	15.77	8.24	61.04	256.21	96.16	8.01	650.69
	Δ L_{ALRC}	21.11	-11.56	22.69	6.25	0.80	22.78	177.86	54.12	5.15	299.20
	Δ L_{ALRC} (%)	86%	-12%	43%	66%	11%	60%	227%	129%	180%	85%
							cis-DCE				
L_{ALRC} [mg d^{-1}]	P&T on -	9.33	1884.98	325.00	0.97	0.07	0.05	1.10	0.27	0.75	2222.52
	P&T off -	37.76	3026.44	1172.35	29.18	0.29	0.78	13.61	3.10	7.61	4291.12
	Δ L_{ALRC}	28.43	1141.46	847.34	28.21	0.23	0.73	12.51	2.82	6.86	2068.60
	Δ L_{ALRC} (%)	305%	61%	261%	2914%	338%	1440%	1137%	1029%	917%	93%
							VC				
L_{ALRC} [mg d^{-1}]	P&T on -	127.83	8030.56	395.35	4.38	2.39	51.95	27.56	1.03	0.08	8641
	P&T off -	655.75	20989.21	2905.31	101.02	18.84	310.17	152.12	1.32E+01	2.15E+00	25147.73
	Δ L_{ALRC}	527.92	12958.65	2509.97	96.64	16.45	258.22	124.56	12.1400	2.0717	16506.61
	Δ L_{ALRC} (%)	413%	161%	635%	2209%	689%	497%	452%	1180%	2561%	191%

Table 4.7. Contaminant loadings reaching the canal (L_{RZ2}) calculated for each transect (T1-T9) in the heterogenous model.

		T1	**T2**	**T3**	**T4**	**T5**	**T6**	**T7**	$\sum \Delta L_{RZ2}$
						PCE			
L_{RZ2} **[mg d^{-1}]**	P&T on -	13.13	132.93	76.48	8.10	0.96	8.61	20.77	271.99
	P&T off -	6.59	79.91	46.05	4.79	0.51	4.79	10.85	160.25
	Δ L_{RZ2}	-6.54	-53.02	-30.44	-3.32	-0.45	-3.82	-9.93	-111.74
	Δ L_{RZ2} (%)	-50%	-40%	-40%	-41%	-47%	-44%	-48%	-41%
						TCE			
L_{RZ2} **[mg d^{-1}]**	P&T on -	164.11	370.09	331.26	23.26	28.85	41.14	568.19	1724.18
	P&T off -	89.93	208.74	198.52	13.56	16.45	23.40	335.66	1017.01
	Δ L_{RZ2}	-74.18	-161.35	-132.75	-9.70	-12.40	-17.73	-232.54	-707.17
	Δ L_{RZ2} (%)	-45%	-44%	-40%	-42%	-43%	-43%	-41%	-41%
						cis-DCE			
L_{RZ2} **[mg d^{-1}]**	P&T on -	8914	24586	78276	3583	282	2027	1737	120129
	P&T off -	6167	16005	63561	2828	179	1379	1047	91695
	Δ L_{RZ2}	-2748	-8580	-14715	-756	-103	-648	-690	-28434
	Δ L_{RZ2} (%)	-31%	-35%	-19%	-21%	-37%	-32%	-40%	-24%
						VC			
L_{RZ2} **[mg d^{-1}]**	P&T on -	56297	331009	592533	39005	2074	28681	15629	1068734
	P&T off -	42606	214679	495887	32229	1414	20875	9805	820139
	Δ L_{RZ2}	-13692	-116330	-96645	-6776	-660	-7806	-5824	-248596
	Δ L_{RZ2} (%)	-24%	-35%	-16%	-17%	-32%	-27%	-37%	-23%

For TCE, ΔL_{ALRC} in the heterogeneous model was mainly positive and erratic among the transects, with values oscillating between 11% and 227%. An exception was T2, where ΔL_{ALRC}=-12%. The highest ΔL_{ALRC} was observed in T7, where the contaminant loadings increased from L_{ALRC}=78 mg d^{-1} to L_{ALRC}=256 mg d^{-1} following the deactivation of the P&T. This increase can be explained considering that k_{RD2} in T7 was the smallest among those found for TCE (Table S4.3 in SM). Correspondingly, Da was also the lowest among the transects where biostimulation is active (Figure 4.8). This means that the abatement of TCE loadings in T7 in the "P&T on" scenario was mostly carried out by the P&T system rather than biodegradation, and consequently its deactivation led to a huge increase of contaminant loadings in T7. The cumulative variation of TCE loading calculated by the homogeneous models was $\sum\Delta L_{ALRC}$ =106% and by the heterogeneous model it was $\sum\Delta L_{ALRC}$ =85%.

For DCE and VC, switching off the P&T generates a strong increase in the loadings, as ΔL_{ALRC} oscillated between 600% and 1800%. The difference was positive in all transects. The homogeneous model provided a cumulative difference in loading $\sum\Delta L_{ALRC}$ = 773% for DCE and $\sum\Delta L_{ALRC}$ = 827% for VC. In the heterogeneous model, however, these differences were ΔL_{ALRC} = 93% for DCE and $\sum\Delta L_{ALRC}$ = 191% for VC.

These results further stress the difference between a heterogeneous and homogeneous parameterization, with the former providing much reduced difference in total loadings than the latter. For practical purposes related to this site, the models suggest that switching off the P&T generates higher loadings released into the canal. Therefore, while inactivating the pumping wells increases the residence time and enhances the biodegradation (as demonstrated by Da), the P&T has a critical role to abate the contaminant mass exfiltrating the site, particularly for the less chlorinated species.

4.3.3.2 At RZ2-RZ3 boundary

Loadings calculated at the boundary between RZ2 and RZ3 in the heterogeneous model (Figure 4.11) show that ΔL_{RZ2} were negative in all transects for each chloroethene. This means that, at the outflow boundary of the biostimulated reaction zone RZ2, the loadings calculated in the "P&T off" scenario were always lower compared to the ones calculated in the "P&T on" scenario. In particular, the decrease in L_{RZ2} without P&T was higher for PCE and TCE (average $\Delta L_{RZ2} < -40\%$) compared to DCE and VC ($\Delta L_{RZ2} > -40\%$).

This result can be ascribed to the impact of the P&T wells on the flow field in RZ2, which affects the ratio between reaction and transport scales, i.e., the Damköhler numbers (Da). When the P&T is off, Da increases for all chloroethenes as a consequence of the reduction of the flow rates, as confirmed by the increase in water travel times within RZ2 calculated with particle tracking. This allows more time for the kinetic reactions to occur, which translated into less contaminants arriving at the outflow boundary. As biodegradation in RZ2 was more efficient for PCE and TCE, deactivating the P&T led to a higher abatement of loadings (i.e., more negative ΔL_{RZ2}) for these species than for DCE and VC.

This behavior was not observed at the ALRC boundary, where ΔL_{ALRC} were more complex to evaluate, especially for PCE and TCE (Figure 4.10). The value of ΔL_{ALRC} was negative for PCE in transects T1 (-17%)

and T2 (-12%) and for TCE in transect T2 (-12%). In the remaining transects ΔL_{ALRC} was always positive, although with very variable values.

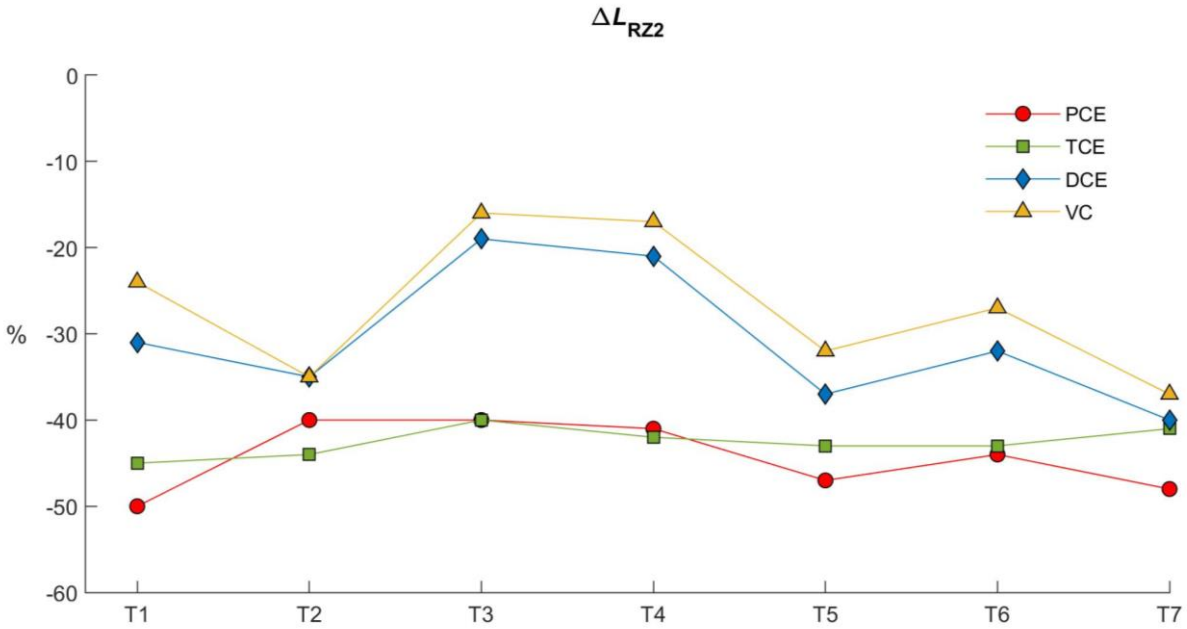

Figure 4.11. Variation (%) of PCE and TCE (a) and DCE and VC (b) loadings exiting the RZ2 (ΔL_{RZ2}) for each transect in the heterogeneous model with the deactivation of the P&T system compared to the initial situation with P&T active.

The different behavior of ΔL_{ALRC} (Figure 4.10) in each transect could be explained as the result of contrasting tendencies.

- In RZ2 the deactivation of the P&T system resulted in increased residence times of contaminants in all transects, as seen before. An increase of residence time resulted in an increase of Da without P&T (see Figure 4.8) that led to a higher destruction of contaminant mass in RZ2 within each transect (negative ΔL_{RZ2} in Figure 4.11).
- At the same time the deactivation of the P&T system means that contaminants were no longer intercepted by the extraction wells and mechanically removed from the system.

Thus, the deactivation of the P&T system had a different effect on PCE and TCE in each transect at the ALRC, depending on the balance between the two aforementioned trends.

Apparently, in transects T1 and T2 for PCE and T2 for TCE, the mass removed by the extraction wells when the P&T system was active was not enough to counterbalance the reduction of mass destruction via biodegradation in RZ2 caused by the presence of the wells themselves (due to shortening of residence times), which resulted in negative ΔL_{ALRC}. As a result, the presence of the P&T system was detrimental for the optimal mass destruction of PCE and TCE in these transects. On the contrary, an opposite situation took place in the remaining transects, where an increase of contaminant loadings was observed for PCE and TCE without the P&T (positive ΔL_{ALRC}), proving the overall beneficial effect of the P&T on the destruction of these two compounds.

For DCE and VC, instead, ΔL_{ALRC} were always positive. For these two contaminants an additional effect had to be taken into consideration: both compounds were also degraded in RZ3 (i.e. the reaction zone downgradient of the P&T wells) via oxidative pathways. Particle tracking simulations carried out with PMPATH proved that the deactivation of the P&T system resulted in a decrease of contaminants residence times between the extraction wells and the canal (i.e. within RZ3 where OX of DCE and VC is active). In this area, the presence of the P&T wells caused, in fact, both a decrease of transport velocity due to decreased hydraulic gradients as well as a deviation of contaminant particles which resulted in a lengthening of particles paths in the proximity of the wells' capture zones. Therefore, the lower residence times obtained with the deactivation of the P&T wells (combined with the absence of mechanical removal of contaminants) resulted in a decreased DCE and VC mass destruction in RZ3. The increase of DCE and VC mass destruction in RZ2 via RD without P&T (negative ΔL_{RZ2} in Figure 4.11) was not enough to counterbalance this effect. This explained the much higher ΔL_{ALRC} values obtained for DCE and VC (generally much higher than 300%) compared to PCE and TCE (always lower than 300%).

4.4 Discussion

4.4.1 Importance of embedding spatial heterogeneity in the model

This work showed that a multidimensional RTM embedding a heterogeneous parameterization of first-order reaction rates (k) can provide critical information about the SBS management. The use of Damköhler numbers (Da) was particularly useful to elucidate the control of the spatial variation of the biochemical processes on the efficiency of the SBS. This metric has been already adopted in several bioremediation modeling studies to relate reaction and transport rates (Fry and Istok, 1994; Henri and Fernàndez-Garcia, 2014; Knapp and Faison, 1997; MacDonald et al., 1999; Zhang et al., 2010). We used Da to epitomize the efficiency of the biodegradation process, which was expected to be strongly variable in the site according to laboratory analyses (Bertolini et al 2021).

The heterogeneous model provided significantly different results than those obtained from the homogeneous model. Given that the heterogeneous model fits better the field observations, we recommend the use of a model embedding a spatially variable parametrization to make decisions for this site. Although the spatially invariant k in the homogeneous model correlate well with the "effective" k obtained from the heterogeneous model (Figure 4), the use of a single homogeneous reaction rate for each reaction zone turned out to be an inaccurate upscaling approach.

A limitation of this study was that the model adopts first-order kinetics. While this type of modeling ap-proach has been widely adopted in bioremediation studies (e.g. Clement et al., 2000; Falta, 2008), it remains a simplified modeling approach that does not consider the interplay of multiple geochemical and environmental factors on the biodegradation rates (Chambon et al., 2013). A more proper approach should consider for instance the availability of hydrogen and other electron donors (e.g., acetate) as a rate limiting factor for

reductive dechlorination, the effect of bacteria concentrations and activity, the competition for electron donors between chloroethenes and alternative terminal electron acceptors (TEAs) such as manganese (IV), iron (III) and sulfate, which are present in high concentrations at the study site. The use of Monod kinetics (e.g. Chambon et al., 2013) would permit to integrate these processes in the computation of degradation rates and reproduce their spatial variation in the model, depending on hydrogen and TEAs concentrations and microbiological content distribution.

However, such an approach would require a proper reproduction of spatial distribution of parameters values, whose accuracy is known to strongly influence the final result of modelling studies (Dalla Libera et al., 2021; Lin et al., 2017; Sidiropoulos et al., 2021; Wheater et al., 2000). This reproduction is generally accomplished with stochastic modeling (Coburn et al., 2006). However, the application of such methods is time-consuming and the accuracy of the reproduction obtained is strongly dependent on data availability in the modeled area. For aquifers that show a significant spatial heterogeneity of key properties (like the one investigated), their accurate characterization represents a time-intensive and costly activity and is, thus, not always feasible. In fact, the limited aquifer characterization of the investigated study site prevented the application of stochastic modeling. Specifically, substrate concentrations are not available and coverage gaps of the site area are present for both TEAs concentrations and microbiological data, especially in the area between the two barriers. Thus, a more extensive characterization of the area from a geochemical and microbiological point of view is suggested in order to implement a more complex and accurate 2D RTM.

4.4.2 Ruling out P&T: a wise decision to cut costs?

Overall, the results obtained from contaminant loadings exfiltrating from the system showed that the deactivation of the P&T would be detrimental for the abatement of contaminants, especially considering that it would bring to a substantial increase of VC which is the more toxic chloroethene.

Even though the P&T method was subject to fierce criticism starting the early 1990s, the results show that this approach is still essential to tackle some extreme contamination situations like the one addressed in this study, in particular when coupled to ISB.

As shown, biodegradation efficiency throughout a site can be quite variable depending on hydrogeological and microbiological heterogeneity (Herrero et al., 2021), and thus render the task of overall optimization of biodegradation arduous.

Whilst great improvements have been made towards the comprehension of microbiological systems and biodegradation in the last decades (Dolinová et al., 2017b; Kouznetsova et al., 2010; Tiehm and Schmidt, 2011), the interaction between different species in microbial communities and how this affects the efficiency of biodegradation of the different contaminants is very complex and far from being completely understood (e.g. Hug et al., 2012; Moreira et al., 2021; Xiao et al., 2020). Therefore, until a better understanding of bioremediation is achieved, a P&T system can be still seen as an established approach to minimize plume spreading to unpolluted areas.

Potentially, only part of the P&T could be deactivated, leaving some wells active. A scenario-based analysis that evaluates the impact of deactivating individual wells could be carried out using our model, in order to obtain quantitative answers in this regard. Such a specific application goes beyond the scientific goals of this study.

Another possible model scenario involves reducing the wells' pumping rates, which is critical to re-duce costs and energy demand of the P&T system (Casasso et al 2021). Several studies have focused on the optimization (i.e. minimization) of pumping rates in P&T systems, which is a demanding task when dealing with heterogeneous systems (Matott et al., 2006; Pedretti, 2020). Advanced techniques exist that permit to take into account the effect of heterogeneities in aquifer properties, in particular hydraulic conductivity distribution which is the factor that above all influences transport (Pedretti, 2020).

If a significant reduction of pumping rates is not achievable and the estimated operational timeframes are long, geothermal exploitation of P&T systems (Casasso et al., 2019) could be taken into consideration as an alternative to achieve an overall reduction of P&T economic burden as well as its environmental impact, by reducing the carbon footprint associated to the remediation process. Using bioremediation sites as aquifer thermal energy storage (ATES) systems has already been proposed (Fleuchaus et al., 2018; Ni et al., 2018, 2016), and existing P&T wells could be an excellent way to inject and recover warm or cold waters to the aquifer. Moreover, warming up groundwater could further enhance microbiological activity, which is favored, within certain limits, at temperatures higher than those normally found in aquifers (e.g. Bradley et al., 2005; Fletcher et al., 2011; Friis et al., 2007; Löffler et al., 2013; Marcet et al., 2018; Truex et al., 2007).

4.5 Summary and conclusion

A 2D RTM was set up for the evaluation of the combined efficiency of the SBS and P&T system active in the study site in carrying out chloroethenes degradation. Both homogeneous and heterogeneous spatial distribution of first order degradation constants were used in order to assess the importance of model parametrization.

Two main conclusions that can be drawn from this work are:

I. Our analysis indicates that a heterogeneous model configuration should be preferred over a homogeneous configuration. In fact, this study showed the importance of considering heterogeneity of degradation in the site in order to obtain a realistic assessment of the overall degradation efficiency as well as a more accurate estimation of contaminant loadings exfiltrating from the remediation system.

II. The application of Da in the heterogeneous model also permitted to distinguish with more accuracy between areas within the site where the biostimulation is more or less effective. This is useful for pinpointing the more critical areas in the site that may benefit most from an adjustment of the biostimulation activity or further interventions.

For the efficiency assessment of the SBS the subdivision of the site area into the transects T1-T9 was considered for both the homogeneous and the heterogeneous model. To evaluate degradation in each of the transects, two indicators were taken into consideration. The first was the Damköhler number (Da) which permitted to estimate the relative efficiency of degradation between transects in RZ2 based on calibrated k_{RD2} values and residence times. The second parameter was the contaminant loading exiting the combined remediation system, which permitted to quantify the mass of contaminant remaining in each transect.

Resulting Da values were very different in the two models.

In the homogeneous model the Da was shown to increase from T1 to T7. Assuming the same value for the degradation constant k_{RD2} in all RZ2, the efficiency estimated with *Da* in each transect was only dependent on the residence time, which increased progressively from T1 to T7

The Da resulting from the heterogeneous model in each transect, instead, showed that the situation was more complicated, since the degradation efficiency expressed as Da depends on both k_{RD2}, which was assumed as spatially variable within RZ2, and the residence times. While the residence time increased progressively from T1 to T7, an inverse trend was generally observed for k_{RD2} and the highest efficiencies were observed for those transects where the optimal combination of the two parameters took place. Contrary to what was observed in the homogeneous model, the transects with the overall highest *Da* for each chloroethene were the middle transects T4 and T5. Much higher Da were also found in T1 compared to the homogeneous model, where degradation efficiency resulted to be very low (Da between 0.9 and 22; Table 4.4).

The calculated loadings of PCE and TCE were overestimated in the homogeneous model compared to the heterogeneous model, while DCE and VC loadings were significantly underestimated, thus leading to an underestimation of PCE and TCE degradation and an overestimation of DCE and VC degradation.
These observations proved that considering heterogeneity is essential to obtain a realistic assessment of effectiveness of the ongoing remediation processes and to be able to use the model to identify critical areas on which further intervention is required.
Moreover, in order to evaluate the effect of the presence of the P&T system on the biodegradation in both the homogeneous and the heterogeneous model, a second scenario without the P&T system was tested.
In both the homogeneous and heterogeneous model, the deactivation of the P&T caused an increase of total contaminant loadings reaching the canal for all chloroethenes (i.e. positive ΔL_{ALRC}), showing that the P&T overall contribution to the abatement of contaminant loadings is significant and thus the deactivation of the whole system is not recommended. However, the heterogeneous model suggested that some wells may be deactivated (or the pumping rates reduced), as the change in loadings between active and inactive P&T is transect-specific and depends on the local efficiency of the biostimulation as well as on the influence of the wells on the flow field.

Conclusion

Overall, the multidisciplinary approach and multiscale experimental activities were fundamental for the characterization of the site, the implementation and the efficiency evaluation of the remediation system.

In chapter 2 (Casiraghi et al., 2022a) laboratory analyses and field-scale piloting tests had demonstrated that chloroethenes could be best removed by means of a sequential bioremediation system (SBS) stimulating reductive dechlorination (RD) and oxidation (OX) in sequence using a combination of injected nutrients and air sparging (Casiraghi et al., 2022a). The operational-scale SBS was created at the end of the experiments and is still working today. It consists of two biobarriers about 400m-long, each one designed to achieve redox conditions favorable to RD (anaerobic biobarrier) or OX (aerobic biobarrier).

In chapter 3 (Casiraghi et al., 2022b) the actual occurrence of bioremediation was investigated combining concentration data and carbon isotopic signature of chloroethenes (obtained by compound specific isotope analysis of carbon, C-CSIA), which were determined on samples collected in piezometers located along a groundwater flow path crossing both biobarriers. Data were interpreted with a 1D reactive transport model (RTM) developed using the code PHREEQC (Parkhurst and Appelo, 2013). The model was able to adequately reproduce the experimental data, providing useful insights about the biodegradation processes taking place at different distances from each biobarrier along the flow path. Specifically, it suggested that anaerobic and aerobic biodegradation were actually being stimulated by the biobarriers.

However, the limited dimensionality of Casiraghi et al. (2022b)'s model was insufficient to properly investigate important aspects associated to the contamination and bioremediation process. Chiefly, the 1D model could not be used to quantify the sitewide mass loading of chloroethenes exfiltrating from the remediation system, nor to generate scenario-based predictions simulating alternative setups of the remediation system that could optimize chloroethenes degradation process.

Thus, in chapter 4 a multidimensional model extended to the whole site area was implemented with RT3D. Hydrogeological homogeneity was assumed in the model, while two parametrizations of different complexities were adopted for the degradation rate constants (k). A "homogeneous" and a "heterogeneous" spatial distribution were applied. The multidimensional model also permitted to integrate the P&T wells located downgradient of the SBS and evaluate the interaction between the two remediation systems by implementing and comparing two scenarios, with and without P&T.

Damköhler numbers (Da) and contaminant loadings of chloroethenes exfiltrating from the remediation system (L) were computed in each scenario and compared. Results showed significant differences between the heterogeneous and the homogeneous model both in terms of spatial variation of degradation efficiency (determined through Da) and L, proving the importance of a less parsimonious and more precise parametrization of k for an accurate assessment of the system efficiency. P&T proved to be important in the abatement of L and essential for the containment of the contamination plume.

The investigations and methods applied in this work allowed to obtain an evaluation of the whole remediation system efficiency and are thus recommended for other sites where sequential bioremediation (and possibly P&T) is adopted for aquifer cleanup.

A substantial improvement to the methodologies used would be the application of stochastic modeling for the reproduction of spatial distribution of input parameters values, which would allow the set-up of a RTM embedding a more complex degradation kinetics such as Monod kinetics. Such a model would permit to simulate degradation rates variable from cell to cell, which would be dependent on the spatial distribution of hydrogeochemical and microbiological data. This approach was not applied in this work due to the insufficient spatial characterization of the study site, especially in the area between the two biobarriers. Thus, an extension of hydrogeochemical and microbiological characterization to the area within the barriers is suggested in order to permit the implementation of a more complex RTM which would in turn permit a more accurate evaluation of the SBS.

References

Abe, Y., Aravena, R., Zopfi, J., Shouakar-Stash, O., Cox, E., Roberts, J.D., Hunkeler, D., 2009. Carbon and Chlorine Isotope Fractionation during Aerobic Oxidation and Reductive Dechlorination of Vinyl Chloride and *cis* -1,2-Dichloroethene. Environ. Sci. Technol. 43, 101–107. https://doi.org/10.1021/es801759k

Alvarez-Zaldívar, P., Centler, F., Maier, U., Thullner, M., Imfeld, G., 2016. Biogeochemical modelling of in situ biodegradation and stable isotope fractionation of intermediate chloroethenes in a horizontal subsurface flow wetland. Ecological Engineering 90, 170–179. https://doi.org/10.1016/j.ecoleng.2016.01.037

Amos, B.K., Christ, J.A., Abriola, L.M., Pennell, K.D., Löffler, F.E., 2007. Experimental Evaluation and Mathematical Modeling of Microbially Enhanced Tetrachloroethene (PCE) Dissolution. Environ. Sci. Technol. 41, 963–970. https://doi.org/10.1021/es061438n

Antelmi, M., Mazzon, P., Höhener, P., Marchesi, M., Alberti, L., 2021. Evaluation of MNA in A Chlorinated Solvents-Contaminated Aquifer Using Reactive Transport Modeling Coupled with Isotopic Fractionation Analysis. Water 13, 2945. https://doi.org/10.3390/w13212945

APAT, 2003. APAT, Protection Agency of Environment and Technical Services. Analytical methods for chemical water analysis, vol. 1. ("Metodi analitici per le acque - Volume I - Sezione 1000". APAT Rapporti 29). IRSA-CNR (Institute for Water Research, National Research Council). In Italian.

Appelo, C.A.J., Postma, D., 2004. Geochemistry, Groundwater and Pollution, 0 ed. CRC Press. https://doi.org/10.1201/9781439833544

Aulenta, F., Majone, M., Tandoi, V., 2006a. Enhanced anaerobic bioremediation of chlorinated solvents: environmental factors influencing microbial activity and their relevance under field conditions. J. Chem. Technol. Biotechnol. 81, 1463–1474. https://doi.org/10.1002/jctb.1567

Aulenta, F., Majone, M., Tandoi, V., 2006b. Enhanced anaerobic bioremediation of chlorinated solvents: environmental factors influencing microbial activity and their relevance under field conditions. Journal of Chemical Technology & Biotechnology 81, 1463–1474. https://doi.org/10.1002/jctb.1567

Baek, W., Lee, J.Y., 2011. Source apportionment of trichloroethylene in groundwater of the industrial complex in Wonju, Korea: a 15-year dispute and perspective: Source apportionment of TCE in groundwater of industrial complex in Wonju. Water and Environment Journal 25, 336–344. https://doi.org/10.1111/j.1747-6593.2010.00226.x

Barajas-Rodriguez, F.J., Murdoch, L.C., Falta, R.W., Freedman, D.L., 2019. Simulation of in situ biodegradation of 1,4-dioxane under metabolic and cometabolic conditions. Journal of Contaminant Hydrology 223, 103464. https://doi.org/10.1016/j.jconhyd.2019.02.006

Barrio-Lage, G.A., Parsons, F.Z., Barbitz, R.M., Lorenzo, P.L., Archer, H.E., 1990. Enhanced anaerobic biodegradation of vinyl chloride in ground water. Environ. Toxicol. Chem. 9, 403–415.

Barrio-Lage, G.A., Parsons, F.Z., Nassars, R.S., Lorenzo, P.L., 1987. Biotransformation of trichloroethene in a variety of subsurface materials. Environ. Toxicol. Chem. 6, 571–578.

Bell, C.H., Wong, J., Parsons, K., Semel, W., McDonough, J., Gerber, K., 2022. First FULL-SCALE IN SITU Propane Biosparging for CO-METABOLIC Bioremediation of 1, 4-DIOXANE. Groundwater Monitoring Rem 42, 54–66. https://doi.org/10.1111/gwmr.12511

Beretta, G.P., Terrenghi, J., 2017. Groundwater flow in the Venice lagoon and remediation of the Porto Marghera industrial area (Italy). Hydrogeol J 25, 847–861. https://doi.org/10.1007/s10040-016-1517-5

Bertolini, M., Zecchin, S., Beretta, G.P., De Nisi, P., Ferrari, L., Cavalca, L., 2021. Effectiveness of Permeable Reactive Bio-Barriers for Bioremediation of an Organohalide-Polluted Aquifer by Natural-Occurring Microbial Community. Water 13, 2442. https://doi.org/10.3390/w13172442

Bianchi, M., Pedretti, D., 2017. Geological entropy and solute transport in heterogeneous porous media. Water Resources Research 53, 4691–4708. https://doi.org/10.1002/2016WR020195

Blum, P., Hunkeler, D., Weede, M., Beyer, C., Grathwohl, P., Morasch, B., 2009. Quantification of biodegradation for o-xylene and naphthalene using first order decay models, Michaelis–Menten kinetics and stable carbon isotopes. Journal of Contaminant Hydrology 105, 118–130. https://doi.org/10.1016/j.jconhyd.2008.11.009

Bostick, B.C., Fendorf, S., 2003. Arsenite sorption on troilite (FeS) and pyrite (FeS2). Geochimica et Cosmochimica Acta, Advances in Oxide and Sulfide Mineral Surface Chemistry 67, 909–921. https://doi.org/10.1016/S0016-7037(02)01170-5

Bostick, B.C., Fendorf, S., Manning, B.A., 2003. Arsenite adsorption on galena (PbS) and sphalerite (ZnS). Geochimica et Cosmochimica Acta, Advances in Oxide and Sulfide Mineral Surface Chemistry 67, 895–907. https://doi.org/10.1016/S0016-7037(02)00959-6

Bouwer, E., Norris, R., Hinchee, R., Brown, R.A., Semprini, L., Wilson, J.T., Kampbell, D.H., Reinhard, M., Borden, R.C., Vogel, T., Thomas, J.M., Ward, C.H., 1994. Bioremediation of Chlorinated Solvents Using Alternate Electron Acceptors. Hanbook of Bioremediation 149–175.

Bradley, P.M., Chapelle, F.H., 1996. Anaerobic Mineralization of Vinyl Chloride in Fe(III)-Reducing, Aquifer Sediments. Environ. Sci. Technol. 30, 2084–2086. https://doi.org/10.1021/es950926k

Bradley, P.M., Chapelle, F.H., Lovley, D.R., 1998. Humic Acids as Electron Acceptors for Anaerobic Microbial Oxidation of Vinyl Chloride and Dichloroethene. Appl Environ Microbiol 64, 3102–3105. https://doi.org/10.1128/AEM.64.8.3102-3105.1998

Bradley, P.M., Richmond, S., Chapelle, F.H., 2005. Chloroethene Biodegradation in Sediments at 4°C. Appl Environ Microbiol 71, 6414–6417. https://doi.org/10.1128/AEM.71.10.6414-6417.2005

Burton, E.D., Johnston, S.G., Kocar, B.D., 2014. Arsenic Mobility during Flooding of Contaminated Soil: The Effect of Microbial Sulfate Reduction. Environ. Sci. Technol. 48, 13660–13667. https://doi.org/10.1021/es503963k

Calloni, A., Sala, P., Pirrotta, S., Tavecchia, S., 2002. Fenomeni di Contaminazione delle Acque Sotterranee. Indagini per l'individuazione dei focolai-Titolo IV-L.R.62/85. Provincia di Milano.

Carraro, A., Fabbri, P., Giaretta, A., Peruzzo, L., Tateo, F., Tellini, F., 2015. Effects of redox conditions on the control of arsenic mobility in shallow alluvial aquifers on the Venetian Plain (Italy). Science of The Total Environment 532, 581–594. https://doi.org/10.1016/j.scitotenv.2015.06.003

Casasso, A., Ferrantello, N., Pescarmona, S., Bianco, C., Sethi, R., 2020. Can Borehole Heat Exchangers Trigger Cross-Contamination between Aquifers? Water 12, 1174. https://doi.org/10.3390/w12041174

Casasso, A., Tosco, T., Bianco, C., Bucci, A., Sethi, R., 2019. How Can We Make Pump and Treat Systems More Energetically Sustainable? Water 12, 67. https://doi.org/10.3390/w12010067

Casiraghi, G., Pedretti, D., Beretta, G.P., Bertolini, M., Bozzetto, G., Cavalca, L., Ferrari, L., Masetti, M., Terrenghi, J., 2022a. Piloting Activities for the Design of a Large-scale Biobarrier Involving In Situ Sequential Anaerobic–aerobic Bioremediation of Organochlorides and Hydrocarbons. Water Air Soil Pollut 233, 425. https://doi.org/10.1007/s11270-022-05886-1

Casiraghi, G., Pedretti, D., Beretta, G.P., Bertolini, M., Bozzetto, G., Cavalca, L., Ferrari, L., Masetti, M., Terrenghi, J., n.d. Piloting Activities for the Design of a Large-scale Biobarrier Involving In Situ

Sequential Anaerobic–aerobic Bioremediation of Organochlorides and Hydrocarbons. Water Air Soil Pollut 233, 425. https://doi.org/10.1007/s11270-022-05886-1

Casiraghi, G., Pedretti, D., Beretta, G.P., Masetti, M., Varisco, S., 2022b. Assessing a Large-Scale Sequential In Situ Chloroethene Bioremediation System Using Compound-Specific Isotope Analysis (CSIA) and Geochemical Modeling. Pollutants 2, 462–486. https://doi.org/10.3390/pollutants2040031

Casiraghi, G., Pedretti, D., Beretta, G.P., Masetti, M., Varisco, S., 2022b. Assessing a Large-Scale Sequential In Situ Chloroethene Bioremediation System Using Compound-Specific Isotope Analysis (CSIA) and Geochemical Modeling. Pollutants 2, 462–485. https://doi.org/10.3390/pollutants2040031

Chambon, J.C., Bjerg, P.L., Scheutz, C., Baelum, J., Jakobsen, R., Binning, P.J., 2013. Review of reactive kinetic models describing reductive dechlorination of chlorinated ethenes in soil and groundwater. Biotechnol. Bioeng. 110, 1–23. https://doi.org/10.1002/bit.24714

Chandra, R. (Ed.), 2016. Biodegradation of Chemical Pollutants of Tannery Wastewater, in: Environmental Waste Management. CRC Press, pp. 385–412. https://doi.org/10.1201/b19243-17

Chapelle, F.H., Haack, S.K., Adriaens, P., Henry, M.A., Bradley, P.M., 1996. Comparison of E_h and H_2 Measurements for Delineating Redox Processes in a Contaminated Aquifer. Environ. Sci. Technol. 30, 3565–3569. https://doi.org/10.1021/es960249+

Chiang, W.-H., Kinzelbach, W., 2003. The advective transport model PMPATH. 3D-Groundwater Modeling with PMWIN: A Simulation System for Modeling Groundwater Flow and Pollution 175–198.

Christensen, T.H., Bjerg, P.L., Banwart, S.A., Jakobsen, R., Heron, G., Albrechtsen, H.-J., 2000. Characterization of redox conditions in groundwater contaminant plumes. Journal of Contaminant Hydrology 45, 165–241. https://doi.org/10.1016/S0169-7722(00)00109-1

Ciampi, P., Esposito, C., Petrageli Papini, M., 2019. Hydrogeochemical model supporting the remediation strategy of a highly contaminated industrial site. Water 11, 1371. https://doi.org/10.3390/w11071371

Cichocka, D., Siegert, M., Imfeld, G., Andert, J., Beck, K., Diekert, G., Richnow, H.-H., Nijenhuis, I., 2007. Factors controlling the carbon isotope fractionation of tetra- and trichloroethene during reductive dechlorination by Sulfurospirillum ssp. and Desulfitobacterium sp. strain PCE-S: Carbon isotope fractionation during reductive dechlorination. FEMS Microbiology Ecology 62, 98–107. https://doi.org/10.1111/j.1574-6941.2007.00367.x

Clapp, L.W., Semmens, M.J., Novak, P.J., Hozalski, R.M., 2004. Model for In Situ Perchloroethene Dechlorination via Membrane-Delivered Hydrogen. J. Environ. Eng. 130, 1367–1381. https://doi.org/10.1061/(ASCE)0733-9372(2004)130:11(1367)

Clement, T.P., 1999. A modular computer code for simulating reactive multi-species transport in 3-dimensional groundwater systems. Pacific Northwest National Lab.(PNNL), Richland, WA (United States).

Clement, T.P., 1997. RT3D—A Modular Computer Code for Simulating Reactive Multi-Species Transport in 3-Dimensional Groundwater Systems. Battelle Pacific Northwest National Laboratory Research Report, PNNL-SA-28967.

Clement, T.P., Johnson, C.D., Sun, Y., Klecka, G.M., Bartlett, C., 2000. Natural attenuation of chlorinated ethene compounds: model development and field-scale application at the Dover site. Journal of Contaminant Hydrology 42, 113–140. https://doi.org/10.1016/S0169-7722(99)00098-4

Coburn, T.C., Yarus, J.M., Chambers, R.L., 2006. Stochastic Modeling and Geostatistics: Principles, Methods, and Case Studies, Volume II. American Association of Petroleum Geologists. https://doi.org/10.1306/CA51063

Corsini, A., Zaccheo, P., Muyzer, G., Andreoni, V., Cavalca, L., 2014. Arsenic transforming abilities of groundwater bacteria and the combined use of Aliihoeflea sp. strain 2WW and goethite in metalloid removal.

Journal of Hazardous Materials, Research Frontiers in Chalcogen Cycle Based Environmental Technologies 269, 89–97. https://doi.org/10.1016/j.jhazmat.2013.12.037

Courbet, C., Rivière, A., Jeannottat, S., Rinaldi, S., Hunkeler, D., Bendjoudi, H., de Marsily, G., 2011a. Complementing approaches to demonstrate chlorinated solvent biodegradation in a complex pollution plume: Mass balance, PCR and compound-specific stable isotope analysis. Journal of Contaminant Hydrology 126, 315–329. https://doi.org/10.1016/j.jconhyd.2011.08.009

Courbet, C., Rivière, A., Jeannottat, S., Rinaldi, S., Hunkeler, D., Bendjoudi, H., de Marsily, G., 2011b. Complementing approaches to demonstrate chlorinated solvent biodegradation in a complex pollution plume: Mass balance, PCR and compound-specific stable isotope analysis. Journal of Contaminant Hydrology 126, 315–329. https://doi.org/10.1016/j.jconhyd.2011.08.009

Cozzarelli, I.M., Suflita, J.M., Ulrich, G.A., Harris, S.H., Scholl, M.A., Schlottmann, J.L., Christenson, S., 2000. Geochemical and Microbiological Methods for Evaluating Anaerobic Processes in an Aquifer Contaminated by Landfill Leachate. Environ. Sci. Technol. 34, 4025–4033. https://doi.org/10.1021/es991342b

Craig, H., 1957. Isotopic standards for carbon and oxygen and correction factors for mass-spectrometric analysis of carbon dioxide. Geochimica et Cosmochimica Acta 12, 133–149. https://doi.org/10.1016/0016-7037(57)90024-8

Cupples, A.M., Spormann, A.M., McCarty, P.L., 2004. Comparative Evaluation of Chloroethene Dechlorination to Ethene by *Dehalococcoides* -like Microorganisms. Environ. Sci. Technol. 38, 4768–4774. https://doi.org/10.1021/es049965z

D'Affonseca, F.M., Prommer, H., Finkel, M., Blum, P., Grathwohl, P., 2011. Modeling the long-term and transient evolution of biogeochemical and isotopic signatures in coal tar-contaminated aquifers: MODELING COAL TAR-CONTAMINATED AQUIFERS. Water Resour. Res. 47. https://doi.org/10.1029/2010WR009108

Dalla Libera, N., Fabbri, P., Mason, L., Piccinini, L., Pola, M., 2018. A local natural background level concept to improve the natural background level: a case study on the drainage basin of the Venetian Lagoon in Northeastern Italy. Environ Earth Sci 77, 487. https://doi.org/10.1007/s12665-018-7672-3

Dalla Libera, N., Pedretti, D., Casiraghi, G., Markó, Á., Piccinini, L., Fabbri, P., 2021. Probability of Non-Exceedance of Arsenic Concentration in Groundwater Estimated Using Stochastic Multicomponent Reactive Transport Modeling. Water 13, 3086. https://doi.org/10.3390/w13213086

Dalla Libera, N., Pedretti, D., Tateo, F., Mason, L., Piccinini, L., Fabbri, P., 2020. Conceptual model of arsenic mobility in the shallow alluvial aquifers near Venice (Italy) elucidated through machine learning and geochemical modeling. Water Resources Research 56, e2019WR026234. https://doi.org/10.1029/2019WR026234

Davis, J.W., Carpenter, C.L., 1990. Aerobic biodegradation of vinyl chloride in groundwater samples. Appl Environ Microbiol 56, 3878–3880. https://doi.org/10.1128/aem.56.12.3878-3880.1990

Devlin, J.F., Katic, D., Barker, J.F., 2004. In situ sequenced bioremediation of mixed contaminants in groundwater. Journal of Contaminant Hydrology 69, 233–261. https://doi.org/10.1016/S0169-7722(03)00156-6

Devlin, J.F., Parker, B.L., 1996. Optimum Hydraulic Conductivity to Limit Contaminant Flux Through Cutoff Walls. Groundwater 34, 719–726. https://doi.org/10.1111/j.1745-6584.1996.tb02060.x

Dey, K., Roy, P., 2009. Degradation of Trichloroethylene by Bacillus sp.: Isolation Strategy, Strain Characteristics, and Cell Immobilization. Curr Microbiol 59, 256–260. https://doi.org/10.1007/s00284-009-9427-6

Doherty, J., Brebber, L., Whyte, P., 1994. PEST: Model-independent parameter estimation. Watermark Computing, Corinda, Australia 122, 336.

Dolfing, J., 2016. Energetic Considerations in Organohalide Respiration, in: Adrian, L., Löffler, F.E. (Eds.), Organohalide-Respiring Bacteria. Springer Berlin Heidelberg, Berlin, Heidelberg, pp. 31–48. https://doi.org/10.1007/978-3-662-49875-0_3

Dolinová, I., Štrojsová, M., Černík, M., Němeček, J., Macháčková, J., Ševců, A., 2017a. Microbial degradation of chloroethenes: a review. Environ Sci Pollut Res 24, 13262–13283. https://doi.org/10.1007/s11356-017-8867-y

Dolinová, I., Štrojsová, M., Černík, M., Němeček, J., Macháčková, J., Ševců, A., 2017b. Microbial degradation of chloroethenes: a review. Environ Sci Pollut Res 24, 13262–13283. https://doi.org/10.1007/s11356-017-8867-y

Domenico, P.A., Schwartz, F.W., 1998. Physical and chemical hydrogeology, 2nd ed. ed. Wiley, New York.

EPA, 2013. EPA superfund remedy report, 14th ed. (No. EPA-542-R-13-016).

EPA, 2007. Treatment technologies for site cleanup: annual status report (ASR), 12th ed. (No. EPA 542-R-07-012). EPA.

EPA, 2001. Cost analyses for selected groundwater cleanup projects: pump and treat systems and permeable reactive barriers (No. EPA 542-R-00-013). U.S. Environmental Protection Agency.

EPA, 1996. Pump-and-Treat Ground-Water Remediation A Guide for Decision Makers and Practitioners (No. 22618). U.S. Environmental Protection Agency, Washington, D.C.

European Environment Agency, 2022. Europe's groundwater, EEA Briefing. Publications Office, LU.

Falta, R.W., 2008. Methodology for Comparing Source and Plume Remediation Alternatives. Ground Water 46, 272–285. https://doi.org/10.1111/j.1745-6584.2007.00416.x

Fennell, D.E., Carroll, A.B., Gossett, J.M., Zinder, S.H., 2001. Assessment of Indigenous Reductive Dechlorinating Potential at a TCE-Contaminated Site Using Microcosms, Polymerase Chain Reaction Analysis, and Site Data. Environ. Sci. Technol. 35, 1830–1839. https://doi.org/10.1021/es0016203

Fennell, D.E., Gossett, J.M., Zinder, S.H., 1997. Comparison of Butyric Acid, Ethanol, Lactic Acid, and Propionic Acid as Hydrogen Donors for the Reductive Dechlorination of Tetrachloroethene. Environ. Sci. Technol. 31, 918–926. https://doi.org/10.1021/es960756r

Fletcher, K.E., Costanza, J., Cruz-Garcia, C., Ramaswamy, N.S., Pennell, K.D., Löffler, F.E., 2011. Effects of Elevated Temperature on *Dehalococcoides* Dechlorination Performance and DNA and RNA Biomarker Abundance. Environ. Sci. Technol. 45, 712–718. https://doi.org/10.1021/es1023477

Fleuchaus, P., Godschalk, B., Stober, I., Blum, P., 2018. Worldwide application of aquifer thermal energy storage – A review. Renewable and Sustainable Energy Reviews 94, 861–876. https://doi.org/10.1016/j.rser.2018.06.057

Foght, J., 2008. Anaerobic Biodegradation of Aromatic Hydrocarbons: Pathways and Prospects. MIP 15, 93–120. https://doi.org/10.1159/000121324

Fralish, M.S., Downs, J.W., 2022. Vinyl Chloride Toxicity, in: StatPearls. StatPearls Publishing, Treasure Island (FL).

Frascari, D., Zanaroli, G., Danko, A.S., 2015. In situ aerobic cometabolism of chlorinated solvents: A review. Journal of Hazardous Materials 283, 382–399. https://doi.org/10.1016/j.jhazmat.2014.09.041

Freeze, R.A., Cherry, J.A., 1989. What Has Gone Wrong? Ground Water 27, 458–464.

Freeze, R.A., Cherry, J.A., 1979. Groundwater. Prentice-Hall, Englewood Cliffs, N.J.

Friis, A.K., Heimann, A.C., Jakobsen, R., Albrechtsen, H.-J., Cox, E., Bjerg, P.L., 2007. Temperature dependence of anaerobic TCE-dechlorination in a highly enriched Dehalococcoides-containing culture. Water Research 41, 355–364. https://doi.org/10.1016/j.watres.2006.09.026

Fritsche, W., Hofrichter, M., 2005. Aerobic Degradation of Recalcitrant Organic Compounds by Microorganisms, in: Jördening, H.-J., Winter, J. (Eds.), Environmental Biotechnology. Wiley-VCH Verlag GmbH & Co. KGaA, Weinheim, FRG, pp. 203–227. https://doi.org/10.1002/3527604286.ch7

Fritsche, W., Hofrichter, M., 2004. Aerobic Degradation of Recalcitrant Organic Compounds by Microorganisms, in: Environmental Biotechnology. John Wiley & Sons, Ltd, pp. 203–227. https://doi.org/10.1002/3527604286.ch7

Fry, V.A., Istok, J.D., 1994. Effectosf rate-limited desorption on the feasibility of in situ bioremediation. Water Resources Research 30, 2413–2422.

Futagami, T., Goto, M., Furukawa, K., 2008. Biochemical and genetic bases of dehalorespiration. Chem. Record 8, 1–12. https://doi.org/10.1002/tcr.20134

Gelhar, L.W., Welty, C., Rehfeldt, K.R., 1992. A critical review of data on field-scale dispersion in aquifers. Water Resour. Res. 28, 1955–1974. https://doi.org/10.1029/92WR00607

Haest, P.J., Springael, D., Smolders, E., 2010. Modelling reactive CAH transport using batch experiment degradation kinetics. Water Research 44, 2981–2989. https://doi.org/10.1016/j.watres.2010.02.031

Häggblom, M.M., Bossert, I.D., 2004. Halogenated Organic Compounds - A Global Perspective, in: Häggblom, M.M., Bossert, I.D. (Eds.), Dehalogenation. Kluwer Academic Publishers, Boston, pp. 3–29. https://doi.org/10.1007/0-306-48011-5_1

Haley, J.L., Hanson, B., Enfield, C.G., Glass, J., 1991. Evaluating the effectivness of ground water extraction systems. Ground Water Monitoring Review 11, 119–124.

Harbaugh, A.W., 2005. MODFLOW-2005 : the U.S. Geological Survey modular ground-water model--the ground-water flow process. Techniques and Methods.

Haritash, A.K., Kaushik, C.P., 2009. Biodegradation aspects of Polycyclic Aromatic Hydrocarbons (PAHs): A review. Journal of Hazardous Materials 169, 1–15. https://doi.org/10.1016/j.jhazmat.2009.03.137

Hartmans, S., de Bont, J.A.M., Tramper, J., Luyben, K.Ch.A.M., 1985. Bacterial degradation of vinyl chloride. Biotechnol Lett 7, 383–388. https://doi.org/10.1007/BF01166208

He, J., Sung, Y., Dollhopf, M.E., Fathepure, B.Z., Tiedje, J.M., Löffler, F.E., 2002. Acetate versus Hydrogen as Direct Electron Donors To Stimulate the Microbial Reductive Dechlorination Process at Chloroethene-Contaminated Sites. Environ. Sci. Technol. 36, 3945–3952. https://doi.org/10.1021/es025528d

He, Y.T., Wilson, J.T., Su, C., Wilkin, R.T., 2015. Review of abiotic degradation of chlorinated solvents by reactive iron minerals in aquifers. Groundwater Monitoring & Remediation 35, 57–75.

Henri, C.V., Fernàndez-Garcia, D., 2014. Toward efficiency in heterogeneous multispecies reactive transport modeling: A particle-tracking solution for first-order network reactions. Water Resour. Res. 50, 7206–7230. https://doi.org/10.1002/2013WR014956

Henschler, D., 1994. Toxicity of Chlorinated Organic Compounds: Effects of the Introduction of Chlorine in Organic Molecules. Angew. Chem. Int. Ed. Engl. 33, 1920–1935. https://doi.org/10.1002/anie.199419201

Herrero, J., Puigserver, D., Nijenhuis, I., Kuntze, K., Parker, B.L., Carmona, J.M., 2021. The role of ecotones in the dehalogenation of chloroethenes in alluvial fan aquifers. Environ Sci Pollut Res 28, 26871–26884. https://doi.org/10.1007/s11356-021-12538-0

Holliger, C., Hahn, D., Harmsen, H., Ludwig, W., Schumacher, W., Tindall, B., Vazquez, F., Weiss, N., Zehnder, A.J.B., 1998. Dehalobacter restrictus gen. nov. and sp. nov., a strictly anaerobic bacterium

that reductively dechlorinates tetra- and trichloroethene in an anaerobic respiration. Archives of Microbiology 169, 313–321. https://doi.org/10.1007/s002030050577

Holliger, C., Schraa, G., Stams, A.J., Zehnder, A.J., 1993. A highly purified enrichment culture couples the reductive dechlorination of tetrachloroethene to growth. Appl Environ Microbiol 59, 2991–2997. https://doi.org/10.1128/aem.59.9.2991-2997.1993

Holliger, Christof, Wohlfarth, G., Diekert, G., 1998. Reductive dechlorination in the energy metabolism of anaerobic bacteria. FEMS Microbiology Reviews 22, 383–398. https://doi.org/10.1111/j.1574-6976.1998.tb00377.x

Hourbron, E., Escoffier, S., Capdeville, B., 2000. Trichloroethylene elimination assay by naural consortia of heterotrophic and methanotrophic bacteria. Water Science and Technology 42, 395–402. https://doi.org/10.2166/wst.2000.0540

Huang, L., Sturchio, N.C., Abrajano, T., Heraty, L.J., Holt, B.D., 1999. Carbon and chlorine isotope fractionation of chlorinated aliphatic hydrocarbons by evaporation. Organic Geochemistry 30, 777–785. https://doi.org/10.1016/S0146-6380(99)00060-1

Hug, L.A., Beiko, R.G., Rowe, A.R., Richardson, R.E., Edwards, E.A., 2012. Comparative metagenomics of three Dehalococcoides-containing enrichment cultures: the role of the non-dechlorinating community. BMC Genomics 13, 327. https://doi.org/10.1186/1471-2164-13-327

Hyun, S.P., Hayes, K.F., 2009. Feasibility of Using In Situ FeS Precipitation for TCE Degradation. Journal of Environmental Engineering 135, 1009–1014. https://doi.org/10.1061/(ASCE)EE.1943-7870.0000073

Jeannottat, S., Hunkeler, D., 2012. Chlorine and Carbon Isotopes Fractionation during Volatilization and Diffusive Transport of Trichloroethene in the Unsaturated Zone. Environ. Sci. Technol. 46, 3169–3176. https://doi.org/10.1021/es203547p

Jeong, H.Y., Hayes, K.F., 2007. Reductive Dechlorination of Tetrachloroethylene and Trichloroethylene by Mackinawite (FeS) in the Presence of Metals: Reaction Rates. Environ. Sci. Technol. 41, 6390–6396. https://doi.org/10.1021/es0706394

Kao, C., 2003. Enhanced PCE dechlorination by biobarrier systems under different redox conditions. Water Research 37, 4885–4894. https://doi.org/10.1016/j.watres.2003.08.001

Kao, C.M., Chen, S.C., Wang, J.Y., Chen, Y.L., Lee, S.Z., 2003. Remediation of PCE-contaminated aquifer by an in situ two-layer biobarrier: laboratory batch and column studies. Water Research 37, 27–38. https://doi.org/10.1016/S0043-1354(02)00254-3

Kawabe, Y., Komai, T., 2019. A Case Study of Natural Attenuation of Chlorinated Solvents Under Unstable Groundwater Conditions in Takahata, Japan. Bull Environ Contam Toxicol 102, 280–286. https://doi.org/10.1007/s00128-019-02546-9

Keely, J.F., 1989. Performance Evaluations of Pump-and-Treat Remediations. Kerr Environmental Research Laboratory, Ada, OK.

Kirk, M.F., Holm, T.R., Park, J., Jin, Q., Sanford, R.A., Fouke, B.W., Bethke, C.M., 2004. Bacterial sulfate reduction limits natural arsenic contamination in groundwater. Geology 32, 953–956. https://doi.org/10.1130/G20842.1

Kirk, M.F., Roden, E.E., Crossey, L.J., Brealey, A.J., Spilde, M.N., 2010. Experimental analysis of arsenic precipitation during microbial sulfate and iron reduction in model aquifer sediment reactors. Geochimica et Cosmochimica Acta 74, 2538–2555. https://doi.org/10.1016/j.gca.2010.02.002

Knapp, R.B., Faison, B.D., 1997. A bioengineering system for in situ bioremediation of contaminated groundwater. J Ind Microbiol Biotechnol 18, 189–197.

Koenig, J., Lee, M., Manefield, M., 2015. Aliphatic organochlorine degradation in subsurface environments. Rev Environ Sci Biotechnol 14, 49–71. https://doi.org/10.1007/s11157-014-9345-3

Kouznetsova, I., Mao, X., Robinson, C., Barry, D.A., Gerhard, J.I., McCarty, P.L., 2010. Biological reduction of chlorinated solvents: Batch-scale geochemical modeling. Advances in Water Resources 33, 969–986. https://doi.org/10.1016/j.advwatres.2010.04.017

Kristensen, P., Whalley, C., Néry, F., Zal, N., Christiansen, T., 2018. European waters: assessment of status and pressures 2018. Publications Office of the European Union, Luxembourg.

Kromann, A., Ludvigsen, L., Albrechtsen, H.-J., Christensen, T.H., Ejlertsson, J., Svensson, B.H., 1998. Degradability of chlorinated aliphatic compounds in methanogenic leachates sampled at eight landfills. Waste Manag Res 16, 54–62. https://doi.org/10.1177/0734242X9801600107

Krumholz, L.R., Sharp, R., Fishbain, S.S., 1996. A freshwater anaerobe coupling acetate oxidation to tetrachloroethylene dehalogenation. Appl Environ Microbiol 62, 4108–4113. https://doi.org/10.1128/aem.62.11.4108-4113.1996

Lai, A., Aulenta, F., Mingazzini, M., Palumbo, M.T., Papini, M.P., Verdini, R., Majone, M., 2017. Bioelectrochemical approach for reductive and oxidative dechlorination of chlorinated aliphatic hydrocarbons (CAHs). Chemosphere 169, 351–360. https://doi.org/10.1016/j.chemosphere.2016.11.072

Lecloux, A.J., 2003. Scientific activities of Euro Chlor in monitoring and assessing naturally and man-made organohalogens. Chemosphere 52, 521–529. https://doi.org/10.1016/S0045-6535(03)00205-4

Lee, I.-S., Bae, J.-H., Yang, Y., McCarty, P.L., 2004. Simulated and experimental evaluation of factors affecting the rate and extent of reductive dehalogenation of chloroethenes with glucose. Journal of Contaminant Hydrology 74, 313–331. https://doi.org/10.1016/j.jconhyd.2004.03.006

Leeson, A., Becvar, E., Parsons, B.H., Fortenberry, J., Coyle, C., 2004. Principles and practices of enhanced Anaerobic bioremediation of chlorinated Solvents (Guidance Document No. 04-203 TR-2250- ENV). ESTCP, 901 N. Stuart Street, Suite 303 Arlington, VA 22203.

Lendvay, J.M., Löffler, F.E., Dollhopf, M., Aiello, M.R., Daniels, G., Fathepure, B.Z., Gebhard, M., Heine, R., Helton, R., Shi, J., Krajmalnik-Brown, R., Major, C.L., Barcelona, M.J., Petrovskis, E., Hickey, R., Tiedje, J.M., Adriaens, P., 2003. Bioreactive Barriers: A Comparison of Bioaugmentation and Biostimulation for Chlorinated Solvent Remediation. Environ. Sci. Technol. 37, 1422–1431. https://doi.org/10.1021/es025985u

Liang, X., Dong, Y., Kuder, T., Krumholz, L.R., Philp, R.P., Butler, E.C., 2007. Distinguishing Abiotic and Biotic Transformation of Tetrachloroethylene and Trichloroethylene by Stable Carbon Isotope Fractionation. Environ. Sci. Technol. 41, 7094–7100. https://doi.org/10.1021/es070970n

Liang, X., Howlett, M.R., Nelson, J.L., Grant, G., Dworatzek, S., Lacrampe-Couloume, G., Zinder, S.H., Edwards, E.A., Sherwood Lollar, B., 2011. Pathway-Dependent Isotope Fractionation during Aerobic and Anaerobic Degradation of Monochlorobenzene and 1,2,4-Trichlorobenzene. Environ. Sci. Technol. 45, 8321–8327. https://doi.org/10.1021/es201224x

Lin, Y.-P., Chen, Y.-W., Chang, L.-C., Yeh, M.-S., Huang, G.-H., Petway, J., 2017. Groundwater Simulations and Uncertainty Analysis Using MODFLOW and Geostatistical Approach with Conditioning Multi-Aquifer Spatial Covariance. Water 9, 164. https://doi.org/10.3390/w9030164

Liu, P., Wang, G., Shang, M., Liu, M., 2021. Groundwater Nitrate Bioremediation Simulation of In Situ Horizontal Well by Microbial Denitrification Using PHREEQC. Water Air Soil Pollut 232, 356. https://doi.org/10.1007/s11270-021-05313-x

Liu, Y., Ngo, H.H., Guo, W., Sun, J., Wang, D., Peng, L., Ni, B.-J., 2017. Modeling aerobic biotransformation of vinyl chloride by vinyl chloride-assimilating bacteria, methanotrophs and ethenotrophs. Journal of Hazardous Materials 332, 97–103. https://doi.org/10.1016/j.jhazmat.2017.03.003

Löffler, F.E., Yan, J., Ritalahti, K.M., Adrian, L., Edwards, E.A., Konstantinidis, K.T., Müller, J.A., Fullerton, H., Zinder, S.H., Spormann, A.M., 2013. Dehalococcoides mccartyi gen. nov., sp. nov., obligately organohalide-respiring anaerobic bacteria relevant to halogen cycling and bioremediation, belong to a novel bacterial class, Dehalococcoidia classis nov., order Dehalococcoidales ord. nov. and family Dehalococcoidaceae fam. nov., within the phylum Chloroflexi. International Journal of Systematic and Evolutionary Microbiology 63, 625–635. https://doi.org/10.1099/ijs.0.034926-0

Luijten, M.L.G.C., de Weert, J., Smidt, H., Boschker, H.T.S., de Vos, W.M., Schraa, G., Stams, A.J.M., 2003. Description of Sulfurospirillum halorespirans sp. nov., an anaerobic, tetrachloroethene-respiring bacterium, and transfer of Dehalospirillum multivorans to the genus Sulfurospirillum as Sulfurospirillum multivorans comb. nov. International Journal of Systematic and Evolutionary Microbiology 53, 787–793. https://doi.org/10.1099/ijs.0.02417-0

Luptakova, A., Kotulicova, I., Macingova, E., Jencarova, J., 2013. Bacterial Elimination of Sulphates from Mine Waters. Chemical Engineering Transactions 35, 853–858. https://doi.org/10.3303/CET1335142

MacDonald, T.R., Kitanidis, P.K., McCarty, P.L., Roberts, P.V., 1999. Mass-Transfer Limitations for Macroscale Bioremediation Modeling and Implications on Aquifer Clogging. Ground Water 37.

Mackay, D.M., Cherry, J.A., 1989. Groundwater contamination: pump-and-treat remediation. Environ. Sci. Technol. 23, 630–636. https://doi.org/10.1021/es00064a001

Mackay, D.M., Wilson, R.D., Brown, M.J., Ball, W.P., Xia, G., Durfee, D.P., 2000. A controlled field evaluation of continuous vs. pulsed pump-and-treat remediation of a VOC-contaminated aquifer: site characterization, experimental setup, and overview of results. Journal of Contaminant Hydrology 41, 81–131. https://doi.org/10.1016/S0169-7722(99)00065-0

Maillard, J., Regeard, C., Holliger, C., 2005. Isolation and characterization of Tn-Dha1, a transposon containing the tetrachloroethene reductive dehalogenase of Desulfitobacterium hafniense strain TCE1. Environ Microbiol 7, 107–117. https://doi.org/10.1111/j.1462-2920.2004.00671.x

Maillard, J., Schumacher, W., Vazquez, F., Regeard, C., Hagen, W.R., Holliger, C., 2003. Characterization of the Corrinoid Iron-Sulfur ProteinTetrachloroethene Reductive Dehalogenase of *Dehalobacterre-strictus*. Appl Environ Microbiol 69, 4628–4638. https://doi.org/10.1128/AEM.69.8.4628-4638.2003

Majone, M., Verdini, R., Aulenta, F., Rossetti, S., Tandoi, V., Kalogerakis, N., Agathos, S., Puig, S., Zanaroli, G., Fava, F., 2015. In situ groundwater and sediment bioremediation: barriers and perspectives at European contaminated sites. New Biotechnology 32, 133–146. https://doi.org/10.1016/j.nbt.2014.02.011

Marcet, T.F., Cápiro, N.L., Yang, Y., Löffler, F.E., Pennell, K.D., 2018. Impacts of low-temperature thermal treatment on microbial detoxification of tetrachloroethene under continuous flow conditions. Water Research 145, 21–29. https://doi.org/10.1016/j.watres.2018.07.076

Marquis Jr, S., 1995. Don't Give Up on Pump and Treat: Enhance It with Bioremediation. Soils & Groundwater Cleanup 46–50.

Mattes, T.E., Alexander, A.K., Coleman, N.V., 2010. Aerobic biodegradation of the chloroethenes: pathways, enzymes, ecology, and evolution. FEMS Microbiology Reviews 34, 445–475. https://doi.org/10.1111/j.1574-6976.2010.00210.x

Mattes, T.E., Alexander, A.K., Richardson, P.M., Munk, A.C., Han, C.S., Stothard, P., Coleman, N.V., 2008. The Genome of *Polaromonas* sp. Strain JS666: Insights into the Evolution of a Hydrocarbon- and

Xenobiotic-Degrading Bacterium, and Features of Relevance to Biotechnology. Appl Environ Microbiol 74, 6405–6416. https://doi.org/10.1128/AEM.00197-08

Matteucci, F., Ercole, C., del Gallo, M., 2015a. A study of chlorinated solvent contamination of the aquifers of an industrial area in central Italy: a possibility of bioremediation. Front. Microbiol. 6. https://doi.org/10.3389/fmicb.2015.00924

Matteucci, F., Ercole, C., del Gallo, M., 2015b. A study of chlorinated solvent contamination of the aquifers of an industrial area in central Italy: a possibility of bioremediation. Frontiers in Microbiology 6.

Maymó-Gatell, X., Chien, Y., Gossett, J.M., Zinder, S.H., 1997. Isolation of a Bacterium That Reductively Dechlorinates Tetrachloroethene to Ethene. Science 276, 1568–1571. https://doi.org/10.1126/science.276.5318.1568

Maymó-Gatell, X., Nijenhuis, I., Zinder, S.H., 2001. Reductive Dechlorination of *cis* -1,2-Dichloroethene and Vinyl Chloride by " *Dehalococcoides ethenogenes* ." Environ. Sci. Technol. 35, 516–521. https://doi.org/10.1021/es001285i

Moore, J.N., Ficklin, W.H., Johns, C., 1988. Partitioning of arsenic and metals in reducing sulfidic sediments. Environmental Science & Technology 22, 432–437.

Moreira, D., Zivanovic, Y., López-Archilla, A.I., Iniesto, M., López-García, P., 2021. Reductive evolution and unique predatory mode in the CPR bacterium Vampirococcus lugosii. Nat Commun 12, 2454. https://doi.org/10.1038/s41467-021-22762-4

Moussa, T.A.A., Khalil, N.M., 2022. Extremozymes from extremophilic microorganisms as sources of bioremediation, in: Microbial Extremozymes. Elsevier, pp. 135–146. https://doi.org/10.1016/B978-0-12-822945-3.00005-1

Mukwevho, M.J., Chirwa, E.M.N., Maharajh, D., 2019. The effect of pH and temperature on biological sulphate reduction. https://doi.org/10.3303/CET1974087

Mutch, R.D., Scott, J.I., Wilson, D.J., 1993. Cleanup of fractured rock aquifers: Implications of matrix diffusion. Environ Monit Assess 24, 45–70. https://doi.org/10.1007/BF00568799

Němeček, J., Marková, K., Špánek, R., Antoš, V., Kozubek, P., Lhotský, O., Černík, M., 2020. Hydrochemical Conditions for Aerobic/Anaerobic Biodegradation of Chlorinated Ethenes—A Multi-Site Assessment. Water 12, 322. https://doi.org/10.3390/w12020322

Neumann, A., Scholz-Muramatsu, H., Diekert, G., 1994. Tetrachloroethene metabolism of Dehalospirillum multivorans. Arch. Microbiol. 162, 295–301. https://doi.org/10.1007/BF00301854

Ni, Z., Van Gaans, P., Rijnaarts, H., Grotenhuis, T., 2018. Combination of aquifer thermal energy storage and enhanced bioremediation: Biological and chemical clogging. Science of The Total Environment 613–614, 707–713. https://doi.org/10.1016/j.scitotenv.2017.09.087

Ni, Z., Van Gaans, P., Smit, M., Rijnaarts, H., Grotenhuis, T., 2016. Combination of aquifer thermal energy storage and enhanced bioremediation: resilience of reductive dechlorination to redox changes. Appl Microbiol Biotechnol 100, 3767–3780. https://doi.org/10.1007/s00253-015-7241-6

Nielsen, P.H., Bjarnadóttir, H., Winter, P.L., Christensen, T.H., 1995. In situ and laboratory studies on the fate of specific organic compounds in an anaerobic landfill leachate plume, 2. Fate of aromatic and chlorinated aliphatic compounds. Journal of Contaminant Hydrology 20, 51–66. https://doi.org/10.1016/0169-7722(95)00026-R

Norris, R.D., 2018. Handbook of bioremediation, First edition. ed. CRC Press, Boca Raton, FL.

Nowak, J., Kirsch, N.H., Hegemann, W., Stan, H.-J., 1996. Total reductive dechlorination of chlorobenzenes to benzene by a methanogenic mixed culture enriched from Saale river sediment. Appl Microbiol Biotechnol 45, 700–709. https://doi.org/10.1007/s002530050751

NRC, 1994. Alternatives for Ground Water Cleanup. National Academies Press, Washington, D.C. https://doi.org/10.17226/2311

O'Day, P.A., Vlassopoulos, D., Root, R., Rivera, N., 2004. The influence of sulfur and iron on dissolved arsenic concentrations in the shallow subsurface under changing redox conditions. Proceedings of the National Academy of Sciences 101, 13703–13708.

Olsen, R.L., Kavanaugh, M.C., 1993. Can groundwater restoration be achieved? Water Environ. Technol. 5, 42–47.

Pandey, V.C., Singh, V. (Eds.), 2020. Bioremediation of pollutants: from genetic engineering to genome engineering. Elsevier, Amsterdam.

Parkhurst, D. L., Appelo, C.A.J., 2013. Description of Input and Examples for PHREEQC Version 3—A Computer Program for Speciation, Batch-Reaction, One-Dimensional Transport, and Inverse Geochemical Calculations. U.S. Geological Survey.

Parkhurst, David L., Appelo, C.A.J., 2013. Description of Input and Examples for PHREEQC Version 3—A Computer Program for Speciation, Batch-Reaction, One-Dimensional Transport, and Inverse Geochemical Calculations. (USGS Technical No. 6(A)43). U.S. Geological Survey, Denver, CO, USA.

Pedretti, D., 2020. Heterogeneity-controlled uncertain optimization of pump-and-treat systems explained through geological entropy. Int J Geomath 11, 22. https://doi.org/10.1007/s13137-020-00158-8

Pedretti, D., Fernàndez-Garcia, D., Bolster, D., Sanchez-Vila, X., 2013. On the formation of breakthrough curves tailing during convergent flow tracer tests in three-dimensional heterogeneous aquifers. Water Resources Research 49, 4157–4173. https://doi.org/10.1002/wrcr.20330

Pedretti, Daniele, Masetti, M., Beretta, G.P., Vitiello, M., 2013. A Revised Conceptual Model to Reproduce the Distribution of Chlorinated Solvents in the Rho Aquifer (Italy). GroundWater Monit R 33, 69–77. https://doi.org/10.1111/gwmr.12017

Pedretti, D., Masetti, M., Marangoni, T., Beretta, G.P., 2012. Slurry wall containment performance: monitoring and modeling of unsaturated and saturated flow. Environ Monit Assess 184, 607–624. https://doi.org/10.1007/s10661-011-1990-1

Petitta, M., Pacioni, E., Sbarbati, C., Corvatta, G., Fanelli, M., Aravena, R., 2013. Hydrodynamic and isotopic characterization of a site contaminated by chlorinated solvents: Chienti River Valley, Central Italy. Applied Geochemistry 32, 164–174. https://doi.org/10.1016/j.apgeochem.2012.09.012

Phelps, T.J., Malachowsky, K., Schram, R.M., White, D.C., 1991. Aerobic mineralization of vinyl chloride by a bacterium of the order Actinomycetales. Appl Environ Microbiol 57, 1252–1254. https://doi.org/10.1128/aem.57.4.1252-1254.1991

Pi, K., Wang, Y., Xie, X., Ma, T., Liu, Y., Su, C., Zhu, Y., Wang, Z., 2017. Remediation of arsenic-contaminated groundwater by in-situ stimulating biogenic precipitation of iron sulfides. Water Research 109, 337–346. https://doi.org/10.1016/j.watres.2016.10.056

Pooley, K.E., Blessing, M., Schmidt, T.C., Haderlein, S.B., MacQuarrie, K.T.B., Prommer, H., 2009. Aerobic Biodegradation of Chlorinated Ethenes in a Fractured Bedrock Aquifer: Quantitative Assessment by Compound-Specific Isotope Analysis (CSIA) and Reactive Transport Modeling. Environ. Sci. Technol. 43, 7458–7464. https://doi.org/10.1021/es900658n

Poulson, S.R., Drever, J.I., 1999. Stable Isotope (C, Cl, and H) Fractionation during Vaporization of Trichloroethylene. Environ. Sci. Technol. 33, 3689–3694. https://doi.org/10.1021/es990406f

Powell, C.L., Goltz, M.N., Agrawal, A., 2014. Degradation kinetics of chlorinated aliphatic hydrocarbons by methane oxidizers naturally-associated with wetland plant roots. Journal of Contaminant Hydrology 170, 68–75. https://doi.org/10.1016/j.jconhyd.2014.10.001

Prommer, H., Anneser, B., Rolle, M., Einsiedl, F., Griebler, C., 2009. Biogeochemical and Isotopic Gradients in a BTEX/PAH Contaminant Plume: Model-Based Interpretation of a High-Resolution Field Data Set. Environ. Sci. Technol. 43, 8206–8212. https://doi.org/10.1021/es901142a

Ravina, M., Facelli, A., Zanetti, M., 2020. Halocarbon Emissions from Hazardous Waste Landfills: Analysis of Sources and Risks. Atmosphere 11, 375. https://doi.org/10.3390/atmos11040375

Reinhart, D., 1993. A Review Of Recent Studies On The Sources Of Hazardous Compounds Emitted From Solid Waste Landfills: A U.S. Experience. Waste Management & Research 11, 257–268. https://doi.org/10.1006/wmre.1993.1025

Renpenning, J., Hitzfeld, K.L., Gilevska, T., Nijenhuis, I., Gehre, M., Richnow, H.-H., 2015. Development and Validation of an Universal Interface for Compound-Specific Stable Isotope Analysis of Chlorine (^{37}Cl/ ^{35}Cl) by GC-High-Temperature Conversion (HTC)-MS/IRMS. Anal. Chem. 87, 2832–2839. https://doi.org/10.1021/ac504232u

Rittle, K.A., Drever, J.I., Colberg, P.J., 1995. Precipitation of arsenic during bacterial sulfate reduction. Geomicrobiology Journal 13, 1–11.

Rügge, K., Bjerg, P.L., Pedersen, J.K., Mosbaek, H., Christensen, T.H., 1999. An anaerobic field injection experiment in a landfill leachate plume, Grindsted, Denmark: 1. Experimental setup, tracer movement, and fate of aromatic and chlorinated compounds. Water Resour. Res. 35, 1231–1246. https://doi.org/10.1029/1998WR900101

Ryoo, D., Shim, H., Canada, K., Barbieri, P., Wood, T.K., 2000. Aerobic degradation of tetrachloroethylene by toluene-o-xylene monooxygenase of Pseudomonas stutzeri OX1. Nat Biotechnol 18, 775–778. https://doi.org/10.1038/77344

Schäfer, W., Kinzelbach, W., 1992. Stochastic modeling of in situ bioremediation in heterogeneous aquifers. Journal of Contaminant Hydrology 10, 47–73. https://doi.org/10.1016/0169-7722(92)90043-E

Scheibe, T.D., Mahadevan, R., Fang, Y., Garg, S., Long, P.E., Lovley, D.R., 2009. Coupling a genome-scale metabolic model with a reactive transport model to describe *in situ* uranium bioremediation: Coupled genome-scale and reactive transport models. Microbial Biotechnology 2, 274–286. https://doi.org/10.1111/j.1751-7915.2009.00087.x

Schmidt, K.R., Tiehm, A., 2008. Natural attenuation of chloroethenes: identification of sequential reductive/oxidative biodegradation by microcosm studies. Water Science and Technology 58, 1137–1145. https://doi.org/10.2166/wst.2008.729

Sharma, P.K., McCarty, P.L., 1996. Isolation and Characterization of a Facultatively Aerobic Bacterium That Reductively Dehalogenates Tetrachloroethene to cis-1,2-Dichloroethene. Appl Environ Microbiol 62, 761–765. https://doi.org/10.1128/aem.62.3.761-765.1996

Shivalkar, S., Singh, V., Sahoo, A.K., Samanta, S.K., Gautam, P.K., 2021. Bioremediation: a potential ecological tool for waste management, in: Bioremediation for Environmental Sustainability. Elsevier, pp. 1–21. https://doi.org/10.1016/B978-0-12-820318-7.00001-0

Sidiropoulos, P., Mylopoulos, N., Vasiliades, L., Loukas, A., 2021. Stochastic nitrate simulation under hydraulic conductivity uncertainty of an agricultural basin aquifer at Eastern Thessaly, Greece. Environ Sci Pollut Res 28, 65700–65715. https://doi.org/10.1007/s11356-021-15555-1

Singh, J., Knapp, H.V., Demissie, M., 2004. Hydrologic modeling of the Iroquois River watershed using HSPF and SWAT. ISWS CR 2004-08. Champaign, Ill.: Illinois State Water Survey.

Sizirici, B., Tansel, B., 2010. Projection of landfill stabilization period by time series analysis of leachate quality and transformation trends of VOCs. Waste Management 30, 82–91. https://doi.org/10.1016/j.wasman.2009.09.006

Slater, G.F., Sherwood Lollar, B., Sleep, B.E., Edwards, E.A., 2001. Variability in Carbon Isotopic Fractionation during Biodegradation of Chlorinated Ethenes: Implications for Field Applications. Environ. Sci. Technol. 35, 901–907. https://doi.org/10.1021/es001583f

Speight, J.G., 2020. Remediation technologies, in: Natural Water Remediation. Elsevier, pp. 263–303. https://doi.org/10.1016/B978-0-12-803810-9.00008-5

Steefel, C.I., Appelo, C.A.J., Arora, B., Jacques, D., Kalbacher, T., Kolditz, O., Lagneau, V., Lichtner, P.C., Mayer, K.U., Meeussen, J.C.L., Molins, S., Moulton, D., Shao, H., Šimůnek, J., Spycher, N., Yabusaki, S.B., Yeh, G.T., 2015. Reactive transport codes for subsurface environmental simulation. Comput Geosci 19, 445–478. https://doi.org/10.1007/s10596-014-9443-x

Stroo, H.F., Leeson, A., Ward, C.H. (Eds.), 2013. Bioaugmentation for groundwater remediation, SERDP and ESTCP remediation technology monograph series. Springer, New York.

Sturman, P.J., Stewart, P.S., Cunningham, A.B., Bouwer, E.J., Wolfram, J.H., 1995. Engineering scale-up of in situ bioremediation processes: a review. Journal of Contaminant Hydrology 19, 171–203. https://doi.org/10.1016/0169-7722(95)00017-P

Suarez, M.P., Rifai, H.S., 1999. Biodegradation Rates for Fuel Hydrocarbons and Chlorinated Solvents in Groundwater. Bioremediat. J 3, 337–362.

Suflita, J.M., Gerba, C.P., Ham, R.K., Palmisano, A.C., Rathje, W.L., Robinson, J.A., 1992. The world's largest landfill. Environ. Sci. Technol. 26, 1486–1495. https://doi.org/10.1021/es00032a002

Sung, Y., Fletcher, K.E., Ritalahti, K.M., Apkarian, R.P., Ramos-Hernández, N., Sanford, R.A., Mesbah, N.M., Löffler, F.E., 2006. *Geobacter lovleyi* sp. nov. Strain SZ, a Novel Metal-Reducing and Tetrachloroethene-Dechlorinating Bacterium. Appl Environ Microbiol 72, 2775–2782. https://doi.org/10.1128/AEM.72.4.2775-2782.2006

Sung, Y., Ritalahti, K.M., Sanford, R.A., Urbance, J.W., Flynn, S.J., Tiedje, J.M., Löffler, F.E., 2003. Characterization of Two Tetrachloroethene-Reducing, Acetate-Oxidizing Anaerobic Bacteria and Their Description as *Desulfuromonas michiganensis* sp. nov. Appl Environ Microbiol 69, 2964–2974. https://doi.org/10.1128/AEM.69.5.2964-2974.2003

Thomas, J.M., Ward, C.H., 1989. In situ biorestoration of organic contaminants in the subsurface. Environ. Sci. Technol. 23, 760–766. https://doi.org/10.1021/es00065a004

Tiehm, A., Schmidt, K.R., 2011. Sequential anaerobic/aerobic biodegradation of chloroethenes—aspects of field application. Current Opinion in Biotechnology, Energy biotechnology – Environmental biotechnology 22, 415–421. https://doi.org/10.1016/j.copbio.2011.02.003

Tillotson, J.M., Borden, R.C., 2017. Rate and Extent of Chlorinated Ethene Removal at 37 ERD Sites. J. Environ. Eng. 143, 04017028. https://doi.org/10.1061/(ASCE)EE.1943-7870.0001224

Tobiszewski, M., Namieśnik, J., 2012. Abiotic degradation of chlorinated ethanes and ethenes in water. Environ Sci Pollut Res 19, 1994–2006. https://doi.org/10.1007/s11356-012-0764-9

Travis, C., Doty, C., 1990. ES&T Views: Can contaminated aquifers at superfund sites be remediated? Environ. Sci. Technol. 24, 1464–1466. https://doi.org/10.1021/es00080a600

Truex, M., Powell, T., Lynch, K., 2007. In Situ Dechlorination of TCE during Aquifer Heating. Groundwater Monitoring & Remediation 27, 96–105. https://doi.org/10.1111/j.1745-6592.2007.00141.x

Van Breukelen, B.M., Hunkeler, D., Volkering, F., 2005. Quantification of Sequential Chlorinated Ethene Degradation by Use of a Reactive Transport Model Incorporating Isotope Fractionation. Environ. Sci. Technol. 39, 4189–4197. https://doi.org/10.1021/es048973c

Van Breukelen, B.M., Thouement, H.A.A., Stack, P.E., Vanderford, M., Philp, P., Kuder, T., 2017. Modeling 3D-CSIA data: Carbon, chlorine, and hydrogen isotope fractionation during reductive dechlorination

of TCE to ethene. Journal of Contaminant Hydrology 204, 79–89. https://doi.org/10.1016/j.jconhyd.2017.07.003

van Warmerdam, E.M., Frape, S.K., Aravena, R., Drimmie, R.J., Flatt, H., Cherry, J.A., 1995. Stable chlorine and carbon isotope measurements of selected chlorinated organic solvents. Applied Geochemistry 10, 547–552. https://doi.org/10.1016/0883-2927(95)00025-9

Vanbroekhoven, K., Van Roy, S., Gielen, C., Maesen, M., Ryngaert, A., Diels, L., Seuntjens, P., 2007. Microbial processes as key drivers for metal (im)mobilization along a redox gradient in the saturated zone. Environ Pollut 148, 759–769. https://doi.org/10.1016/j.envpol.2007.01.036

Varisco, S., Beretta, G.P., Raffaelli, L., Raimondi, P., Pedretti, D., 2021. Model-Based Analysis of the Link between Groundwater Table Rising and the Formation of Solute Plumes in a Shallow Stratified Aquifer. Pollutants 1, 66–86. https://doi.org/10.3390/pollutants1020007

Vidali, M., 2001. Bioremediation. An overview. Pure and Applied Chemistry 73, 1163–1172. https://doi.org/10.1351/pac200173071163

Vogel, T.M., McCarty, P.L., 1985. Biotransformation of tetrachloroethylene to trichloroethylene, dichloroethylene, vinyl chloride, and carbon dioxide under methanogenic conditions. Appl Environ Microbiol 49, 1080–1083. https://doi.org/10.1128/aem.49.5.1080-1083.1985

Vogt, C., Kleinsteuber, S., Richnow, H.-H., 2011. Anaerobic benzene degradation by bacteria. Microbial Biotechnology 4, 710–724. https://doi.org/10.1111/j.1751-7915.2011.00260.x

Wang, C.-C., Li, C.-H., Yang, C.-F., 2019. Acclimated methanotrophic consortia for aerobic co-metabolism of trichloroethene with methane. International Biodeterioration & Biodegradation 142, 52–57. https://doi.org/10.1016/j.ibiod.2019.05.002

Wheater, H.S., Tompkins, J.A., van Leeuwen, M., Butler, A.P., 2000. Uncertainty in groundwater flow and transport modelling?a stochastic analysis of well-protection zones. Hydrol. Process. 14, 2019–2029. https://doi.org/10.1002/1099-1085(20000815/30)14:11/12<2019::AID-HYP52>3.0.CO;2-H

Widdowson, M.A., 2004. Modeling Natural Attenuation of Chlorinated Ethenes Under Spatially Varying Redox Conditions. Biodegradation 15, 435–451. https://doi.org/10.1023/B:BIOD.0000044680.39094.cc

Wiegert, C., Mandalakis, M., Knowles, T., Polymenakou, P.N., Aeppli, C., Macháčková, J., Holmstrand, H., Evershed, R.P., Pancost, R.D., Gustafsson, Ö., 2013. Carbon and Chlorine Isotope Fractionation During Microbial Degradation of Tetra- and Trichloroethene. Environ. Sci. Technol. 47, 6449–6456. https://doi.org/10.1021/es305236y

Wood, J.A., Porter, M.L., 1987. Hazardous Pollutants in Class II Landfills. JAPCA 37, 609–615. https://doi.org/10.1080/08940630.1987.10466250

Xiao, Z., Jiang, W., Chen, D., Xu, Y., 2020. Bioremediation of typical chlorinated hydrocarbons by microbial reductive dechlorination and its key players: A review. Ecotoxicology and Environmental Safety 202, 110925. https://doi.org/10.1016/j.ecoenv.2020.110925

Yang, J., Meng, L., Guo, L., 2018. In situ remediation of chlorinated solvent-contaminated groundwater using ZVI/organic carbon amendment in China: field pilot test and full-scale application. Environ Sci Pollut Res 25, 5051–5062. https://doi.org/10.1007/s11356-017-9903-7

Yang, Y., Higgins, S.A., Yan, J., Şimşir, B., Chourey, K., Iyer, R., Hettich, R.L., Baldwin, B., Ogles, D.M., Löffler, F.E., 2017. Grape pomace compost harbors organohalide-respiring Dehalogenimonas species with novel reductive dehalogenase genes. ISME J 11, 2767–2780. https://doi.org/10.1038/ismej.2017.127

Yang, Y., McCarty, P.L., 2002. Comparison between Donor Substrates for Biologically Enhanced Tetrachloroethene DNAPL Dissolution. Environ. Sci. Technol. 36, 3400–3404. https://doi.org/10.1021/es011408e

Yu, S., Dolan, M.E., Semprini, L., 2005. Kinetics and Inhibition of Reductive Dechlorination of Chlorinated Ethylenes by Two Different Mixed Cultures. Environ. Sci. Technol. 39, 195–205. https://doi.org/10.1021/es0496773

Yu, S., Semprini, L., 2004. Kinetics and modeling of reductive dechlorination at high PCE and TCE concentrations. Biotechnol. Bioeng. 88, 451–464. https://doi.org/10.1002/bit.20260

Zalesak, M., Ruzicka, J., Vicha, R., Dvorackova, M., 2017. Cometabolic degradation of dichloroethenes by Comamonas testosteroni RF2. Chemosphere 186, 919–927. https://doi.org/10.1016/j.chemosphere.2017.07.156

Zhang, C., Kang, Q., Wang, X., Zilles, J.L., Müller, R.H., Werth, C.J., 2010. Effects of Pore-Scale Heterogeneity and Transverse Mixing on Bacterial Growth in Porous Media. Environ. Sci. Technol. 44, 3085–3092. https://doi.org/10.1021/es903396h

Zheng, C., Bennett, G.D., 2002. Applied contaminant transport modeling, 2nd ed. ed. Wiley-Interscience, New York.

Zimmermann, J., Halloran, L.J.S., Hunkeler, D., 2020. Tracking chlorinated contaminants in the subsurface using compound-specific chlorine isotope analysis: A review of principles, current challenges and applications. Chemosphere 244, 125476. https://doi.org/10.1016/j.chemosphere.2019.125476